

Dissertation zur Erlangung des Doktorgrades
der Fakultät für Chemie und Pharmazie
der Ludwig-Maximilians-Universität München

Optimised Freezing and Thawing of Monoclonal Antibody Solutions



Oliver Blümel

aus

Fulda, Deutschland

2021

Erklärung

Diese Dissertation wurde im Sinne von §7 der Promotionsordnung vom 28. November 2011 von Herrn Prof. Dr. Wolfgang Frieß betreut.

Eidesstattliche Versicherung

Diese Dissertation wurde eigenständig und ohne unerlaubte Hilfe erarbeitet.

München, 30. Oktober 2021

Oliver Blümel

Oliver Blümel

Dissertation eingereicht am: 13.12.2021

1. Gutachter: Prof. Dr. Wolfgang Frieß

2. Gutachter: Prof. Dr. Gerhard Winter

Mündliche Prüfung am: 03.02.2022

„Jede Lösung eines Problems ist ein neues Problem.“

Johann Wolfgang von Goethe

Acknowledgements

First and foremost, I would like to thank my supervisors Prof. Dr. Wolfgang Frieß and Dr. Karoline Bechtold-Peters. Their honest advice, constructive feedback, ambitious guidance, and mindset that there is always room for improvement are the main reasons this work was possible.

I am thankful for the motivating and challenging meetings and discussions with the co-authors of the manuscripts, Dr. Jakob W. Bücheler, Dr. Astrid Hauptmann, Dr. Georg Hölzl, Dr. Miguel A. Rodrigues, Dr. Vitor Geraldes, Moritz Anuschek, and Dr. Andraž Pavlišič.

My deepest gratitude to Professor Dr. Wolfgang Frieß, Prof. Dr. Gerhard Winter, and Prof. Dr. Olivia Merkel for giving me the opportunity to spend this period of life at the Department of Pharmaceutical Technology and Biopharmaceutics.

Furthermore, many thanks to AK Frieß, AK Winter, and AK Merkel for numerous joint hiking trips, winter retreats, Oktoberfest visits, and countless parties. It was great to see colleagues becoming close friends. I would especially like to emphasise Inas ElBialy and Fabian Moll, my Damensauna labmates, and Eduard Trenkenschuh, the lifetime Damensauna honorary member, for always having a sympathetic ear and for making the time at the LMU so precious. Thanks to Natalie Deiringer and Dr. Hristo Svilenov, who anytime lent a helping hand. I don't want to miss a single coffee break with Dr. Martin Domnowski, which often resulted in fruitful discussions and are still ongoing. Many thanks to Imke Leitner and Sabine Kohler, who keep things ticking over.

I would like to express my deepest gratitude to my family for their support through the years. Without their help I would never have been given the chance to study pharmacy and to start my PhD project in Munich.

Most importantly, I thank my wife Luisa, the love of my life. She continuously supports me, lifts the burden from my shoulders, and encourages me. I am more than thankful for having you and am looking forward to spending the rest of my life with you. The sky is the limit as long as you are by my side.

Funding Acknowledgements

This work was funded by the Novartis AG, Basel.

Table of Contents

Chapter 1	General Introduction	1
1.1	Freezing and Thawing of Monoclonal Antibody Solutions.....	1
1.2	Stresses During Freezing and Thawing	2
1.2.1	Cryoconcentration Upon Freezing and Concentration Gradients Upon Thawing	2
1.2.2	Cold Denaturation.....	2
1.2.3	Denaturation at the Ice-Liquid Interface.....	3
1.2.4	Crystallisation and pH Shifts	3
1.2.5	Additional Stresses.....	4
1.3	Process Optimisation and Storage	4
1.4	Scale-Down Devices.....	5
1.4.1	Approaches to Scale-Down Freezing and Thawing.....	6
1.4.2	Computational Fluid Dynamic Simulations.....	6
1.4.3	2 L Scale-Down Device	6
1.4.4	Micro Scale-Down Device.....	7
	References.....	8
	Aim and Outline of the Thesis	12
Chapter 2	Cryoconcentration and 3D Temperature Profiles during Freezing of mAb Solutions in Large-Scale PET Bottles and a Novel Scale-Down Device	14
2.1	Abstract	15
2.2	Introduction.....	16
2.3	Materials and Methods.....	18
2.3.1	Materials	18
2.3.2	Development of a Scale-Down Device Assisted by Computational Fluid Dynamics	18
2.3.3	Design of the Scale-Down Device.....	20
2.3.4	Preparation of Protein Samples.....	20

Table of Contents

2.3.5	Temperature Mapping During Freezing	21
2.3.6	Analysis of Cryoconcentration	22
2.3.7	Viscosity Measurements	22
2.4	Results and Discussion	23
2.4.1	Matching Thermal History Between a 2 L Bottle and the Scale-Down Container.....	23
2.4.2	Comparison of 3D Temperature Profiles During Freezing.....	24
2.4.3	Comparison of Cryoconcentration.....	27
2.4.4	Influence of Initial mAb Concentration on Cryoconcentration.....	30
2.4.4.1	Concentration-Dependent and Temperature-Dependent Viscosity Measurements	31
2.4.4.2	Effect of mAb Concentration on Cryoconcentration.....	31
2.5	Conclusion	34
	Acknowledgements.....	35
	References.....	36
Chapter 3	Scaling Down Large-Scale Thawing of mAb Solutions – 3D Temperature Profiles, Changes in Concentration, and Density Gradients.....	39
3.1	Abstract.....	40
3.2	Introduction.....	41
3.3	Materials and Methods.....	43
3.3.1	Materials	43
3.3.2	Scale-Down Device	44
3.3.3	Preparation of Protein Samples.....	44
3.3.4	Temperature Mapping during Thawing.....	45
3.3.5	Analysis of Concentration Gradients after Thawing	45
3.3.5.1	Quantification of mAb and Histidine.....	45
3.3.5.2	Quantification of PS80.....	46

Table of Contents

3.3.6	Diffusion of Solution Components after Thawing.....	47
3.3.7	Analysis of Density Gradients	47
3.4	Results and Discussion	48
3.4.1	Comparison of 3D Temperature Profiles during Thawing	48
3.4.2	Comparison of Concentration Gradients after Thawing.....	51
3.4.3	Comparison of Density Gradients after Thawing	57
3.4.4	Perspective	58
3.5	Conclusion	59
	Acknowledgements.....	59
	References.....	60
Chapter 4	The Effect of mAb and Excipient Cryoconcentration on Long-Term Frozen Storage Stability – Part 1: Higher Molecular Weight Species and Subvisible Particle Formation	63
4.1	Abstract.....	64
4.2	Introduction.....	65
4.3	Materials and Methods.....	67
4.3.1	Materials	67
4.3.2	Sample Preparation	68
4.3.3	Stability Analysis	68
4.3.3.1	Flow Imaging Microscopy.....	68
4.3.3.2	Size-Exclusion Chromatography	69
4.3.4	Determination of T_g'	69
4.4	Results.....	70
4.4.1	Long-Term Storage at -80 °C	70
4.4.2	Long-Term Storage at -20 °C	71
4.4.3	Long-Term Storage at -10 °C	72
4.4.4	Determination of T_g'	74

Table of Contents

4.5	Discussion.....	75
4.6	Conclusion.....	79
	Acknowledgements.....	80
	References.....	81
Chapter 5	The Effect of mAb and Excipient Cryoconcentration on Long-Term Frozen Storage Stability – Part 2: Aggregate Formation and Oxidation.....	84
5.1	Abstract.....	85
5.2	Introduction.....	86
5.3	Materials and Methods.....	88
5.3.1	Materials.....	88
5.3.2	Sample Preparation.....	88
5.3.3	Stability Analysis.....	89
5.3.3.1	Flow Imaging Microscopy.....	90
5.3.3.2	Size-Exclusion Chromatography.....	90
5.3.3.3	Optical Density at 350 nm.....	90
5.3.3.4	Protein A Analytical Chromatography.....	90
5.3.4	Determination of the Interaction Parameter k_D	91
5.4	Results.....	91
5.4.1	Formation of HMWS.....	92
5.4.2	Formation of Subvisible Particles.....	94
5.4.3	Optical Density at 350 nm.....	95
5.4.4	MAb Oxidation.....	96
5.4.5	Interaction Parameter k_D	98
5.5	Discussion.....	98
5.6	Conclusion.....	101
	Acknowledgements.....	102

Table of Contents

References.....	103
Chapter 6 Evaluation of Two Novel Scale-Down Devices for Testing mAb Aggregation during Large-Scale Freezing.....	106
6.1 Abstract.....	107
6.2 Introduction.....	109
6.3 Materials and Methods.....	111
6.3.1 Materials	111
6.3.2 Preparation of Protein Samples.....	112
6.3.3 SDD and mSDD.....	112
6.3.4 Freezing and Thawing.....	113
6.3.5 Stability Analysis	113
6.3.5.1 Flow Imaging Microscopy.....	113
6.3.5.2 Size-Exclusion Chromatography	114
6.3.5.3 Dynamic Light Scattering.....	114
6.3.5.4 Optical Density at 350 nm	114
6.3.6 Temperature Mapping in the mSDD.....	114
6.4 Results and Discussion	115
6.4.1 MAb Aggregation in the 2 L Bottle, 125 mL Bottle, and the SDD.....	115
6.4.2 MAb Aggregation in 10 mL Vials and the mSDD	121
6.5 Conclusion	125
Acknowledgements.....	125
References.....	126
Chapter 7 Computational Fluid Dynamic Simulations of Temperature, Cryoconcentration, and Local Stress during Large-Scale Freezing and Thawing of mAb Solutions	129
7.1 Abstract.....	130
7.2 Introduction.....	131

Table of Contents

7.3	Materials and Methods.....	131
7.3.1	Materials	131
7.3.2	Temperature Mapping during Freezing and Thawing	131
7.3.3	Analysis of Changes in Concentration.....	132
7.3.4	Computational Fluid Dynamics Modeling.....	133
7.4	Results and Discussion	134
7.4.1	Comparison of Temperature Profiles during Freezing	134
7.4.2	Comparison of Cryoconcentration.....	136
7.4.3	Comparison of Temperature Profiles during Thawing	137
7.4.4	Comparison of Concentration Gradients upon Thawing	138
7.4.5	Additional Parameters Derived from the CFD Simulations	139
7.5	Conclusion	141
	References.....	142
Chapter 8	Summary	143

Chapter 1 General Introduction

1.1 Freezing and Thawing of Monoclonal Antibody Solutions

Therapeutic proteins, especially monoclonal antibodies (mAbs), are essential in the treatment of severe diseases and part of a growing market (1–3). During production, mAb bulk drug substance is commonly frozen and subsequently thawed (4–7). Thereby, physical and chemical degradation reactions are inhibited or sufficiently slowed down, microbial growth minimised, and ultimately shelf life increased (4,5). Additionally, flexibility is gained during biopharmaceutical manufacturing by decoupling drug substance and drug product processing (5,8,9). Frozen transportation, in comparison to liquid, reduces the risk of agitation, foaming, and shaking (10). These numerous advantages over liquid storage might be outbalanced by a variety of possible detrimental effects that are associated with freezing and thawing of mAb solutions (Figure 1) as well as by economic considerations.

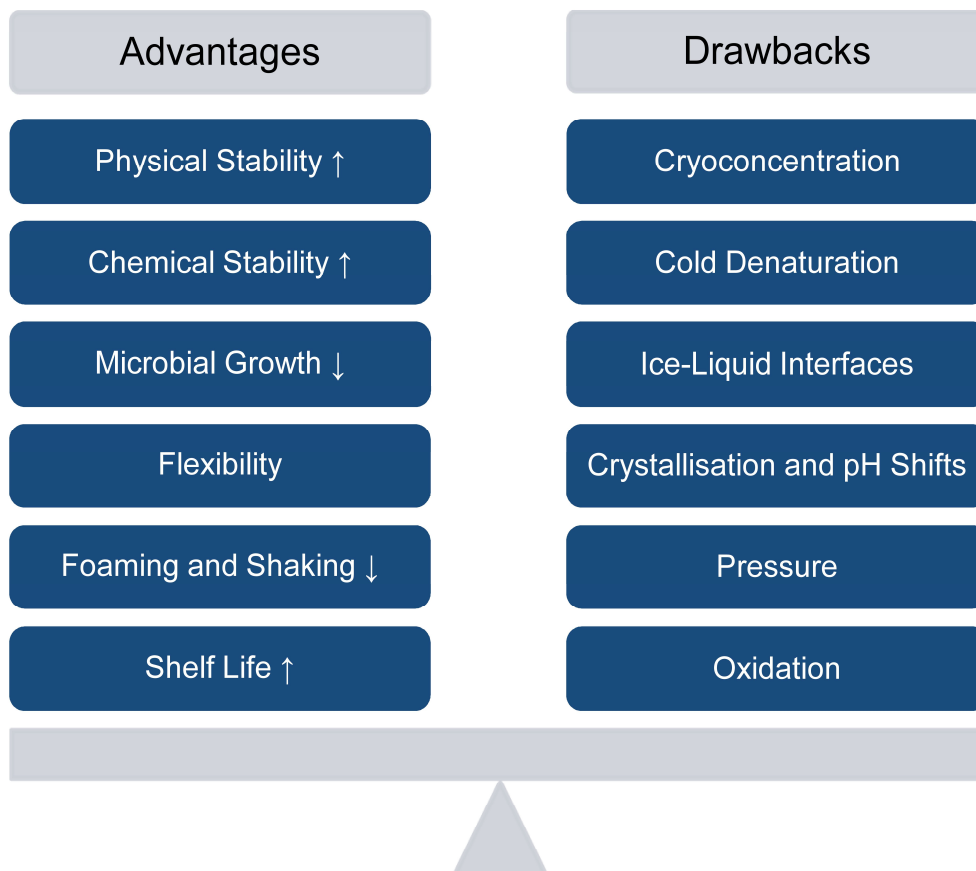


Figure 1 Possible positive and negative effects associated with freezing and thawing of mAb solutions.

1.2 Stresses During Freezing and Thawing

1.2.1 Cryoconcentration Upon Freezing and Concentration Gradients Upon Thawing

Changes in concentration upon freezing (7,11–13), referred to as cryoconcentration, and concentration gradients upon thawing (3,10) can have a negative impact on mAb stability. On a microscopic scale, growing ice crystals exclude proteins and excipients during freezing (9,14–16). In between these ice crystals the solutes' concentration increases and a freeze-concentrated matrix (FCM) is formed. The composition of the FCM is characterised by phase or state diagrams (17–19). Macroscopically, the mAb and excipients are transported into unfrozen regions by natural convection and diffusion (5,6,16). This leads to a spatial heterogeneity within the frozen bulk. Thus, some regions consist mostly of ice crystals, while others contain large patches of cryoconcentrated mAb solution (19). Both, the microscopic and macroscopic composition differ throughout the bulk and are influenced by diffusivity (7,18,20). During thawing, the FCM melts out of the ice and a concentration gradient develops (3,10,21). Ice that consists mainly of water dilutes the top region, whereas the highly concentrated FCM sinks to the bottom due to its higher density (10). Cryoconcentration upon freezing as well as concentration gradients after thawing are associated with mAb aggregation (3,12,16). By increasing cooling and heating rates, cryoconcentration and concentration gradients can be effectively reduced (5,9,18).

1.2.2 Cold Denaturation

Unfolding of proteins at high temperatures upon heating is a well-known phenomenon. Intuitively, storage at low temperatures is associated with decelerated reaction kinetics and an increase in storage stability. However, the impact of low temperatures on stability behaves counter-intuitive (22). The Gibbs free energy of unfolding ΔG as a function of temperature is an arched curve (9,22,23). Consequently, two unfolding transition points are observed, the melting temperature T_m and the cold denaturation temperature T_c (22,23). When these temperatures are passed, unfolding of proteins is thermodynamically favoured. The phenomenon of protein unfolding due to low temperatures is referred to as cold denaturation (1,2,6,22–24). Because of the inference with ice at temperatures below the freezing temperature, cold denaturation is not easily experimentally accessible. Recently, studies using proteins with a cold denaturation temperature above freezing temperature proved to be a promising strategy (22). Another approach is to prevent the formation of ice

through isochoric cooling using a special device (23,24). Thereby, the effect of storage temperature as well as excipients on protein aggregation as a result of cold denaturation has been evaluated. Molecular dynamic simulation demonstrated that the presence of ice negatively affects cold denaturation (1,2). In the vicinity of ice, water molecules are slowed down. Thus, hydrogen bonds with the protein, especially with the nonpolar patches in the protein core, facilitate unfolding (1).

1.2.3 Denaturation at the Ice-Liquid Interface

An additional possibly detrimental effect is denaturation at the interface between ice and the FCM (1,13,25). Although extensively studied, the mechanism of adsorption and denaturation is not completely understood (1). Direct adsorption to the interface (26), a pH shift and a lack of stabilisers in the vicinity of the ice surface (27), accumulation of air bubbles (17), pressure-induced unfolding (17,27), as well as enhanced cold denaturation (2) are discussed. While faster freezing reduces cryoconcentration, it leads to a higher number of smaller ice crystals (1,6,12,25). Consequently, faster freezing correlates with a larger interfacial area and the net effect on mAb stability cannot be generalised. In contrast, faster thawing reduces the exposure time of mAbs to interfaces and inhibits Ostwald ripening; thereby, additional interfaces during thawing can be prevented (6).

1.2.4 Crystallisation and pH Shifts

Due to cryoconcentration, excipients might exceed their solubility limit and salts or stabilisers crystallise (6,9,28–31). Studies revealed that crystallisation of the cryoprotectant trehalose during frozen storage significantly affects mAb stability (28,30). Crystallisation deprives the mAb of the cryoprotectant, but at the same time trehalose crystals introduce another denaturing surface (28,30). During thawing, crystallisable excipients in a metastable state might recrystallise and cause additional stress (6,9).

However, not only the crystallisation of cryoprotectants directly impacts mAb stability. Crystallisation of buffer salts can result in significant pH shifts potentially creating an unfavourable environment that facilitates mAb aggregation (6,8,32). The most prominent example is the shift in pH of sodium phosphate buffers. Eutectic crystallisation of disodium phosphate during freezing can lead to a shift in pH from pH 7 to approximately pH 4 (6,8,32). Even without exceeding the solubility limit of a buffer salt, the temperature dependence of the pK_a can cause a pH shift but typically by less than 1 pH unit (8). Upon thawing a slight hysteresis is observed, most likely due to cryoconcentration and increased

buffer strength (8). It has been shown that the protein itself can effectively suppress crystallisation and thereby sufficiently high mAb concentrations can have a self-stabilising effect (31,33). In addition, highly concentrated mAb solutions possess a high self-buffering capacity and thereby attenuate pH shifts (34).

1.2.5 Additional Stresses

In addition to these extensively studied stresses, recently mechanical stress, local pressure, and oxidation have been proposed as additional possibly detrimental factors (17). The volume expansion during ice formation leads to a significant increase in pressure. This could result in pressure-induced mAb destabilisation (17). A theoretical pressure exceeding 2 kBar has been estimated (1,17). A high-pressure form of ice that was detected in frozen protein solutions via high-resolution synchrotron X-ray diffraction underlines this theory (27). When liquid regions in a container are enclosed by ice, the pressure in the container can reach 10 bar leading to deformation or breakage of the container. This outcome is influenced by the direction of ice growth during freezing (17).

Furthermore, oxidation could be relevant during frozen storage (17,35). The solubility of oxygen increases during cooling. An increase of the oxygen concentration in aqueous solution by a factor of three when lowering the temperature from 25 °C to -20 °C has been stated (17). Additionally, dissolved gases cryoconcentrate upon freezing. When the solubility limit of gases is reached, predominantly oxygen and nitrogen form gas bubbles. This does not only introduce additional surfaces, but might facilitate mAb oxidation (17). The cryoconcentration of excipients further reduces the solubility of gases and enhances gas bubble formation.

1.3 Process Optimisation and Storage

All these stresses must be considered when optimising freezing and thawing processes. The parameter that can be directly adapted is the rate. It should be noted that in literature no general definition of the terms *slow* and *fast* can be found and the rates that are mentioned in that context vary tremendously (6). Often processing rates that are considered as slow in small-scale studies cannot be achieved in large-scale setups. However, some general assumptions apply to the processing rate. Faster cooling and heating reduces cryoconcentration upon freezing and concentration gradients upon thawing, respectively (5,9,18). Concurrently, the exposure time to critical effects is reduced (6). Thus, thawing should generally be as fast as possible (6,9). However, the multiple effects during freezing

are more complex and no general recommendation for ideal cooling rates can be established. Although faster freezing prevents cryoconcentration, it also results in smaller crystals and larger interfacial area. Hence, the ideal setup must be evaluated on a case-by-case basis.

In respect of the ideal frozen storage temperature, the glass transition temperature of the maximally freeze-concentrated solution (T_g') is a key parameter (8,36). A glassy state, described as a solid solution of cryoconcentrated solutes and unfrozen, amorphous water, is formed below T_g' (37). The viscosity of this vitrified FCM is in the order of 10^{14} Pas and molecular mobility reduced to mm/year (38,39). During heating the viscosity drops when T_g' is passed (40). Above T_g' , the viscosity decreases exponentially with increasing temperature (41). This reduction in viscosity allows increased molecular mobility and eventually facilitates aggregation (39,40). In addition, crystallisation of excipients is much more likely to occur upon storage above T_g' (28,30). Crystallisation of trehalose was most detrimental on mAb stability, when samples were stored only slightly above T_g' (29). Storage at a temperature significantly above T_g' reduced the negative impact of trehalose crystallisation, potentially due to a higher molecular mobility, which allows mAb refolding and re-established interactions with amorphous trehalose (28,30). Storage below T_g' effectively prevents aggregation and is therefore generally considered as the ideal storage condition (18,28,29).

1.4 Scale-Down Devices

A variety of containers along with various freezer configurations are available for processing mAb bulk solutions. The combination of plastic bottles with static air storage rooms or freezers/thawers with forced air convection is widely applied (42). It is self-evident that the use of disposable large-scale bottles comes with different challenges than freezing and thawing in disposable plastic bags or reusable stainless-steel jacketed tanks. Another level of complexity is added as bottles differ in geometry, size, and material. Nonetheless, no device to scale down freezing and thawing in large-scale bottles is currently commercially marketed. Ideally, such a scale-down device (SDD) preserves the characteristics of large-scale freezing and thawing, displays the same level of the numerous possible stresses, but requires only a fraction of the material.

1.4.1 Approaches to Scale-Down Freezing and Thawing

Typically, small-scale studies in vials or tubes are used to optimise the freezing and the thawing process as well as the mAb formulation or to unveil aggregation mechanisms (5,8,28,30,32,33,43,44). Although such studies support a better understanding of freezing and thawing, they do not reflect realistic large-scale scenarios. The exposure time of the protein to numerous stresses, cryoconcentration, processing rates, and the interface between ice and the FCM are not transferable (18,19,45,46). Other approaches manipulate cooling and heating so that small containers match temperature-time profiles observed during large-scale processing (46,47). However, by adapting cooling and heating rates, critical phenomena, e.g. natural convection or nucleation, differ between both scales (5,46,48). Computational Fluid Dynamics (CFD) simulations of freezing and thawing of mAb solutions can help to overcome this limitation and to develop more rational SDDs (46,48).

1.4.2 Computational Fluid Dynamic Simulations

Following this approach, SmartFreeZ developed two devices to mimic freezing and thawing in large-scale 2 L PharmaTainer™ bottles – the SDD and the micro SDD (mSDD). CFD simulations can be used to divide the large-scale bulk into control volumes of approximately 1 mm³. For each control volume the time to go from ice nucleation to glass transition can be calculated and transferred into a cumulative thermal history of the bulk. This period can be considered as most detrimental. After the formation of ice, proteins are exposed to the interface between ice and the FCM, the high excipient concentrations in the FCM, and cold denaturation. Below T_g' , the contribution of these stresses to protein destabilisation are drastically reduced and therefore neglected (18,28,29). By adapting heat exchange in 125 mL PharmaTainer™ bottles or 10 mL PharmaTainer™ stability vials, an equivalent thermal history as in the large-scale 2 L bottle can be reached with significantly less fill volume.

1.4.3 2 L Scale-Down Device

Length and width of a 125 mL bottle is roughly half the distance of the 2 L bottle. By insulating two walls of the 125 mL bottle with a specially designed cover (Figure 2), cooling and heating rates can effectively be manipulated. Thereby, matching thermal histories between the SDD and the 2 L bottle are generated. This approach has the advantage that the SDD can be processed simultaneously to the large-scale bottle. Thus,

the SDD allows a generic application regardless of the freezing and thawing device that is used.

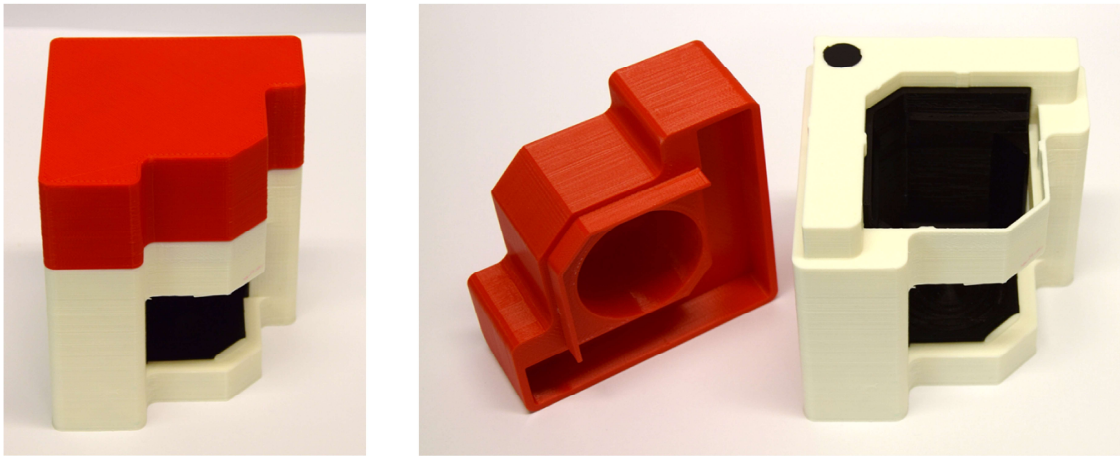


Figure 2 SDD by SmartFreeZ.

1.4.4 Micro Scale-Down Device

The material that is needed to mimic large-scale freezing and thawing behaviour in a 2 L bottle was further reduced by SmartFreeZ in a novel mSDD (Figure 3). The mSDD operates with vials instead of bottles. Nonetheless, the same CFD based approach that was realised in the SDD was applied to generate matching thermal histories. The significantly lower volume and different geometries do not allow to adapt cooling and heating rates by insulating the vials. Instead, heat exchange is controlled from the bottom through a stainless-steel plate. To assure comparability between different vials and runs, the vials are controlled nucleated at the beginning of a run.

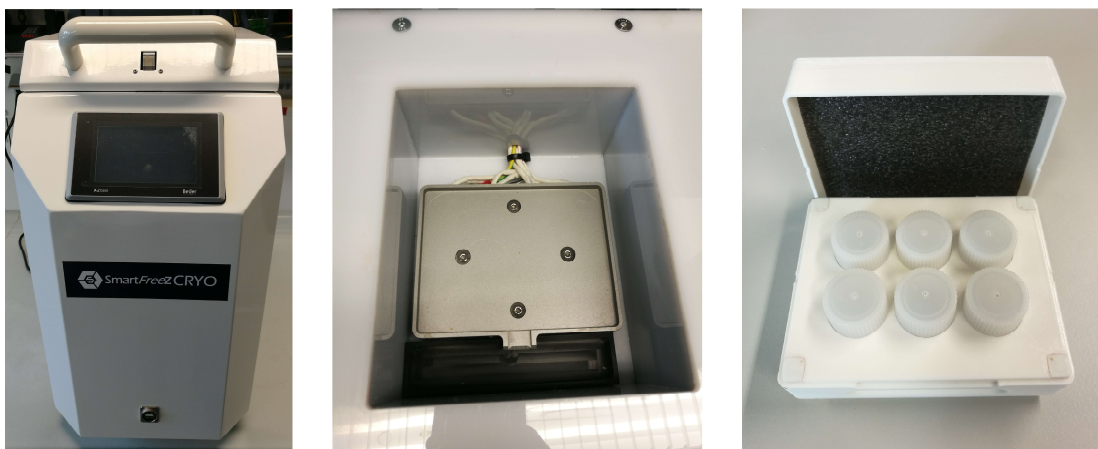


Figure 3 mSDD by SmartFreeZ.

References

1. Arsiccio A, Pisano R. The Ice-Water Interface and Protein Stability: A Review. *J Pharm Sci.* 2020 Jul;109(7):2116–30.
2. Arsiccio A, McCarty J, Pisano R, Shea J-E. Heightened Cold-Denaturation of Proteins at the Ice–Water Interface. *J Am Chem Soc.* 2020 Mar 25;142(12):5722–30.
3. Mehta SB, Subramanian S, D’Mello R, Brisbane C, Roy S. Effect of protein cryoconcentration and processing conditions on kinetics of dimer formation for a monoclonal antibody: A case study on bioprocessing. *Biotechnol Prog.* 2019 Jul 15;35(4):1–7.
4. Padala C, Jameel F, Rathore N, Gupta K, Sethuraman A. Impact of Uncontrolled vs Controlled Rate Freeze-Thaw Technologies on Process Performance and Product Quality. *PDA J Pharm Sci Technol.* 2010;64(4):290–8.
5. Rodrigues MA, Miller MA, Glass MA, Singh SK, Johnston KP. Effect of Freezing Rate and Dendritic Ice Formation on Concentration Profiles of Proteins Frozen in Cylindrical Vessels. *J Pharm Sci.* 2011 Apr;100(4):1316–29.
6. Singh SK, Kolhe P, Wang W, Nema S. Large-Scale Freezing of Biologics A Practitioner’s Review, Part One: Fundamental Aspects. *Bioprocess Int.* 2009;7(9):32–44.
7. Kolhe P, Mehta AP, Lary AL, Chico SC, Singh SK. Large-Scale Freezing of Biologics (Part III). *BioPharm Int.* 2012;25(October):40–8.
8. Kolhe P, Amend E, K. Singh S. Impact of freezing on pH of buffered solutions and consequences for monoclonal antibody aggregation. *Biotechnol Prog.* 2009 Dec 28;26(3):727–33.
9. Rathore N, Rajan RS. Current Perspectives on Stability of Protein Drug Products during Formulation, Fill and Finish Operations. *Biotechnol Prog.* 2008 Jun 6;24(3):504–14.
10. Kolhe P, Badkar A. Protein and solute distribution in drug substance containers during frozen storage and post-thawing: A tool to understand and define freezing-thawing parameters in biotechnology process development. *Biotechnol Prog.* 2011 Mar;27(2):494–504.
11. Roessl U, Leitgeb S, Nidetzky B. Protein freeze concentration and micro-segregation analysed in a temperature-controlled freeze container. *Biotechnol Reports.* 2015 Jun;6:108–11.
12. Hauptmann A, Hoelzl G, Loerting T. Distribution of Protein Content and Number of Aggregates in Monoclonal Antibody Formulation After Large-Scale Freezing. *AAPS PharmSciTech.* 2019 Feb 10;20(2):72.
13. Duarte A, Rego P, Ferreira A, Dias P, Geraldés V, Rodrigues MA. Interfacial Stress and Container Failure During Freezing of Bulk Protein Solutions Can Be Prevented by Local Heating. *AAPS PharmSciTech.* 2020 Oct 1;21(7):251.

14. Bhatnagar BS, Pikal MJ, Bogner RH. Study of the Individual Contributions of Ice Formation and Freeze-Concentration on Isothermal Stability of Lactate Dehydrogenase during Freezing. *J Pharm Sci.* 2008 Feb;97(2):798–814.
15. Webb SD, Webb JN, Hughes TG, Sesin DF, Kincaid AC. Freezing Biopharmaceuticals Using Common Techniques — and the Magnitude of Bulk-Scale Freeze-Concentration. *BioPharm.* 2002;15(5):22–34.
16. Minatovicz B, Sun L, Foran C, Chaudhuri B, Tang C (Xiaolin), Shameem M. Freeze-concentration of solutes during bulk freezing and its impact on protein stability. *J Drug Deliv Sci Technol.* 2020 Aug;58(April):101703.
17. Authelin J-R, Rodrigues MA, Tchessalov S, Singh SK, McCoy T, Wang S, et al. Freezing of Biologicals Revisited: Scale, Stability, Excipients, and Degradation Stresses. *J Pharm Sci.* 2020 Jan;109(1):44–61.
18. Miller MA, Rodrigues MA, Glass MA, Singh SK, Johnston KP, Maynard JA. Frozen-State Storage Stability of a Monoclonal Antibody: Aggregation is Impacted by Freezing Rate and Solute Distribution. *J Pharm Sci.* 2013 Apr;102(4):1194–208.
19. Rodrigues MA, Balzan G, Rosa M, Gomes D, de Azevedo EG, Singh SK, et al. The importance of heat flow direction for reproducible and homogeneous freezing of bulk protein solutions. *Biotechnol Prog.* 2013 Sep;29(5):1212–21.
20. Bluemel O, Buecheler JW, Rodrigues MA, Geraldes V, Hoelzl G, Bechtold-Peters K, et al. Cryoconcentration and 3D Temperature Profiles During Freezing of mAb Solutions in Large-Scale PET Bottles and a Novel Scale-Down Device. *Pharm Res.* 2020 Sep 30;37(9):179.
21. Maity H, Karkaria C, Davagnino J. Mapping of solution components, pH changes, protein stability and the elimination of protein precipitation during freeze–thawing of fibroblast growth factor 20. *Int J Pharm.* 2009 Aug;378(1–2):122–35.
22. Sanfelice D, Temussi PA. Cold denaturation as a tool to measure protein stability. *Biophys Chem.* 2016 Jan;208:4–8.
23. Rosa M, Lopes C, Melo EP, Singh SK, Geraldes V, Rodrigues MA. Measuring and Modeling Hemoglobin Aggregation below the Freezing Temperature. *J Phys Chem B.* 2013 Aug 18;117(30):8939–46.
24. Correia C, Tavares E, Lopes C, Silva JG, Duarte A, Geraldes V, et al. Stability of Protein Formulations at Subzero Temperatures by Isochoric Cooling. *J Pharm Sci.* 2020 Jan;109(1):316–22.
25. Cao E, Chen Y, Cui Z, Foster PR. Effect of freezing and thawing rates on denaturation of proteins in aqueous solutions. *Biotechnol Bioeng.* 2003 Jun 20;82(6):684–90.
26. Strambini GB, Gabellieri E. Proteins in frozen solutions: evidence of ice-induced partial unfolding. *Biophys J.* 1996 Feb 1;70(2):971–6.
27. Bhatnagar B, Zakharov B, Fisyuk A, Wen X, Karim F, Lee K, et al. Protein/Ice Interaction: High-Resolution Synchrotron X-ray Diffraction Differentiates Pharmaceutical Proteins from Lysozyme. *J Phys Chem B.* 2019 Jul 11;123(27):5690–9.

28. Connolly BD, Le L, Patapoff TW, Cromwell MEM, Moore JMR, Lam P. Protein Aggregation in Frozen Trehalose Formulations: Effects of Composition, Cooling Rate, and Storage Temperature. *J Pharm Sci.* 2015 Dec;104(12):4170–84.
29. Singh SK, Kolhe P, Mehta AP, Chico SC, Lary AL, Huang M. Frozen State Storage Instability of a Monoclonal Antibody: Aggregation as a Consequence of Trehalose Crystallization and Protein Unfolding. *Pharm Res.* 2011 Apr 7;28(4):873–85.
30. Hauptmann A, Podgoršek K, Kuzman D, Srčić S, Hoelzl G, Loerting T. Impact of Buffer, Protein Concentration and Sucrose Addition on the Aggregation and Particle Formation during Freezing and Thawing. *Pharm Res.* 2018 May 19;35(5):101.
31. Piedmonte DM, Hair A, Baker P, Brych L, Nagapudi K, Lin H, et al. Sorbitol Crystallization-Induced Aggregation in Frozen mAb Formulations. *J Pharm Sci.* 2015 Feb;104(2):686–97.
32. Pikal-Cleland KA, Rodríguez-Hornedo N, Amidon GL, Carpenter JF. Protein Denaturation during Freezing and Thawing in Phosphate Buffer Systems: Monomeric and Tetrameric β -Galactosidase. *Arch Biochem Biophys.* 2000 Dec;384(2):398–406.
33. Thorat AA, Munjal B, Geders TW, Suryanarayanan R. Freezing-induced protein aggregation - Role of pH shift and potential mitigation strategies. *J Control Release.* 2020 Jul;323(April):591–9.
34. Gokarn YR, Kras E, Nodgaard C, Dharmavaram V, Fesinmeyer RM, Hultgen H, et al. Self-Buffering Antibody Formulations. *J Pharm Sci [Internet].* 2008 Aug 1 [cited 2021 Jun 8];97(8):3051–66. Available from: <https://linkinghub.elsevier.com/retrieve/pii/S0022354916326430>
35. Takenaka N, Ueda A, Daimon T, Bandow H, Dohmaru T, Maeda Y. Acceleration Mechanism of Chemical Reaction by Freezing: The Reaction of Nitrous Acid with Dissolved Oxygen. *J Phys Chem.* 1996 Jan;100(32):13874–84.
36. Alhalaweh A, Alzghoul A, Mahlin D, Bergström CAS. Physical stability of drugs after storage above and below the glass transition temperature: Relationship to glass-forming ability. *Int J Pharm.* 2015 Nov;495(1):312–7.
37. Lim M, Wu H, Breckell M, Birch J. Influence of the glass transition and storage temperature of frozen peas on the loss of quality attributes. *Int J Food Sci Technol.* 2006 May;41(5):507–12.
38. Kasper JC, Friess W. The freezing step in lyophilization: Physico-chemical fundamentals, freezing methods and consequences on process performance and quality attributes of biopharmaceuticals. *Eur J Pharm Biopharm.* 2011 Jun;78(2):248–63.
39. Pansare SK, Patel SM. Practical Considerations for Determination of Glass Transition Temperature of a Maximally Freeze Concentrated Solution. *AAPS PharmSciTech.* 2016 Aug 18;17(4):805–19.
40. Franks F. Freeze-drying of bioproducts: Putting principles into practice. *Eur J Pharm Biopharm.* 1998;45(3):221–9.
41. Seifert I, Friess W. Freeze concentration during freezing: How does the maximally freeze concentrated solution influence protein stability? *Int J Pharm.* 2020 Nov;589(June):119810.

42. Singh SK, Kolhe P, Wang W, Nema S. Large-Scale Freezing of Biologics: A Practitioner's Review, Part 2: Practical Advice. *Bioprocess Int.* 2009;7(10):34–42.
43. Kuelto LA, Wang W e. i., Randolph TW, Carpenter JF. Effects of Solution Conditions, Processing Parameters, and Container Materials on Aggregation of a Monoclonal Antibody during Freeze-Thawing. *J Pharm Sci.* 2008 May;97(5):1801–12.
44. Zhang A, Singh SK, Shirts MR, Kumar S, Fernandez EJ. Distinct Aggregation Mechanisms of Monoclonal Antibody Under Thermal and Freeze-Thaw Stresses Revealed by Hydrogen Exchange. *Pharm Res.* 2012 Jan 30;29(1):236–50.
45. Shamlou PA, Breen LH, Bell W V., Pollo M, Thomas BA. A new scalable freeze–thaw technology for bulk protein solutions. *Biotechnol Appl Biochem.* 2007 Jan 1;46(1):13.
46. Geraldés V, Gomes DC, Rego P, Fegley D, Rodrigues MA. A New Perspective on Scale-Down Strategies for Freezing of Biopharmaceuticals by Means of Computational Fluid Dynamics. *J Pharm Sci.* 2020 Jun;109(6):1978–89.
47. Rayfield WJ, Kandula S, Khan H, Tugcu N. Impact of Freeze/Thaw Process on Drug Substance Storage of Therapeutics. *J Pharm Sci.* 2017 Aug;106(8):1944–51.
48. Roessl U, Jajcevic D, Leitgeb S, Khinast JG, Nidetzky B. Characterization of a Laboratory-Scale Container for Freezing Protein Solutions with Detailed Evaluation of a Freezing Process Simulation. *J Pharm Sci.* 2014 Feb;103(2):417–26.

Aim and Outline of the Thesis

Monoclonal antibodies (mAbs) play an important role in the treatment of severe diseases. During large-scale production, bulk drug substance is regularly frozen and subsequently thawed to increase stability and shelf life. However, a variety of possible drawbacks, e.g. cryoconcentration, interface effects between ice and the freeze-concentrated matrix (FCM), and oxidation, need to be considered. Therefore, a deeper understanding of freezing and thawing and possible limitations is essential to improve the process and to optimise storage. Though small-scale experiments might help to gain a general understanding, they do not reflect realistic large-scale conditions. Thus, ideally large-scale experiments would be performed to rationally characterise mAb stability. Nevertheless, particularly during early-stage development, material for process optimisation and stability studies is limited. Hence, scale-down devices (SDD) that preserve the characteristics of large-scale freezing and thawing but require only a fraction of the material are needed. Computational Fluid Dynamics (CFD) simulations can be used to develop such SDDs.

This thesis shall give insights into the characterisation of a novel SDD that was designed to mimic freezing and thawing in large-scale rectangular bottles. Therefore, the freezing and the thawing process and associated stability affecting phenomena were analysed and compared to large-scale bottles. To underline the impact of the SDD, results were compared to a small-scale bottle. Furthermore, we evaluated the effect cryoconcentration, which comes with a shift in mAb to buffer ratio, can have on long-term frozen storage stability above and below the glass transition temperature of the maximally freeze-concentrated solution (T_g').

In **Chapter 2**, the SDD is characterised in respect of freezing. Therefore, 3D temperature profiles and cryoconcentration of a mAb and the buffer histidine in the SDD are compared to a large-scale 2 L bottle and a small-scale 125 mL bottle. Furthermore, the effect of the initial mAb concentration on freeze-concentration is addressed.

In **Chapter 3**, the performance of the SDD during thawing is assessed. 3D temperature profiles and concentration gradients of mAb, the buffer histidine, and the surfactant polysorbate 80 after thawing are compared to the 125 mL and the 2 L bottle. The density gradient that builds up during and after thawing is quantified.

Chapter 4 describes the impact cryoconcentration, associated with shifts in mAb to histidine ratio, has on long-term frozen storage stability. Samples are stored up to

12 months at -80 °C, -20 °C, and -10 °C and soluble as well as insoluble aggregate levels are analysed. An optimised sample preparation is established to determine T_g' of protein samples that do not contain glass formers via differential scanning calorimetry.

In **Chapter 5**, the aim is to generate a general understanding of the impact small changes in mAb and buffer concentration due to cryoconcentration have on long-term frozen storage. A second mAb is included in the study and aggregation as well as oxidation are assessed after six-month storage at -10 °C. The impact of the ionic strength on protein-protein interactions is evaluated via the interaction parameter k_D .

In **Chapter 6**, mAb aggregation upon repeated freeze-thaw cycles in the SDD is compared to the 2 L and the 125 mL bottle. Soluble and insoluble aggregation after up to five freezing and thawing cycles of three different mAb formulations are determined. In addition, the predictive power of a novel micro-scale down device for large-scale freezing and thawing stress, which further reduces the material needs, is evaluated.

Chapter 7 compares the experimental findings to results obtained by optimised CFD simulations.

Chapter 8 is the summary and conclusion of this thesis.

Chapter 2 Cryoconcentration and 3D Temperature Profiles during Freezing of mAb Solutions in Large-Scale PET Bottles and a Novel Scale-Down Device

This chapter is published as:

Oliver Bluemel¹, Jakob W. Buecheler², Miguel A. Rodrigues³, Vitor Geraldes⁴, Georg Hoelzl⁵, Karoline Bechtold-Peters², Wolfgang Friess¹

Cryoconcentration and 3D Temperature Profiles during Freezing of mAb Solutions in Large-Scale PET Bottles and a Novel Scale-Down Device

In *Pharmaceutical Research*, 2020, 37:179

1 Pharmaceutical Technology and Biopharmaceutics, Department of Pharmacy, Ludwig-Maximilians-Universitaet Muenchen, 81377 Munich, Germany

2 Technical Research and Development, Novartis Pharma AG, 4002 Basel, Switzerland

3 Centro de Química Estrutural, Department of Chemical Engineering, Instituto Superior Técnico, Lisboa 1049-001, Portugal

4 CeFEMA, Department of Chemical Engineering, Instituto Superior Técnico, Lisboa 1049-001, Portugal

5 Sandoz GmbH, 6336 Langkampfen, Austria

Note from the authors:

The version included in this thesis is identical with the published article apart from minor changes.

The published article can be assessed online via:

<https://doi.org/10.1007/s11095-020-02886-w>

Author contributions:

O.B., W.F., and K.B.P. conceived the study. J.W.B. and G.H. provided guidance on the methodology of the cryoconcentration analysis. M.A.R. and V.G. developed the scale-down device. O.B. performed the experiments and evaluated the data. O.B. and M.A.R. wrote the paper. W.F., J.W.B., K.B.P., and G.H. contributed to the discussion of the results and revised the manuscript. W.F. and K.B.P. supervised the work.

2.1 Abstract

Purpose: Small-scale models that simulate large-scale freezing of bulk drug substance of biopharmaceuticals are highly needed to define freezing and formulation parameters based on process understanding. We evaluated a novel scale-down device (SDD), which is based on a specially designed insulation cover, with respect to changes in concentration after freezing, referred to as cryoconcentration, and 3D temperature profiles. Furthermore, the effect of the initial monoclonal antibody (mAb) concentration on cryoconcentration was addressed.

Methods: 2 L and 125 mL bottles were utilised. Temperatures were mapped using type T thermocouples. Frozen blocks were cut and mAb and histidine concentrations were analysed by HPLC. In addition, concentration- and temperature-dependent viscosities were measured.

Results: 3D freezing profiles in the SDD were comparable to large-scale bottles. The SDD accurately predicted cryoconcentration of both mAb and histidine of large-scale freezing. Concentric changes in concentration were evident as well as an unforeseen diluted core at the last point to freeze. At low initial mAb concentration cryoconcentration was substantial, while high initial mAb concentration suppressed cryoconcentration almost completely.

Conclusion: The novel SDD gives detailed insights into large-scale freezing of mAb solutions using only a fraction of the simulated volume. It is a promising material- and cost-saving tool to understand large-scale freezing processes.

Keywords: cryoconcentration, frozen storage, large-scale freezing, monoclonal antibody, scale-down device

Abbreviations: CFD – Computational Fluid Dynamics, CF – Cryoconcentration factor, mAb – Monoclonal antibody, PET – Polyethylene terephthalate, SDD – Scale-down device, TC – Thermocouple, VOF – Volume of Fluid

2.2 Introduction

Therapeutic proteins are highly important for the treatment of several severe diseases with a constantly and rapidly growing market (1–4). In order to preserve the integrity and enhance the stability of bulk drug substance in large-scale industrial production, the biopharmaceuticals are often stored frozen (1,5–9). In comparison to liquid storage the shelf life of bulk drug substances can be increased due to halted microbial growth, slower reaction rates and prevention of foaming and agitation during transportation (1,5–8,10,11). Nevertheless, freezing of protein formulations could be associated with the potential drawbacks of cold denaturation caused by the low temperature itself, denaturation at the ice surface, crystallisation of excipients and cryoconcentration (5,12–15). During freezing, ice crystals grow and exclude excipients and proteins (10,11,16). Hereby, the concentration increases in between the formed ice crystals and in between the ice dendrites, which is referred to as cryoconcentration on a microscopic scale (4,11). Concurrently, excipients and proteins are progressively transported away from the freezing front by diffusion and natural convection (6,12). This leads to a macroscopic cryoconcentration within the entity (4,11). Cryoconcentration in general may cause changes in ionic strength, osmolality and pH (7,17). In our work, macroscopic cryoconcentration will be further referred to as “cryoconcentration”. The extent of cryoconcentration within the sample is strongly dependent on the sample size, the container dimensions and the freezing device. Additionally, the freezing process itself influences the described phenomena (7). Whereas slow cooling and freezing cause strong concentration gradients, fast cooling and freezing can prevent macroscopic cryoconcentration (4,6,7,10,11,18). In order to understand and optimise the freezing process, it is therefore recommended to perform freezing experiments at the relevant scale (12,17–19). However, material for stability studies and freezing experiments is often limited, particularly during early-stage development.

Currently, various freezers along with different containers are marketed. Reusable stainless-steel jacketed tanks or large-scale disposable plastic bags attribute different challenges and show different limitations compared to bottle freezing systems. Another level of complexity is added, as the bottles used differ in size, material and geometry and thereby significantly in freezing times and behaviour. Thus, different scale-down approaches have been described, which ideally conserve the relevant dimensions and process parameters (5).

Especially the combination of disposable plastic bottles/carboys with blast freezers (forced air convection) and passive (static air) walk-in storage freezers or deep freezing chambers is widely spread. However, until now no scale-down device (SDD) is commercially available. The challenge is to develop a SDD, which preserves the freezing characteristic and behaviour of industrially used bottles/carboys and can be used regardless of the freezer employed. Possible stresses, e.g. cryoconcentration, should be mapped in this SDD and limitations of the formulation or the process itself unveiled. SmartFreeZ provided such a device, following a novel and innovative scale-down approach to mimic large-scale freezing behaviour.

This novel SDD was developed via Computational Fluid Dynamics (CFD) and experimental optimisation. CFD simulations were used to calculate the time that it takes each control volume (of approximately 1 mm^3) to go from ice nucleation to glass transition. This period can be considered as stress-time. When ice crystals grow into a control volume, protein molecules become exposed to ice interfaces, low temperature and high concentrations. However, the contribution of these factors to protein destabilisation is expected to be null below the glass transition temperature, because the solution reaches a glassy state and mobility is arrested. Therefore, the distribution of local stress-times (at the millimetre scale) characterises in greater detail the thermal history of a frozen solution than classical approaches, as for example considering only the global freezing time or the temperature profile at a single point. An alternative scale-down strategy is therefore to impose an equivalent distribution of local freezing rates and thereby stress-time (20). In this work, the overall simulated stress-time distribution within the 2 L bottle was imposed to the 125 mL bottle by partially insulating this container. Thereby, the population fractions that experience the same stress are matched between both entities.

In our study we evaluated the performance of this novel device. We compared 3D temperature profiles in the SDD to a 125 mL and a 2 L bottle at distinct positions. Furthermore, we challenged the SDD regarding changes in concentration after freezing and its possibility to reveal unforeseen events. Because of this, we did not only quantify cryoconcentration for the mAb, but also for the buffer component. Eventually, we analysed the influence of the initial mAb concentration on the resulting cryoconcentration using the novel SDD.

2.3 Materials and Methods

2.3.1 Materials

125 mL and 2 L PharmaTainer™ polyethylene terephthalate (PET) bottles were purchased from Cella S.A. (Bascharage, Luxembourg). Polyethersulfone syringe filters (0.2 μm) were acquired from VWR International GmbH (Darmstadt, Germany).

A 187.7 mg/mL IgG1 mAb stock solution in a 20 mM histidine buffer pH 5.5 was provided by Novartis AG (Basel, Switzerland). L-histidine and L-histidine monohydrochloride monohydrate both were purchased from Merck KGaA (Darmstadt, Germany).

Analytical grade potassium dihydrogen phosphate and dipotassium hydrogen phosphate for the preparation of a mobile phase were purchased from VWR International GmbH (Darmstadt, Germany).

2.3.2 Development of a Scale-Down Device Assisted by Computational Fluid Dynamics

The 2 L bottle was frozen inside an aluminium wind tunnel (45 cm diameter and 50 cm height) in a flow of gaseous CO₂ that was accelerated by a fan to an average velocity of 3 m/s. Velocity was measured using a testo 405i hot-wire anemometer (Testo Inc., West Chester, PA, USA). The wind tunnel was inside an insulated chamber containing dry ice to maintain the gas temperature near -80 °C. This tunnel was placed on top of a grid 15 cm above the bottom of the chamber to allow a directed vertical gas flow (Figure 1). The gas temperature and the temperature of the solution inside the container were mapped using type T thermocouples (TCs) and an interface NI USB-9162 from National Instruments Corporation (Austin, Texas, USA).

During the adjustment of the SDD's insulation alternative designs were tested. The SDD performance was evaluated by comparing temperature profiles of devices that were frozen simultaneously with a 2 L bottle to ensure that both containers would experience the same gas flow temperature and global heat transfer coefficients. The analysis of the thermal history was carried out using a CFD model further described below.

The freezing simulations were carried out using a solver program, developed specifically for this system, using the CFD OpenFOAM 5.0 open source C++ library (21). The mathematical model assumes that the biomixture is an aqueous solution of an osmolyte (sucrose) and a protein (BSA). When the ice crystallises, the model assumes that the matrix

of ice dendrites in equilibrium with interstitial concentrated liquid solution constitutes a continuous slushy region of ice, with an average volumetric ice fraction. The liquid solution can percolate through these slushy regions by gravity forces or by pressure gradients, originating macroscopic cryoconcentration of solutes. The mathematical model consists on the Navier-Stokes, energy, continuity and solute continuity equations, together with the equations for thermo-physical properties (heat capacity, thermal conductivity, viscosity and density). The volumetric expansion of the biomixture caused by the formation of ice was simulated by introducing a compressible air phase on the top of the liquid mixture, using the same Volume of Fluid (VOF) Method implemented in the standard solver compressibleInterFoam available in the OpenFOAM package (21). A detailed description of the mathematical model is described elsewhere (22). The CFD simulations were performed using meshes with control volumes of about 1 mm^3 . After the simulation, a post-processing program computed the stress-time of the protein in each control volume to generate a histogram of the stress-time distributions and a cumulative curve of the total mass fraction versus stress-time.

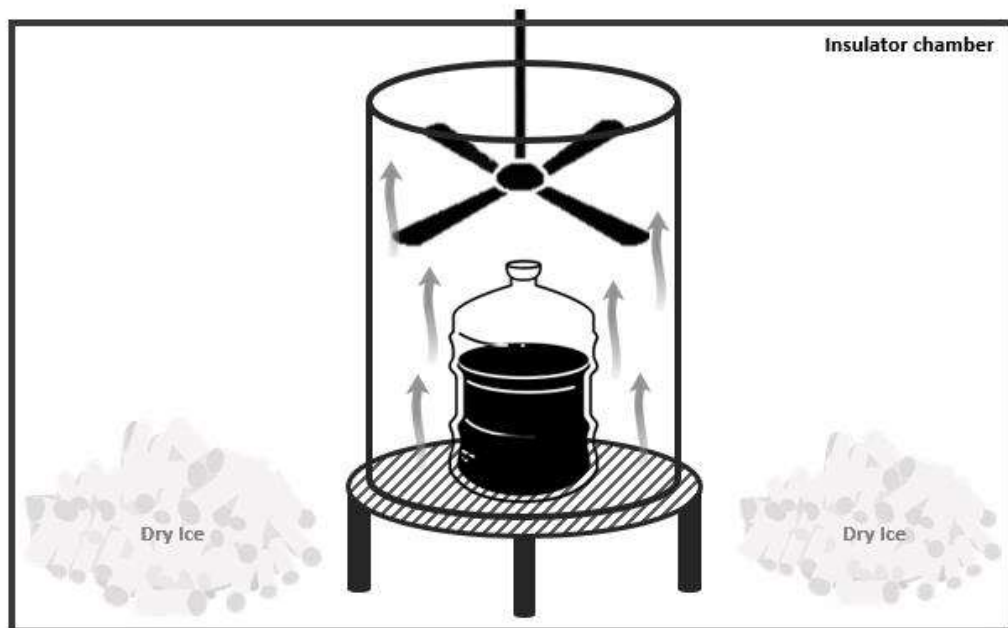


Figure 1 Schematic illustration of the freezing chamber used during the development of the SDD. The containers were placed in a flow of CO_2 at approximately $-80 \text{ }^\circ\text{C}$ and with a vertical velocity of 3 m/s .

2.3.3 Design of the Scale-Down Device

Width and length of the 125 mL PharmaTainer™ bottles is roughly half the distance of the 2 L bottle. Hence, by insulating approximately two walls, the 125 mL bottle could be used to mimic the freezing behaviour of one fourth of a 2 L bottle. The 2 L SDD (Figure 2), provided by SmartFreeZ (Porto Salvo, Portugal), consists of a holder made out of hard polylactic acid and a soft polymer insert. This insert prevents the circulation of air and heat transfer between the bottle and the holder under high convection. The holder has a cavity for a phase change liquid (1% ethanol) to insulate approximately two walls of the 125 mL PharmaTainer™ bottle. A top cover protects the bottle from radiation. For lateral freezing conditions two SDDs were used back-to-back, one for shielding and a second one for analysis.

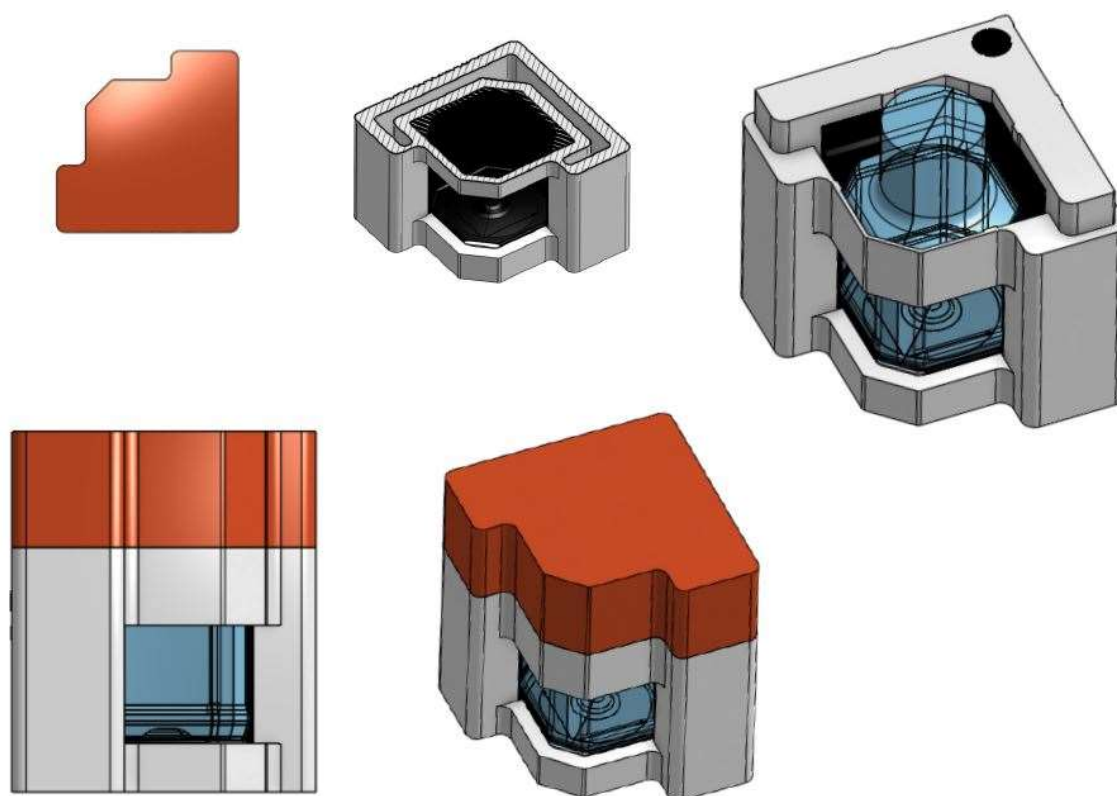


Figure 2 Final design of the 2 L SDD with a 125 mL PharmaTainer™ PET bottle.

2.3.4 Preparation of Protein Samples

Solutions containing 0.5 mg/mL, 5 mg/mL and 150 mg/mL mAb in a 20 mM histidine buffer pH 5.5 were prepared from the stock solution. All formulations were filtered through a 0.2 μm filter and quantified via UV at 280 nm with a NanoDrop One from Thermo Fisher

Scientific Inc. (Waltham, MA, USA). Bottles were filled with 100 mL and 1.6 L, respectively.

2.3.5 Temperature Mapping During Freezing

3D temperature profiles were obtained using type T TCs connected to HH520 handheld data logger thermometers by OMEGA Engineering GmbH (Deckenpfronn, Germany). For the precise and reproducible placement of six TCs, a holder with stainless steel capillaries (Acufirm Ernst Kratz GmbH, Berlin, Germany) was developed in-house for both bottle sizes (Figure 3). TC 1 – TC 5 were placed at 50% liquid level to cover the full freezing path in the 125 mL bottle. TC 6 was positioned at 75% liquid level above TC 1 to analyse the effect caused by variations in height. The 2 L bottle was equipped at corresponding positions in one fourth of the bottle.

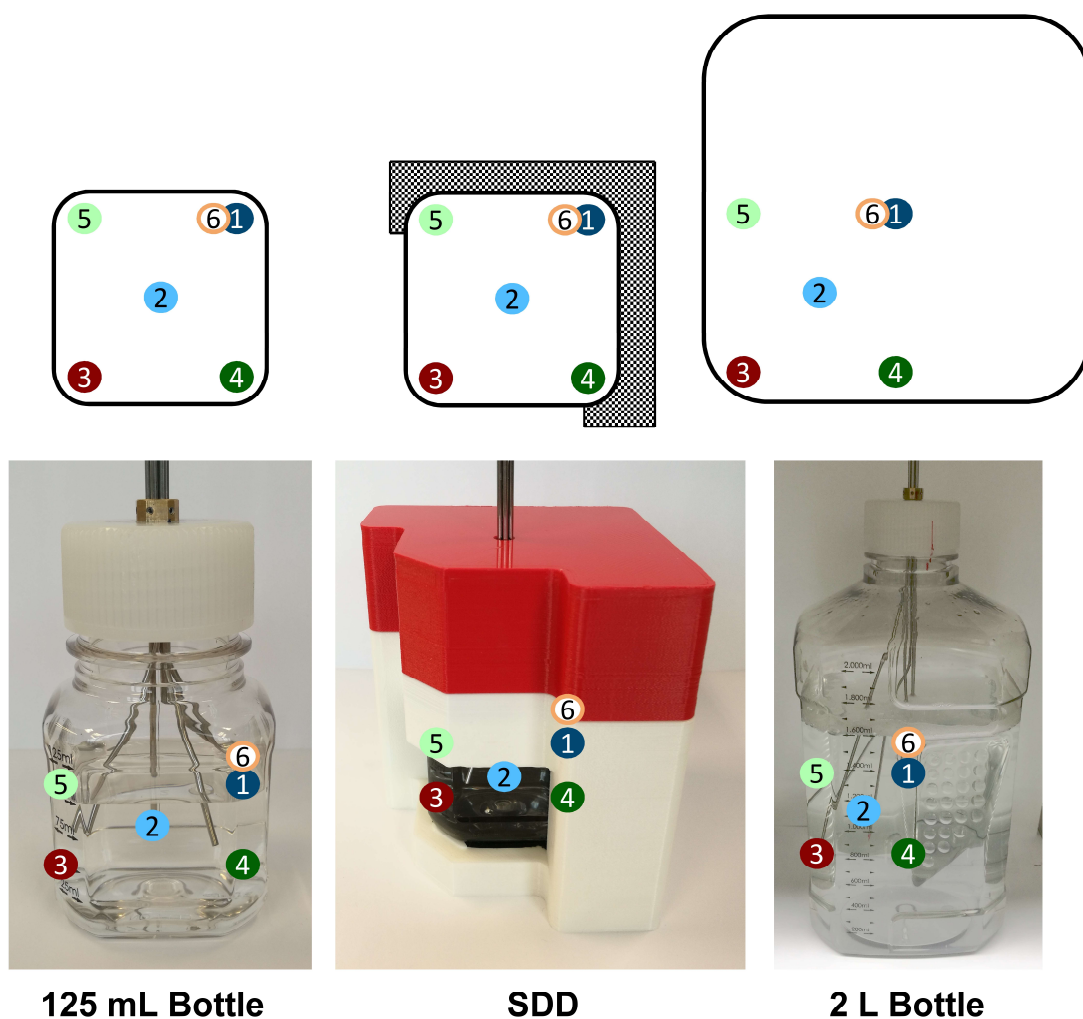


Figure 3 Positioning of TCs with holder (top: schematic representation in cross-section, below: picture of 125 mL bottle unshielded, bottle as inserted into SDD and 2 L bottle).

Bottles filled with solution containing 5 mg/mL mAb were frozen in an MKF 240 air-blast climate chamber (Binder GmbH, Tuttlingen, Germany). After 1 hour of acclimatisation at 20 °C, the bottles were cooled to -40°C at maximum cooling rate. After 9 hours at a constant temperature of -40 °C the set temperature was reached at all mapped positions. Each experiment was executed in triplicates. For every TC the temperature was measured in 1 min time steps.

2.3.6 Analysis of Cryoconcentration

The 125 mL and 2 L bottles as well as the 2 L SDD were compared regarding cryoconcentration after freezing. All three devices were filled with a 5 mg/mL mAb solution. The applied freezing programme and setup for the temperature mapping were also used for these experiments. The studies with the 125 mL bottle and the 2 L SDD were executed in triplicates. The 2 L bottle results were obtained by cutting one bottle due to material constraints. Additionally, cryoconcentration of 0.5 mg/mL and 150 mg/mL mAb solutions in the 2 L SDD was studied.

Frozen samples were cut into equal segments of approximately 3 mL for the 125 mL bottles and 7 mL for the 2 L bottle, respectively. The frozen test material was processed with a PBS 171 ESC bench-top band saw by Berg & Schmid GmbH (Remseck, Germany). MAb and histidine were quantified via size-exclusion chromatography on an Agilent 1200 HPLC equipped with a diode array detector (Agilent Technologies, Santa Clara, California, USA) at 280 nm and 210 nm after thawing. A TSKgel G3000 SWxl column by Tosoh Bioscience GmbH (Griesheim, Germany) as stationary phase and a 150 mM potassium phosphate buffer at pH 6.5 as mobile phase were used.

2.3.7 Viscosity Measurements

Dynamic viscosities were measured using a Physica MCR 100 rheometer by Anton Paar (Graz, Austria) equipped with a plane plate with 25 mm in diameter and a gap of 0.25 mm. Shear rate was kept constant at 1000 s⁻¹. Concentration-dependent viscosities (0.5 mg/mL – 200 mg/mL) were measured at 20 °C and results averaged over ten measurements with a 10 s interval. Temperature-dependent measurements were performed for a 20 mM histidine buffer and protein solutions containing 0.5 mg/mL, 5 mg/mL and 150 mg/mL mAb. Samples were measured every 10 s with a temperature ramp of 1 °C/min. The measurements were stopped as soon as the formation of ice prevented further analysis.

2.4 Results and Discussion

2.4.1 Matching Thermal History Between a 2 L Bottle and the Scale-Down Container

The 2 L freezing experiment was simulated by implementing in the model's boundary conditions the heat transfer coefficient and temperature imposed by the gas-flow, measured during the experiment. Figure 4a shows the calculated and the experimentally determined temperature profiles of a 2 L bottle at the geometrical centre and at half of the centre's width at same height. The experimental and simulated temperatures were congruent for most of the freezing period, showing that the model is correctly predicting the solution's thermal history. Therefore, the prediction of the stress-time, i.e. the time that each control volume stays in between freezing temperature and glass transition temperature, should have equivalent accuracy.

Stress-time distributions were generated for the 2 L bottle and for several scale-down variants, which consisted in different insulations for the 125 mL bottle with more or less exposed areas (not shown). Figure 4b shows the stress-time distribution of the SDD (illustrated in Figure 2) that was closest to the stress-time distribution of the 2 L bottle.

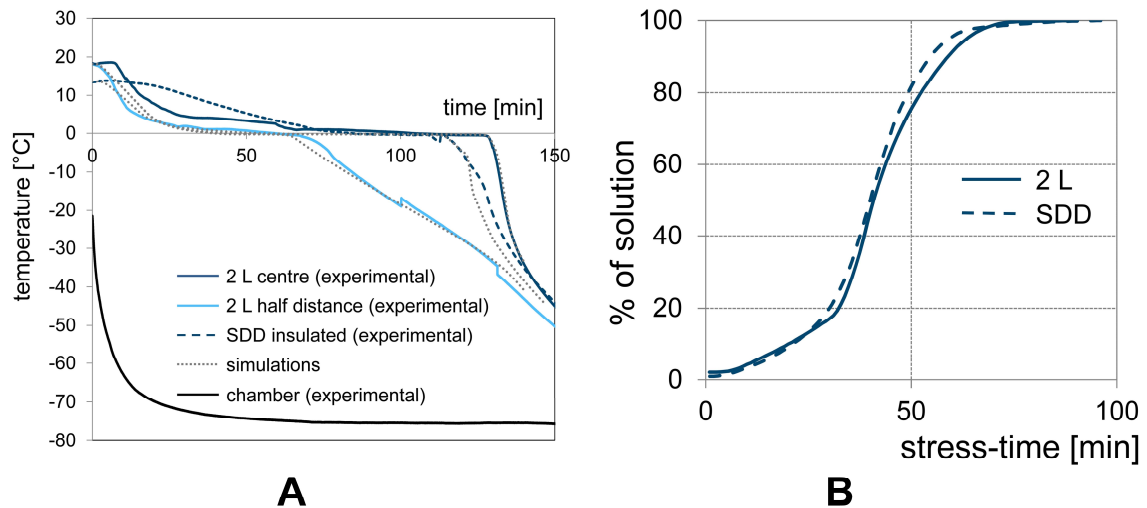


Figure 4 (a) shows temperature profiles measured during the freezing of an aqueous solution containing 5% (w/w) sucrose and 19% (w/w) BSA at locations 1 and 2 (as identified by the colours in Figure 3). The black line highlights the temperature in the chamber during the experiment. The dashed grey lines are simulated temperature profiles for corresponding locations. The SDD was filled with 100 mL and had an exposed area of 37 cm². (b) shows the stress-time distributions for the frozen solutions calculated by CFD for the 2 L bottle and the SDD.

Matching the stress-time distribution is a different approach to scale down than matching the total freezing time. For example, while the stress-time distributions between the two scales matched almost perfectly, the freezing time at the last point to freeze, inferred from Figure 4a, was slightly differing. If containers of different dimensions are frozen in the same period of time, the ice front proceeds slower in the small SDD than in the large-scale bottle. Conversely, if ice velocities are matched, the smaller container will be completely frozen in a shorter time span.

2.4.2 Comparison of 3D Temperature Profiles During Freezing

The SDD was designed to match the thermal history and not the absolute freezing time of the 2 L bottle. Nevertheless, width and length of a 125 mL bottle, which is used in the SDD, is approximately half of the distance of a 2 L bottle. Thus, temperature measurements are an important tool to evaluate the influence of the SDD on the freezing process and to characterise its performance in comparison to large-scale freezing. Consequently, a 125 mL PharmaTainer™ bottle, a 2 L PharmaTainer™ bottle and the 2 L SDD were equipped at corresponding positions with TCs. Freezing time is generally considered as the time between nucleation and completion of water crystallisation (3,12). This period is indicated by a plateau in the temperature profile (3,6). After this plateau no latent heat of crystallisation is released into the system and the temperature drops. In our experiments the onset of nucleation could not be clearly identified and we therefore defined an effective freezing time as the time span between the beginning of cooling and the end of the plateau. Furthermore, the term process time is used as the time needed to reach -38 °C after acclimatisation.

The temperature profiles obtained at six defined positions in the 125 mL bottle and the 2 L SDD are shown in Figure 5. The TCs in the 125 mL bottle can be grouped into two different regions. TC 1 and TC 3 to TC 6 recorded similar profiles. These TCs were positioned at the edges. Freezing time at these positions was approximately 60 minutes, while the process time was 2.5 hours. Data obtained for the geometrical centre (TC 2) showed a prolonged freezing time (1.6 hours), but the same process time as for TC 1 and TC 3 to TC 6.

In the SDD freezing started at the exposed edge (TC 3) and proceeded over the geometrical centre (TC 2) towards the insulated edge (TC 1 and TC 6). Freezing time for the exposed TC 3 was 1.5 hours and thereby nearly reached the maximum observed in the 125 mL bottle. Freezing time further increased for TC 2 with 2.8 hours and up to 4.2 hours for TC 1

and TC 6. Thus, the freezing time at the last point to freeze was increased nearly threefold by using the SDD. The positions that were only partially exposed (TC 4 and TC 5) needed 2.5 hours to freeze completely. Both showed a similar freezing profile to TC 2 in the centre. Process times were equal for all six positions with nearly 7.5 hours. In comparison to the 125 mL bottle, the SDD changed the direction of freezing and prolonged freezing times as well as process times significantly.

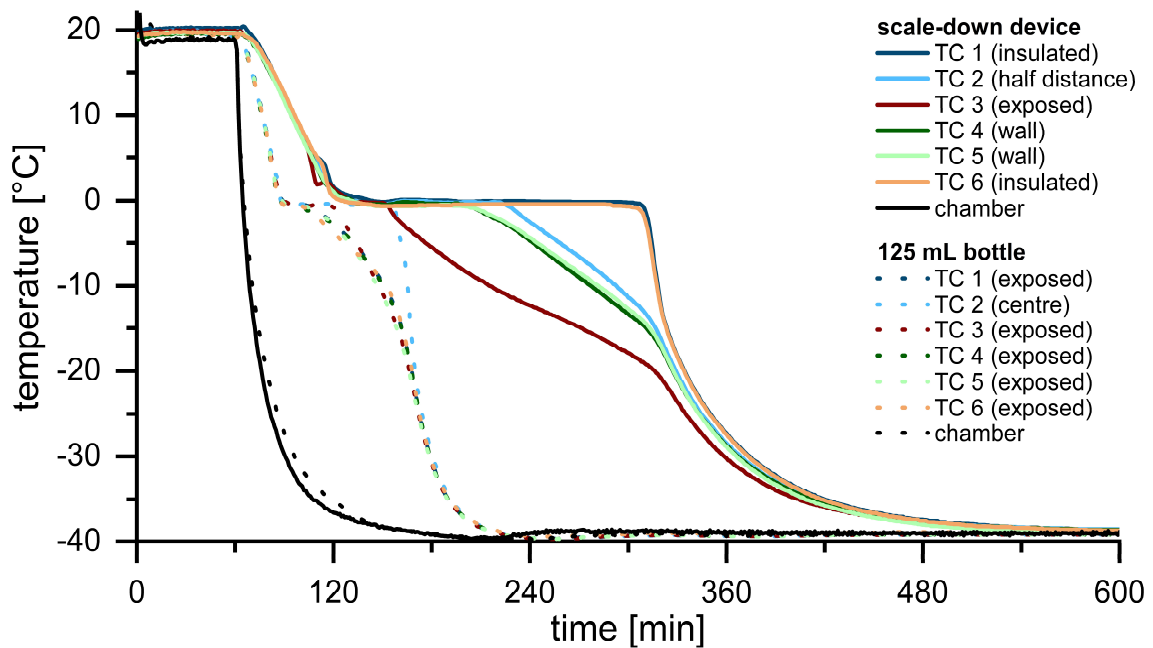


Figure 5 Temperature profiles at different positions within the container during freezing in a 125 mL bottle (dotted lines) and the 2 L SDD (solid lines).

One fourth of a 2 L bottle was equipped at corresponding positions. TC 1 to TC 5 covered the full freezing path at 50% liquid level. TC 6 detected the temperature in the geometrical centre at 75% filling level. Results are shown in comparison to the SDD in Figure 6. Freezing started at the exposed edge (TC 3) and took 1.1 hours. Freezing times at the two monitored walls (TC 4 and TC 5) were only slightly prolonged by 20 minutes and 34 minutes, respectively. Freezing at half height and half freezing path length (TC 2) was completed after 3.6 hours. The last point to freeze was the geometrical centre of the 2 L bottle (TC 1 and TC 6) with a freezing time of 4.6 hours. The height positioning of the TC did not influence the outcome. After the whole content was frozen, temperature quickly merged within the bottle. Thereby, process times were similar throughout the 2 L bottle with approximately 7.5 hours.

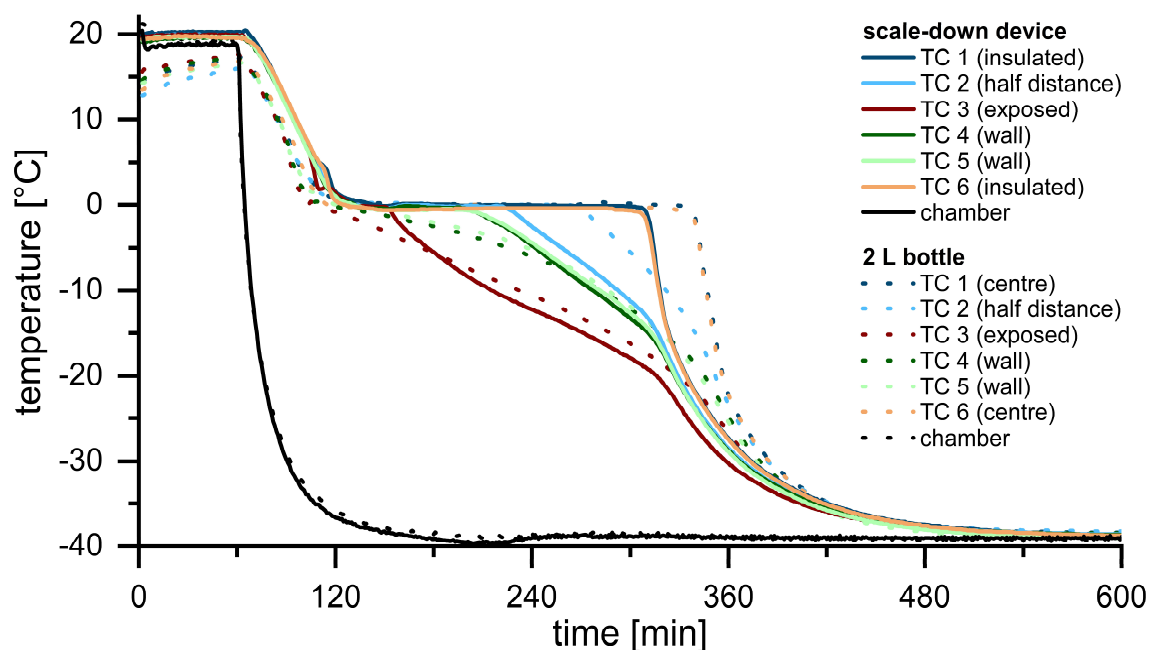


Figure 6 Temperature profiles at different positions within the container during freezing in a 2 L bottle (dotted lines) and the 2 L SDD (solid lines).

In the 125 mL bottle freezing started at the exposed areas. These areas were in contact with the surrounding chilled air through the wall and thereby experienced the highest heat exchange. The freezing front proceeded towards the centre of the bottle, which was the last point to freeze. As a consequence of the small volume, freezing and process times were short in comparison to large-scale freezing.

The large-scale 2 L bottle started to freeze at the exposed edge. This region experienced heat exchange from both surrounding walls. The TCs at the two walls also faced direct heat exchange, nevertheless slightly less, because only one wall transported heat away. As a consequence, freezing at the walls started slightly later and showed a decreased cooling rate after the temperature dropped below 0 °C. The freezing front proceeded towards the last point to freeze, which again was the geometrical centre of the bottle. As long as the bottle was not fully frozen, the latent heat of crystallisation kept the surrounding environment at the freezing temperature (6,23). Hence, a plateau was observable for the different TCs. When fully frozen, the temperature merged within the entire container and the further cooling proceeded similarly for all positions. The larger bulk volume prolonged freezing and process time by a factor of three in comparison to the 125 mL bottle.

The use of the SDD did not only lead to a comparable outcome regarding freezing direction as the 2 L bottle, but also to similar freezing times at the defined positions. Freezing started

at the exposed edge and proceeded over the geometrical centre towards the insulated edge. Thereby, the insulated edge and no longer the geometrical centre of the bottle was the last point to freeze. Freezing time was slightly overestimated for the TCs at the exposed edge and the simulated walls. In contrast, the freezing time was slightly less in the insulated regions compared to the centre of the 2 L bottle. Nonetheless, the process time was the same in the SDD and the 2 L bottle.

The SDD changed the direction of freezing and strongly increased freezing as well as process times compared to the 125 mL bottle, though both were filled with 100 mL. The SDD preserved the freezing path of the 2 L bottle filled with 1.6 L and accurately reflected the 2 L bottle's process time. Therefore, we consider the SDD as an appropriate and material-saving model to simulate large-scale freezing processes.

2.4.3 Comparison of Cryoconcentration

Among others, cryoconcentration is an important stress factor during large-scale freezing of drug bulk substance, potentially influencing protein stability (4,6,13,16,17,24–26). As cryoconcentration is not only influenced by the volume used, but is additionally determined by the freezing protocol, a SDD which accurately reflects cryoconcentration in larger volumes but consumes far less material is highly needed.

In this study, changes in concentration of a mAb as well as histidine were quantified. Changes were expressed as the “Cryoconcentration Factor” (CF), which is defined as

$$CF = \frac{\text{concentration}_{\text{sample}}}{\text{concentration}_{\text{initial}}} = \frac{c_x}{c_0} \quad (1)$$

CF values in the 125 mL bottle ranged between 0.72 and 1.13 for mAb and between 0.53 and 1.41 for histidine. Figure 7 shows the results in comparison to the cryoconcentration in a 2 L PharmaTainer™ PET bottle and the SDD. The CF of the mound in the centre of the 125 mL bottle was close to 1. Throughout the bottle, concentration increased from top to bottom and towards the geometrical centre. Thus, a cross-shaped distribution for both components was evident. The ratio between the CF values for mAb and histidine significantly varied throughout the bulk. The mAb to histidine ratio was shifted towards

mAb at the walls and in the top layer. In contrast, the cryoconcentration of histidine exceeded that of the mAb in the bottom layer and in the centre.

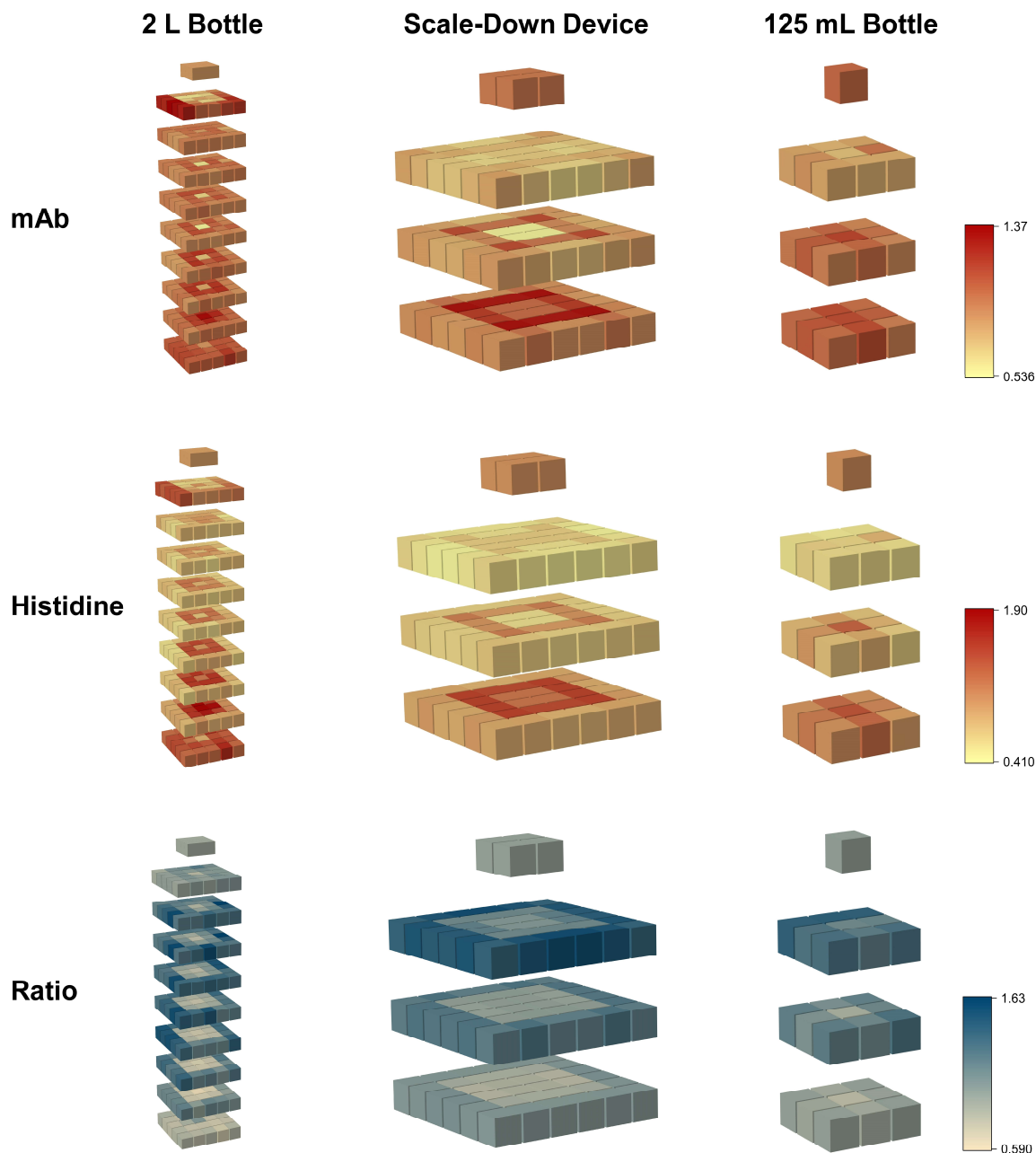


Figure 7 Cryoconcentration of mAb and histidine as well as mAb to histidine ratio in a 2 L PharmaTainer™ PET bottle, the SDD and a 125 mL PharmaTainer™ PET bottle. Results for the SDD were symmetrically quadruplicated to allow the comparison with the 2 L bottle.

In the 2 L bottle, the CF values ranged between 0.54 and 1.37 for mAb and between 0.48 and 2.27 for histidine. As for the 125 mL bottle, the concentration of the mound was close to the initial concentration for both components. The top layer showed two rows of highly concentrated cubes facing the fan and the door of the freezing chamber. The following

layers emphasized concentric changes with a diluted outer circle and a concentrated inner circle. The centre cube was concentrated at the bottom, but strongly diluted in the geometrical centre and at the last point to freeze. In general, mAb and histidine concentration increased from top to bottom. The mAb to histidine ratio was also markedly shifted towards mAb at the walls. Histidine was favoured at the bottom and in the centre and, contrary to the results for the 125 mL bottle, also slightly in the top layer.

The SDD rendered CF values between 0.54 and 1.32 for mAb and between 0.41 and 1.51 for histidine. The results obtained in the SDD were symmetrically quadruplicated to allow for comparison with the 2 L bottle. Visual inspection of the bottle highlighted a mound no longer on top of the geometrical centre, but in the insulated edge of the device. Its concentration was close to the initial 5 mg/mL mAb and 20 mM histidine. Two concentric layers followed an evenly distributed top layer. Similar to the results seen in the 2 L bottle, a highly diluted core was obtained for the last point to freeze. The mAb to histidine ratios were comparable to the outcome in the 2 L bottle. The only exception was the ratio in the top layer. While histidine was slightly favoured in the top layer of the 2 L bottle, in the SDD the mAb to histidine ratio was near 1 in the centre, but strongly shifted to mAb near the wall.

The cooling rate and the related proceeding of the freezing front strongly influence the range of cryoconcentration (4,6,7,10,11,18). In general, protein samples that are frozen faster show less cryoconcentration (6,7,10). The 125 mL bottle froze significantly faster than both the 2 L bottle and the SDD. Thus, cryoconcentration was suppressed in the small bottle. Heat exchange was highest in the edges and therefore these areas were the first to freeze. The ice excluded the solutes, leading to an increased mAb and histidine concentration at the solid-liquid interface. At this interface both components will be transported away by diffusion and natural convection, which is driven by changes in density, temperature and concentration, and the freeze concentrate will only be partially entrapped in the ice (6). This is why the solutes concentrated in the last point to freeze. Additionally, a general increase from top to bottom was evident. Histidine was less entrapped in the regions at the wall, but was strongly concentrated in the centre and at the bottom. We hypothesize that the higher diffusion coefficient allowed the smaller histidine molecules to diffuse further away from the freezing front as compared to the large mAb molecules. Therefore, histidine was especially found at the last point the freeze and at the bottom.

As mentioned in the section above, the 2 L bottle required significantly more time to reach a fully frozen state. Thus, cryoconcentration was enhanced in comparison to the 125 mL bottle. Freezing started at the walls, where heat exchange was highest. Similar to the freezing procedure described for the 125 mL bottle, solutes were partially excluded and concentrated towards the last point to freeze and the bottom. Thereby, concentric changes towards the liquid core were formed. Surprisingly, the geometrical centre and last point to freeze showed a strongly diluted core. We assume that an ice crust forms on top of the liquid during freezing. As freezing of the remaining solution proceeds, the expanding volume of the ice continuously increases the pressure until the remaining liquid core is pushed through this ice crust. Consequently, a mound is formed and highly concentrated rows in the uppermost layer result. This theory is further supported by the mAb to histidine ratio. While the mAb to histidine ratio was above 1 at the walls, it was below 1 in the centre. Ratios similar to the one in the centre were observed in the mound and the top layer.

In general, the 3D distribution of mAb and histidine as well as the extent of cryoconcentration in the 2 L bottle were preserved in the SDD. Unexpected events, such as the diluted core, were evident as well as the concentric changes in concentration. Differences in the degree of cryoconcentration between mAb and histidine could also be highlighted using the SDD. Nevertheless, the maximum histidine concentration was underestimated. In addition, the highly concentrated rows of cubes could not be shown in the SDD. The fewer samples for the SDD possibly averaged the cryoconcentration in the top layer.

In addition to the good agreement of the temperature and freezing profiles in the SDD and the 2 L bottle, the SDD accurately predicted cryoconcentration. Unforeseen events were detected as well as the 3D distribution of both protein and buffer. Thus, we conclude that the SDD can be used to simulate the freezing behaviour and to predict the stability of mAb solutions during large-scale freezing by using only 100 mL.

2.4.4 Influence of Initial mAb Concentration on Cryoconcentration

Natural convection within the entity and diffusion coefficients at the freezing front are two important parameters that mainly determine the degree of cryoconcentration (6,12). Both are influenced by the dynamic viscosity of the solution. Viscosity itself is formulation dependent and increases upon cooling. Therefore, not only the initial mAb concentration of the solution, but also the drop in temperature during cooling strongly changes the

outcome. Hence, we performed concentration-dependent and temperature-dependent dynamic viscosity measurements for the mAb used in this study.

2.4.4.1 Concentration-Dependent and Temperature-Dependent Viscosity Measurements

The dynamic viscosity increased exponentially for a dilution series between 0.5 mg/mL – 200 mg/mL mAb from 1.8 mPas – 19.1 mPas (Figure 8). In addition, viscosity was measured for pure histidine buffer and 0.5 mg/mL, 5 mg/mL and 150 mg/mL mAb solutions in dependence of temperature. The viscosity of 0.5 mg/mL and 5 mg/mL mAb solutions slightly increased during cooling and was comparable to that of the histidine buffer. In contrast, the viscosity of a solution containing 150 mg/mL mAb was 7.7 mPas at 20 °C and increased up to approximately 30 mPas upon cooling to -7 °C.

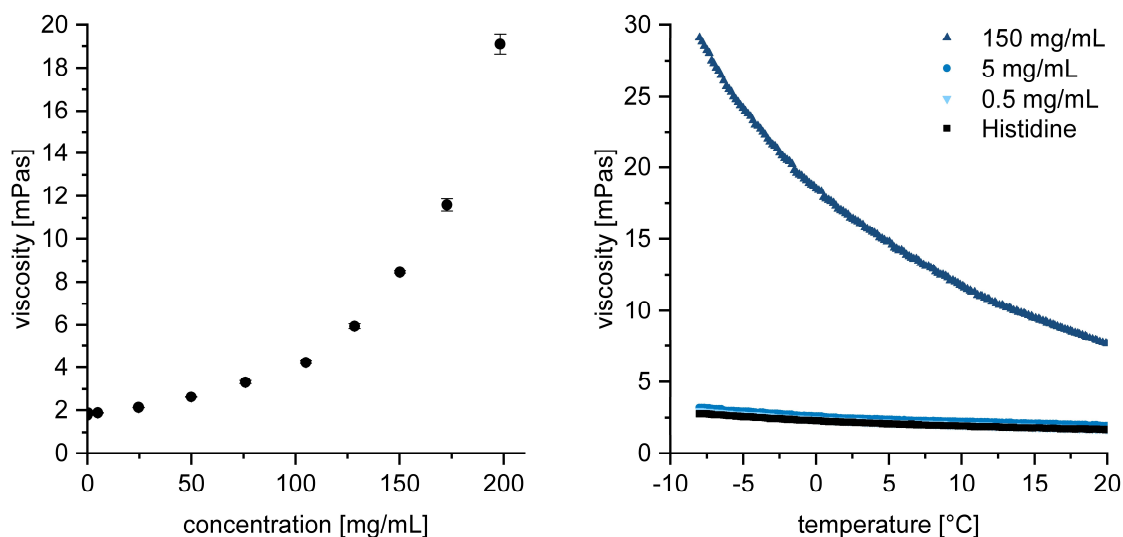


Figure 8 Concentration-dependent and temperature-dependent dynamic viscosity.

2.4.4.2 Effect of mAb Concentration on Cryoconcentration

To evaluate the effect of changes in viscosity on cryoconcentration, we characterised cryoconcentration for solutions containing 0.5 mg/mL and 150 mg/mL mAb. Due to a similar temperature-dependence of the viscosity of 0.5 mg/mL and 5 mg/mL mAb solutions we assumed similar changes in concentration upon freezing. In contrast, cryoconcentration effects should change at 150 mg/mL due to the higher viscosity. Figure 9 provides a comparison between cryoconcentration of the mAb, histidine and the ratio between both for the three mAb concentrations.

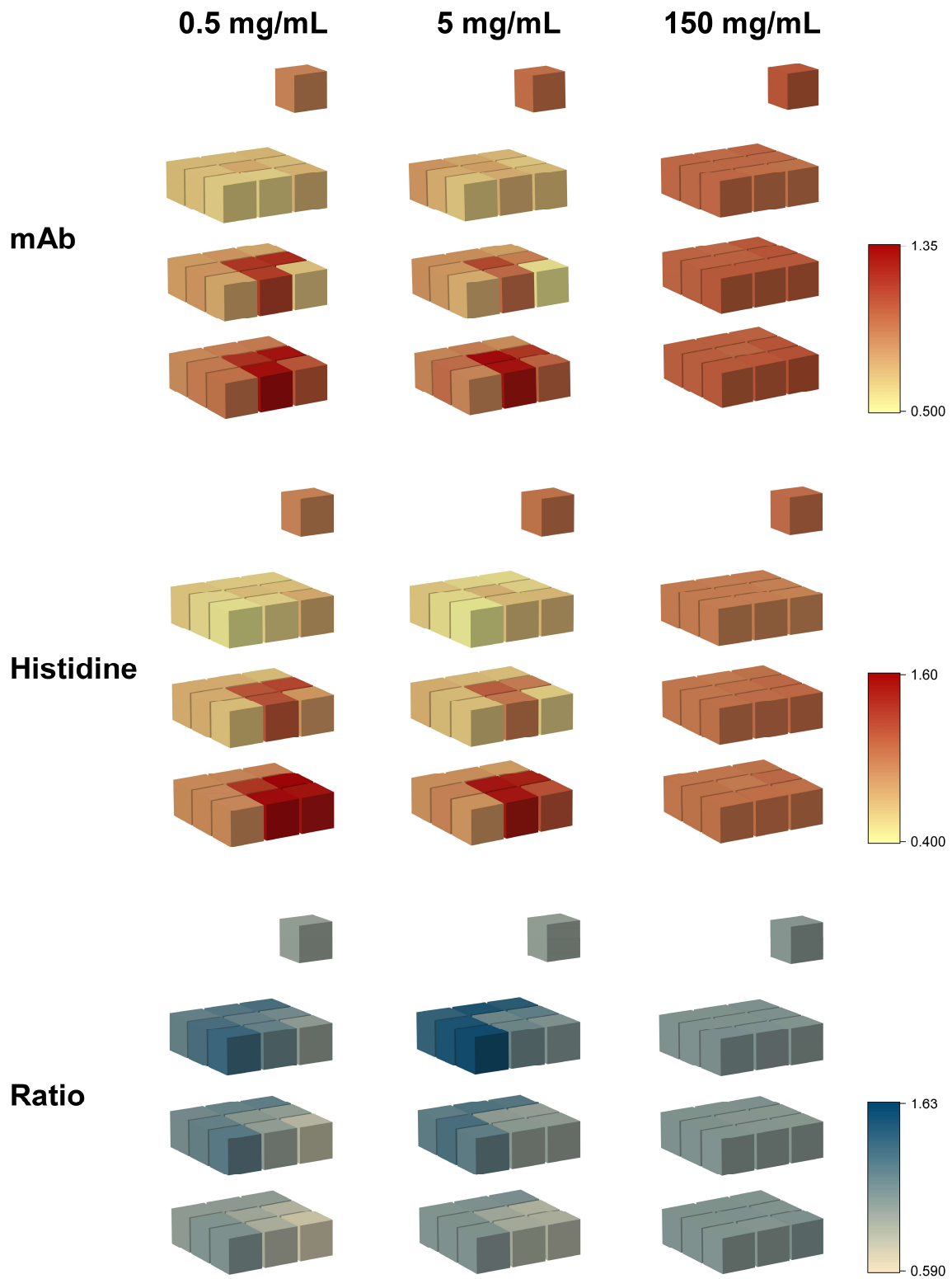


Figure 9 Cryoconcentration of mAb and histidine as well as mAb to histidine ratio for solutions containing 0.5 mg/mL, 5 mg/mL and 150 mg/mL mAb.

At 5 mg/mL mAb CF values were between 0.54 and 1.32 for mAb and between 0.41 and 1.51 for histidine. CF values for the bottles containing only 0.5 mg/mL mAb ranged between 0.60 and 1.31 for mAb and between 0.45 and 1.60 for histidine. Similar to the results discussed for 5 mg/mL, in the frozen 0.5 mg/mL mAb solution both components were evenly distributed in the top layer, followed by two layers with concentric changes towards the last point to freeze. In the insulated edge the samples were again highly diluted in the middle layer, but significantly concentrated at the bottom. The ratio between both components was in good agreement with the outcome at 5 mg/mL. The mAb cryoconcentration exceeded the histidine cryoconcentration in the top region and near the wall, while histidine was more cryoconcentrated in the centre and bottom regions.

For 150 mg/mL mAb CF values were only between 0.91 – 1.07 for mAb and between 0.90 and 1.06 for histidine. Both solutes were slightly diluted in the top layer and concentration marginally increased towards the bottom. The highest and the lowest concentrations were detected in the insulated edge in the bottom and top region, respectively. Nevertheless, changes in concentration became negligible when compared to the outcome of solutions at lower mAb concentrations. The mAb to histidine ratio was unchanged throughout the bulk. The main driving forces for cryoconcentration are diffusion and free convection (6,12). The diffusion can be described by the Stokes-Einstein equation,

$$D = \frac{\kappa_B T}{6\pi\eta r} \quad (2)$$

where D is the diffusion constant, κ_B is the Boltzmann's constant, T the absolute temperature, η is the dynamic viscosity and r the radius of a particle. The flow resulting from natural convection near the bottle wall can be estimated by the Grashof number Gr

$$Gr = \frac{force_{buoyancy}}{force_{viscous}} = \frac{g\beta(T_s - T_\infty)L^3}{\left(\frac{\eta}{\rho}\right)^2} \quad (3)$$

where g is the acceleration due to Earth's gravity, β is the coefficient of thermal expansion, T_s is the surface temperature, T_∞ is the bulk temperature, L is the vertical length and ρ the density.

Thus, the dynamic viscosity of the freezing solution directly influences both natural convection and diffusion. At high protein concentration resulting in high viscosity, the natural flow at the ice interface is strongly reduced and limiting freeze concentration. At the same time the high viscosity limits the diffusional movement of molecules, which reduces formation of a concentration difference between small and large solutes. We already discussed that at low mAb concentrations of 0.5 or 5 mg/mL differences in diffusion coefficients were relevant. The large mAb is partially entrapped in the ice, while histidine diffuses away from the freezing front. Consequently, the ratio shifts towards histidine in the regions that freeze the latest, namely the bottom and insulated edge. This is in agreement with the results from Singh et al., who demonstrated that the protein's cryoconcentration is lagging behind (27). As the temperature-dependent viscosity was similar at 0.5 mg/mL and 5 mg/mL mAb, natural convection proceeded similarly, resulting in the same 3D changes in concentration. At 150 mg/mL mAb the initial viscosity was markedly higher, which further substantially increased with cooling. This suppressed the natural convection within the bottle and thereby strongly reduced cryoconcentration for the mAb and histidine. Additionally, mAb and histidine were similarly distributed within the whole entity since the higher viscosity drastically slows down the diffusion of both mAb and histidine, so that diffusion is not affecting cryoconcentration of the solutes.

In addition to freezing also thawing is a key aspect potentially effecting product stability (17,28). Thus, a detailed description of the performance of the SDD during thawing is the focus of current studies.

2.5 Conclusion

Cryoconcentration during large-scale freezing of biologics is highly process- and container-related. It cannot be easily simulated by small-scale experiments (5,12). So far, no SDD is marketed to predict freezing and cryoconcentration in industrially widely used disposable bottles. In this study, we examined 3D freezing as well as the resulting cryoconcentration of a mAb and histidine in 125 mL and 2 L PharmaTainer™ PET bottles in comparison to an innovative SDD. This device mimics one fourth of a 2 L bottle by insulating two walls

of a 125 mL bottle. In addition, we used the SDD to characterise the influence of dynamic viscosity of a mAb solution on cryoconcentration.

3D temperature profiles and cryoconcentration strongly differed between the 125 mL and the 2 L bottle. Overall process time in the 125 mL bottle was short with 2.5 hours and significantly reduced in comparison to the 2 L bottle (7.5 hours). Consequently, the degree of cryoconcentration and the 3D distribution of the mAb and histidine were not preserved. Thus, the 125 mL PharmaTainer™ bottle itself cannot be used to mimic large-scale freezing processes.

In contrast, the 2 L SDD showed similar results for the overall freezing behaviour and cryoconcentration effects. Concentric changes in concentration towards the last point to freeze and the degree of cryoconcentration were mimicked. Unforeseen phenomena, such as a diluted core in the centre of the 2 L bottle and differences in local distribution of the mAb in comparison to histidine, were evident in the SDD. Therefore, we consider the SDD to be a good device to simulate large-scale freezing processes and to unveil possible limitations.

The SDD supported our theory that the dynamic viscosity influences cryoconcentration and the ratio between the components by influencing natural convection and diffusion. A similarly low viscosity of 0.5 mg/mL and 5 mg/mL mAb solutions led to similar cryoconcentration and significant differences in 3D distribution of mAb and histidine. The higher initial viscosity of a solution with 150 mg/mL mAb, which further increased upon cooling, limited concentration changes.

Acknowledgements

This work was funded by the Novartis Pharma AG.

References

1. Rodrigues MA, Balzan G, Rosa M, Gomes D, de Azevedo EG, Singh SK, et al. The importance of heat flow direction for reproducible and homogeneous freezing of bulk protein solutions. *Biotechnol Prog.* 2013 Sep;29(5):1212–21.
2. Singh SK, Kolhe P, Mehta AP, Chico SC, Lary AL, Huang M. Frozen State Storage Instability of a Monoclonal Antibody: Aggregation as a Consequence of Trehalose Crystallization and Protein Unfolding. *Pharm Res.* 2011 Apr 7;28(4):873–85.
3. Roessl U, Leitgeb S, Nidetzky B. Protein freeze concentration and micro-segregation analysed in a temperature-controlled freeze container. *Biotechnol Reports.* 2015 Jun;6:108–11.
4. Hauptmann A, Hoelzl G, Loerting T. Distribution of Protein Content and Number of Aggregates in Monoclonal Antibody Formulation After Large-Scale Freezing. *AAPS PharmSciTech.* 2019 Feb 10;20(2):72.
5. Padala C, Jameel F, Rathore N, Gupta K, Sethuraman A. Impact of Uncontrolled vs Controlled Rate Freeze-Thaw Technologies on Process Performance and Product Quality. *PDA J Pharm Sci Technol.* 2010;64(4):290–8.
6. Rodrigues MA, Miller MA, Glass MA, Singh SK, Johnston KP. Effect of Freezing Rate and Dendritic Ice Formation on Concentration Profiles of Proteins Frozen in Cylindrical Vessels. *J Pharm Sci.* 2011 Apr;100(4):1316–29.
7. Miller MA, Rodrigues MA, Glass MA, Singh SK, Johnston KP, Maynard JA. Frozen-State Storage Stability of a Monoclonal Antibody: Aggregation is Impacted by Freezing Rate and Solute Distribution. *J Pharm Sci.* 2013 Apr;102(4):1194–208.
8. Radmanovic N, Serno T, Joerg S, Germershaus O. Understanding the Freezing of Biopharmaceuticals: First-Principle Modeling of the Process and Evaluation of Its Effect on Product Quality. *J Pharm Sci.* 2013 Aug;102(8):2495–507.
9. Wöll AK, Desombre M, Enghauser L, Hubbuch J. A phase diagram-based toolbox to assess the impact of freeze/thaw ramps on the phase behavior of proteins. *Bioprocess Biosyst Eng.* 2020 Feb 28;43(2):179–92.
10. Rathore N, Rajan RS. Current Perspectives on Stability of Protein Drug Products during Formulation, Fill and Finish Operations. *Biotechnol Prog.* 2008 Jun 6;24(3):504–14.
11. Webb SD, Webb JN, Hughes TG, Sesin DF, Kincaid AC. Freezing Biopharmaceuticals Using Common Techniques — and the Magnitude of Bulk-Scale Freeze-Concentration. *BioPharm.* 2002;15(5):22–34.
12. Singh SK, Kolhe P, Wang W, Nema S. Large-Scale Freezing of Biologics A Practitioner’s Review, Part One: Fundamental Aspects. *Bioprocess Int.* 2009;7(9):32–44.

Cryoconcentration and 3D Temperature Profiles during Freezing of mAb Solutions in Large-Scale PET Bottles and a Novel Scale-Down Device

13. Hauptmann A, Podgoršek K, Kuzman D, Srčić S, Hoelzl G, Loerting T. Impact of Buffer, Protein Concentration and Sucrose Addition on the Aggregation and Particle Formation during Freezing and Thawing. *Pharm Res.* 2018 May 19;35(5):101.
14. Arakawa T, Prestrelski SJ, Kenney WC, Carpenter JF. Factors affecting short-term and long-term stabilities of proteins. *Adv Drug Deliv Rev.* 2001 Mar;46(1–3):307–26.
15. Zhang A, Singh SK, Shirts MR, Kumar S, Fernandez EJ. Distinct Aggregation Mechanisms of Monoclonal Antibody Under Thermal and Freeze-Thaw Stresses Revealed by Hydrogen Exchange. *Pharm Res.* 2012 Jan 30;29(1):236–50.
16. Bhatnagar BS, Pikal MJ, Bogner RH. Study of the Individual Contributions of Ice Formation and Freeze-Concentration on Isothermal Stability of Lactate Dehydrogenase during Freezing. *J Pharm Sci.* 2008 Feb;97(2):798–814.
17. Kolhe P, Badkar A. Protein and solute distribution in drug substance containers during frozen storage and post-thawing: A tool to understand and define freezing-thawing parameters in biotechnology process development. *Biotechnol Prog.* 2011 Mar;27(2):494–504.
18. Lashmar UT, Vanderburgh M, Little SJ. Bulk Freeze–Thawing of Macromolecules. *Bioprocess Int.* 2007;44–54.
19. Authelin J-R, Rodrigues MA, Tchessalov S, Singh SK, McCoy T, Wang S, et al. Freezing of Biologicals Revisited: Scale, Stability, Excipients, and Degradation Stresses. *J Pharm Sci.* 2020 Jan;109(1):44–61.
20. Geraldés V, Gomes DC, Rego P, Fegley D, Rodrigues MA. A New Perspective on Scale-Down Strategies for Freezing of Biopharmaceuticals by Means of Computational Fluid Dynamics. *J Pharm Sci.* 2020 Jun;109(6):1978–89.
21. Weller H, Greenshields C, Rouvray C de. Download v5.0 | Source Pack | OpenFOAM [Internet]. [cited 2020 Jan 7]. Available from: <https://openfoam.org/download/5-0-source/>
22. Barata FJF. Modelling of macro-cryoconcentration phenomena during the freezing of biopharmaceutical aqueous solutions [Internet]. IST University of Lisbon; 2019 [cited 2020 Jan 7]. Available from: <https://fenix.tecnico.ulisboa.pt/cursos/meq/dissertacao/1691203502343641>
23. Singh SK, Nema S. Freezing and Thawing of Protein Solutions. In: *Formulation and Process Development Strategies for Manufacturing Biopharmaceuticals*. Hoboken, NJ, USA: John Wiley & Sons, Inc.; 2010. p. 625–75.
24. Bhatnagar BS, Bogner RH, Pikal MJ. Protein Stability During Freezing: Separation of Stresses and Mechanisms of Protein Stabilization. *Pharm Dev Technol.* 2007 Jan 7;12(5):505–23.
25. Barnard JG, Singh S, Randolph TW, Carpenter JF. Subvisible Particle Counting Provides a Sensitive Method of Detecting and Quantifying Aggregation of Monoclonal Antibody Caused by Freeze-Thawing: Insights Into the Roles of Particles in the Protein Aggregation Pathway. *J Pharm Sci.* 2011 Feb;100(2):492–503.

26. Wang W, Nema S, Teagarden D. Protein aggregation—Pathways and influencing factors. *Int J Pharm.* 2010 May;390(2):89–99.
27. Kolhe P, Mehta AP, Lary AL, Chico SC, Singh SK. Large-Scale Freezing of Biologics (Part III). *BioPharm Int.* 2012;25(October):40–8.
28. Mehta SB, Subramanian S, D’Mello R, Brisbane C, Roy S. Effect of protein cryoconcentration and processing conditions on kinetics of dimer formation for a monoclonal antibody: A case study on bioprocessing. *Biotechnol Prog.* 2019 Jul 15;35(4):1–7.

Chapter 3 Scaling Down Large-Scale Thawing of mAb Solutions – 3D Temperature Profiles, Changes in Concentration, and Density Gradients

This chapter is published as:

**Oliver Bluemel¹, Jakob W. Buecheler², Astrid Hauptmann³, Georg Hoelzl³,
Karoline Bechtold-Peters², Wolfgang Friess¹**

1 Pharmaceutical Technology and Biopharmaceutics, Department of Pharmacy, Ludwig-Maximilians-
Universitaet Muenchen, 81377 Munich, Germany

2 Technical Research and Development, Novartis Pharma AG, 4002 Basel, Switzerland

3 Sandoz GmbH, 6336 Langkampfen, Austria

Note from the authors:

The version included in this thesis is identical with the published article apart from minor
changes.

The published article can be assessed online via:

<https://doi.org/10.1007/s11095-021-03117-6>

Author contributions:

O.B., W.F., and K.B.P. conceived the study. O.B. performed the experiments and evaluated
the data. O.B. wrote the paper. W.F., J.W.B., K.B.P., G.H., and A.H. contributed to the
discussion of the results and revised the manuscript. W.F. and K.B.P. supervised the work.

3.1 Abstract

Purpose: Scale-down devices (SDD) are designed to simulate large-scale thawing of protein drug substance, but require only a fraction of the material. To evaluate the performance of a new SDD that aims to predict thawing in large-scale 2 L bottles, we characterised 3D temperature profiles and changes in concentration and density in comparison to 125 mL and 2 L bottles. Differences in diffusion between a monoclonal antibody (mAb) and histidine buffer after thawing were examined.

Methods: Temperature profiles at six distinct positions were recorded with type T thermocouples. Size-exclusion chromatography allowed quantification of mAb and histidine. Polysorbate 80 was quantified using a fluorescent dye assay. In addition, the solution's density at different locations in bottles and the SDD was identified.

Results: The temperature profiles in the SDD and the large-scale 2 L bottle during thawing were similar. Significant concentration gradients were detected in the 2 L bottle leading to marked density gradients. The SDD slightly overestimated the dilution in the top region and the maximum concentrations at the bottom. Fast diffusion resulted in rapid equilibration of histidine.

Conclusion: The innovative SDD allows a realistic characterisation and helps to understand thawing processes of mAb solutions in large-scale 2 L bottles. Only a fraction of material is needed to gain insights into the thawing behaviour that is associated with several possible detrimental limitations.

Keywords: concentration gradient, freeze-thaw, large-scale thawing, monoclonal antibody, scale-down device

Abbreviations: bis-ANS – 4,4'-dianilino-1,1'-binaphthyl-5,5'-disulfonic acid dipotassium salt, CFD – Computational Fluid Dynamics, CF – Cryoconcentration factor, DPBS - Dulbecco's phosphate buffered saline, FCM - Freeze-concentrated matrix, FT – Freezing and thawing, HPLC - High-performance liquid chromatography, LPTF - Last point to freeze, LPTT – Last point to thaw, mAb – Monoclonal antibody, PET – Polyethylene terephthalate, PS80 – Polysorbate 80, SDD – Scale-down device, SEC – Size-exclusion chromatography, TC – Thermocouple, T_g' - Glass transition temperature of the maximally freeze-concentrated solution

3.2 Introduction

Therapeutic proteins, especially monoclonal antibodies (mAbs), are of significant importance in a constantly growing market and number of indications (1–3). During large-scale production of biopharmaceuticals freezing is a commonly used processing step to enhance physical and chemical stability and to increase shelf life (4,5). In comparison to liquid storage, frozen storage and transport offers flexibility for the manufacturing process by decoupling drug substance and drug product processing, decreased risk of microbial growth and reduced foaming, shaking and agitation (4–6). While freezing and thawing (FT) is intentional during production of bulk drug substances and drug products (7), commercial products may also be frozen multiple times accidentally by mishandling. Despite its apparent simplicity and undoubted advantages, freezing can be associated with a variety of possible drawbacks. Cold denaturation (8), cryoconcentration on a microscopic and macroscopic scale (2,3,9), crystallisation of cryoprotectants (10,11) or buffer salts, associated with significant pH shifts (12), interactions at the ice interface (13), and ultimately conformational and colloidal instability (14) are well known, although not fully understood. In addition, Authelin et al. address enhanced oxidation, the formation of air bubbles, local pressure, and mechanical stresses as further considerable occurrences that are so far not well examined (15). The FT process becomes even more complex as the described phenomena are not only relevant during freezing but also during thawing. Especially crystallisation (7,16) during and concentration gradients (17,18) after thawing can lead to denaturation, aggregation and precipitation of proteins (18,19).

During freezing, growing ice crystals exclude proteins and other excipients. Consequently, the concentration of the remaining unfrozen solution increases. The microenvironment of the protein between the ice crystals can be described as a freeze-concentrated matrix (FCM). Under ideal equilibrium conditions its maximum concentration is characterised by state diagrams (1,15). The glass transition temperature of the maximally freeze concentrated solution (T_g') is the temperature of complete solidification of the FCM. Macroscopically, the cryoconcentrated solution near the freezing front is transported away into unfrozen regions by diffusion and convection. This leads to a substantial heterogeneity throughout the frozen bulk (1,20). During the thawing process the FCM melts out of the frozen bulk leaving nearly pure ice behind. Due to the high density of the FCM and the low density of the ice, ice floats on top and dilutes the top region as it melts (19). Several studies report a tremendous concentration gradient in post-thawed large-scale bottles (17–19).

These gradients can be associated with decreased protein stability. Protein precipitation can occur in the top layer due to lack of stabilisers or at the bottom because of a salting out effect (17,19).

The complex and interdependent processes have been studied using small-scale experiments and specific scale-down devices (SDDs) (2,6,10,14,16,21,22). Such experiments support finding of the optimal formulation, revealing limitations during processing and storage, and unveiling aggregation mechanisms under the chosen FT setup. However, the experiments do not reflect the large-scale FT rates, cryoconcentration, surface area of ice, and exposure time of protein to the numerous stresses and therefore cannot be straightly extrapolated to large-scale (1,20,23,24).

Using Computational Fluid Dynamics (CFD) the heat transfer can be adapted so that mass fractions in small- and large-scale containers experience equivalent stress. Based on this approach SmartFreeZ developed a SDD assisted by CFD following a novel and innovative approach to representatively scale down FT behaviour in a 2 L bottle. The scale-down strategy by CFD has been described previously (24). In contrast to matching FT profiles at the last point to freeze (LPTF) or the last point to thaw (LPTT), simulations were used to divide the bulk into control volumes of approximately 1 mm³. The time between the beginning of freezing in the container and reaching T_g' in the control volume can be calculated. This time span is most detrimental for protein molecules as they become exposed to the ice liquid interface and concentrated together with the other solutes. When passing T_g' , the viscosity of the FCM increases considerably and the decreased mobility prevents aggregation (1,11,25). The thermal history of a protein solution during large-scale FT was translated into the cumulative thermal history in the SDD. The SDD, which matches the thermal history of a large-scale 2 L bottle, consists of a 125 mL bottle surrounded by a unique holder that controls heat exchange.

Previously, we characterised the performance of this innovative SDD during freezing, revealing a good agreement between the SDD and large-scale 2 L bottles (26). It still needs to be evaluated whether this SDD also reflects thawing at large-scale. Large-scale thawing can affect protein stability. Several studies highlighted significant concentration gradients that evolve during thawing and its negative impact on mAb stability (17–19). The thawing process is more time-consuming than freezing under similar conditions. Thus, the protein is exposed to an unfavourable environment significantly longer. If the bottle is not homogenised immediately after thawing, this time span extends even further. Until now no

SDD is marketed that can adequately mimic the thawing process in widely used rectangular bottles.

While our previous study focused on the validation of the SDD during freezing (26), this study aims to validate the SDD in respect of thawing. Therefore, we compared temperature profiles at several locations in the SDD to a 125 mL and a 2 L bottle. We found significant changes in protein and excipient concentrations in the 2 L bottle that were predicted by the SDD. Excipients play a critical role in ensuring protein stability during freezing and subsequent thawing. Therefore, we did not only compare a model mAb but also the buffer species histidine and the surfactant polysorbate 80 (PS80) at different locations in the SDD to the commercially utilised 2 L bottle. We used these results to assess the density gradient that evolves during thawing an, to our knowledge, has not been examined. Finally, we underline the importance of diffusion, which leads to a rapid equilibration of histidine in the SDD.

3.3 Materials and Methods

3.3.1 Materials

Polyethersulfone bottle top and syringe filters (0.2 μm) were purchased from VWR International GmbH (Darmstadt, Germany). Cellon S.A. (Bascharage, Luxembourg) provided 2 L and 125 mL PharmaTainer™ polyethylene terephthalate (PET) bottles.

Dipotassium hydrogen phosphate and potassium dihydrogen phosphate needed for the preparation of the mobile phase for the high-performance liquid chromatography (HPLC) were obtained from Merck KGaA (Darmstadt, Germany).

Novartis AG (Basel, Switzerland) provided a 185 mg/mL IgG1 mAb stock solution in a 20 mM histidine buffer at pH 5.5. For the dilution L-histidine monochloride monohydrate and L-histidine were purchased from Merck KGaA (Darmstadt, Germany). Super Refined™ PS80 from Croda International plc (Snaith, UK) was used.

Dulbecco's phosphate buffered saline 1X (DPBS) without calcium and magnesium chloride, needed for the quantification of PS80, were obtained from Gibco™ (Thermo Fisher Scientific Inc., Waltham, MA, USA). The fluorescence probe 4,4'-dianilino-1,1'-binaphthyl-5,5'-disulfonic acid dipotassium salt (bis-ANS) was purchased from Invitrogen™ (Thermo Fisher Scientific Inc., Waltham, MA, USA).

3.3.2 Scale-Down Device

SmartFreeZ (Porto Salvo, Portugal) provided the SDDs used in this study. A detailed description of the development assisted by CFD can be found elsewhere (26). The specific SDD was designed to predict thawing in a rectangular 2 L PharmaTainer™ bottle

The 3D printed SDD covers a 125 mL PharmaTainer™ bottle and uses 1% ethanol as a phase change liquid to insulate approximately two walls (Figure 1). Thereby, a 125 mL bottle shall be utilised to mimic FT processes in a large-scale 2 L bottle. A soft polymer insert prevents circulation of air between the SDD and the bottle. To avoid radiation, a top cover shields the bottle from above. Two SDDs were used simultaneously in back-to-back orientation during measurements. One SDD, filled with highly purified water, was needed for shielding. A second one containing the sample was used for experiments.

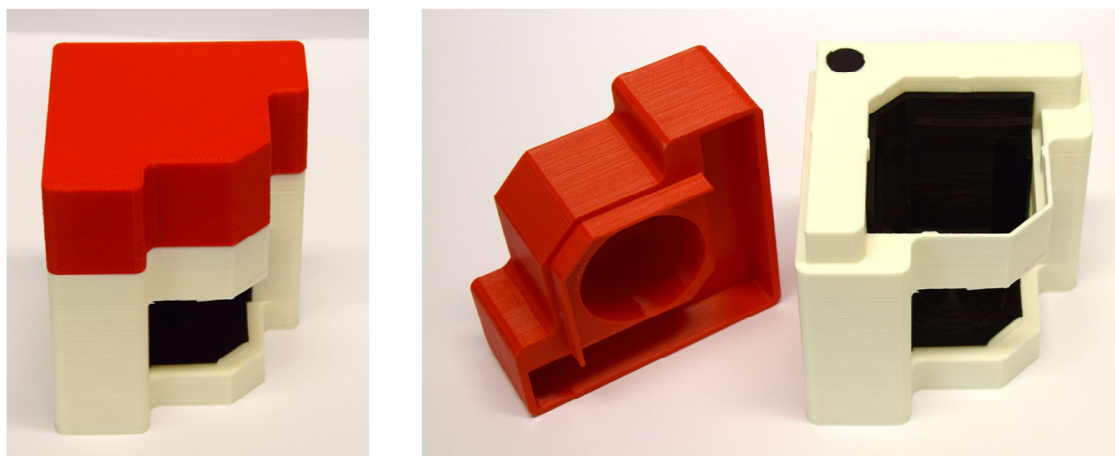


Figure 1 SDD by SmartFreeZ

3.3.3 Preparation of Protein Samples

The stock solution was diluted to a final concentration of 5 mg/mL mAb in 20 mM histidine at pH 5.5. The concentration was determined via UV absorption at 280 nm with a NanoDrop One by Thermo Fisher Scientific Inc. (Waltham, MA, USA). Samples containing 0.4 mg/mL PS80 were prepared by spiking a 10 mg/mL PS80 stock solution. All solutions were filtered through a 0.2 μ m bottle top or syringe filter. 2 L and 125 mL bottles were 80% filled with 1.6 L and 100 mL, respectively.

3.3.4 Temperature Mapping during Thawing

The temperature measurements were performed as previously described (26). Briefly, five type T thermocouples (TCs) connected to an HH520 handheld data logger thermometer (OMEGA Engineering GmbH, Deckenpfronn, Germany) were positioned at half liquid height in the edges and the centre of the 125 mL bottle using stainless steel capillaries (Acufirm Ernst Kratz GmbH, Berlin, Germany) for reproducible placement (Figure 2). A sixth TC (TC 6) was placed at the exact position of TC 1 but at 75% liquid level. Six TCs were arranged at equivalent positions in the 2 L bottle. After acclimatisation at 20 °C for 1 hour in an MKF 240 air-blast climate chamber (Binder GmbH, Tuttlingen, Germany), the chamber was cooled at maximum rate to -40 °C and the temperature held for 10 hours. Subsequently, the temperature was set to 20 °C with maximum heating rate and the solution thawed until the set temperature was reached at all positions. All temperature measurements were executed in triplicates in independent runs.

3.3.5 Analysis of Concentration Gradients after Thawing

Concentration gradients after FT were analysed, once in the 2 L bottle and in triplicates in the SDD and the 125 mL bottle. Samples were taken from nine (2 L bottle) or five (SDD and 125 mL bottle) layers. For each layer five 1 mL samples were taken, four in the edges and a fifth from the centre. Samples were taken with a 1 mL serological glass pipette or 1 mL syringes (B. Braun Melsungen AG, Melsungen, Germany) equipped with a Sterican® 0.80 x 120 mm needle (Braun Melsungen AG, Melsungen, Germany).

3.3.5.1 Quantification of mAb and Histidine

Size-exclusion chromatography (SEC) on an Agilent 1200 HPLC with a diode array detector (Agilent Technologies, Santa Clara, CA, USA) allowed the separation and simultaneous quantification of mAb and histidine. Therefore, samples were diluted 1:4 or 1:10 with mobile phase. After centrifugation for 2 min at 25700 x g with a Heraeus™ Megafuge™ 16R (Thermo Fisher Scientific Inc., Waltham, MA, USA) 5 µL of each sample were injected. As stationary phase a TSKgel G3000 SWxl column (Tosoh Bioscience GmbH, Griesheim, Germany) and as mobile phase a 150 mM potassium phosphate buffer pH 6.5 at a flow rate of 0.4 mL/min were used. Histidine was quantified at 210 nm and mAb at 280 nm by comparing the areas under the curve to standard curves ($R^2 = 0.9999$ and $R^2 = 0.9994$).

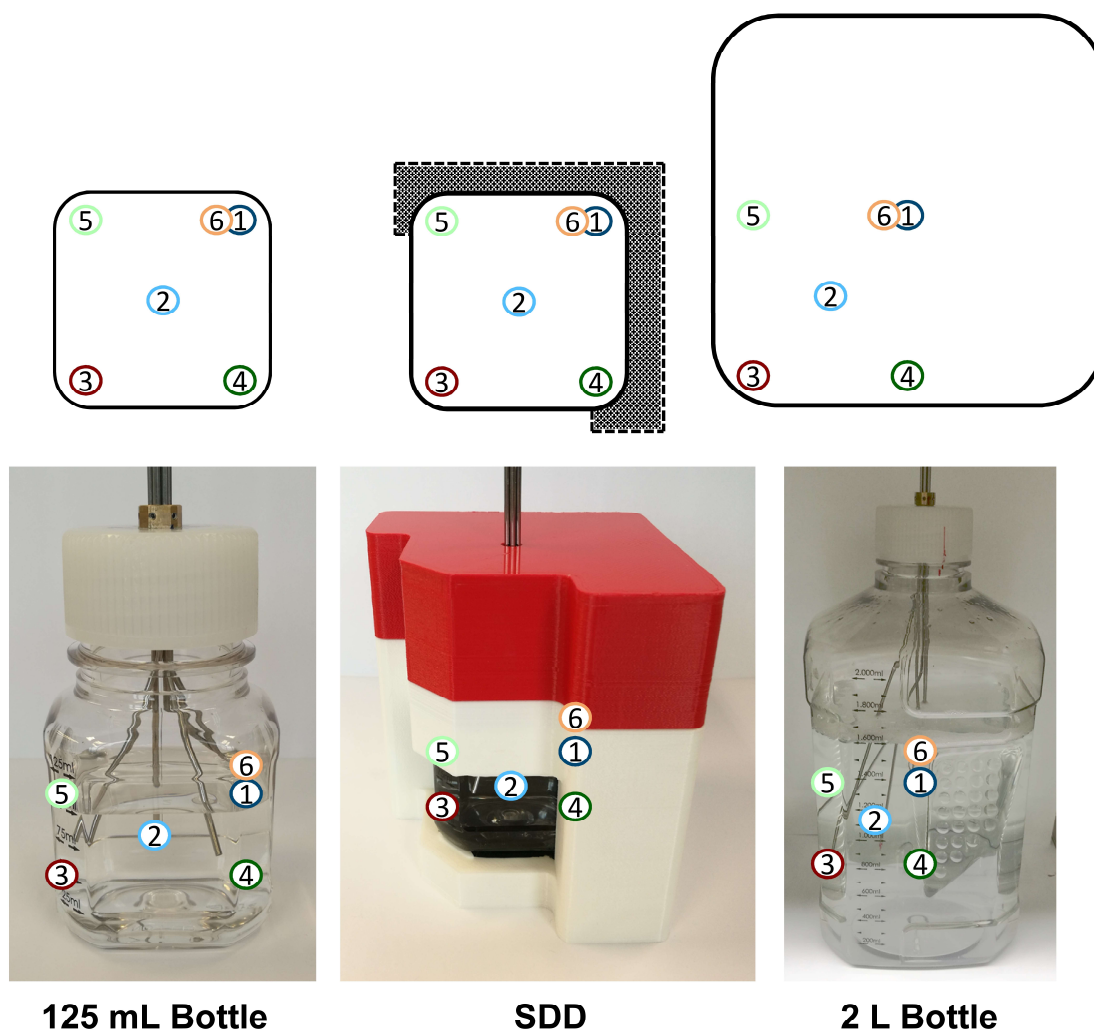


Figure 2 Positioning of TCs in the 125 mL bottle, the SDD and a 2 L PharmaTainer™ bottle (bottom: representative pictures of the positions of the TCs; top: schematic drawing in cross-section from above). Figure adapted from Bluemel et al. (26).

3.3.5.2 Quantification of PS80

The method for the PS80 quantification was adapted from Zheng et al. (27). Samples were diluted 1:4 or 1:10 with DPBS and subsequently heated for 5 min at 99 °C. Afterwards, samples were centrifuged for 5 min at 25700 x g. 190 μ L supernatant were mixed with 10 μ L of 1 mM bis-ANS and vortexed for 5 s. 60 μ L of each sample were analysed in a Varian Cary Eclipse fluorescence spectrophotometer (Agilent Technologies, Santa Clara, CA, USA) using a quartz cuvette at 380 nm excitation and 500 nm emission with both slits set to 5 nm. A calibration curve of PS80 in DPBS allowed the quantification of PS80 between 0.005 mg/mL and 0.15 mg/mL ($R^2 = 0.9988$).

3.3.6 Diffusion of Solution Components after Thawing

The diffusion of mAb and histidine after complete thawing of the solution in the SDD was mapped. Samples were taken after complete thawing of the solution (16 hours at 20 °C) as well as after additional 24 hours and 48 hours. To minimise any possible influence of the removed volume on subsequent results, only 0.25 mL were taken per sample. Samples were obtained from the edges in the top layer, the middle layer and at the bottom. Mixing was avoided by tightly attaching the SDD to the grid in the air-blast climate chamber and taking samples slowly with a 1 mL syringe equipped with a needle.

The DynaPro Plate Reader III (Wyatt Technology, Dernbach, Germany) was used to determine diffusion coefficients of mAb and PS80 via dynamic light scattering. Samples with 10 mg/mL mAb or PS80, respectively, were prepared and filtered. 100 µL of each sample was pipetted in triplicates into a 96-well clear bottom plate (Corning Inc., Corning, NY, USA) and ten acquisitions of 5 s at 25 °C taken. The Dynamics V7.8.2.18 software was used for all calculations.

3.3.7 Analysis of Density Gradients

The changes in density after FT were assessed using a portable density meter DMA 35 Standard (Anton Paar Group AG, Graz, Austria). 15 mL samples were prepared according to concentrations found for each layer during the analysis of the concentration gradients after thawing (Table 1). After a pre-rinse, density was measured in triplicates at room temperature. The density meter extrapolated results to 20 °C.

Table 1 Mean concentrations for mAb, histidine and PS80 as determined after thawing in the 2 L bottle, the SDD and the 125 mL bottle. Corresponding 15 mL samples were prepared to assess changes in density.

Device	Liquid Level Indicator [mL]	mAb [mg/mL]	Histidine [mM]	PS80 [mg/mL]
2 L Bottle	1600	2.72	12.02	0.24
	1400	3.76	15.38	0.32
	1200	4.19	16.85	0.35
	1000	4.19	16.91	0.34
	800	4.50	18.26	0.36
	600	4.62	18.86	0.37
	400	4.69	19.35	0.38
	200	5.90	28.91	0.50
	bottom	14.38	52.97	1.10
SDD	100	1.21	6.40	0.11
	75	1.50	7.71	0.13
	50	2.72	15.17	0.23
	25	4.93	30.31	0.39
	bottom	16.50	44.90	1.32
125 mL Bottle	100	3.13	12.70	0.28
	75	3.38	13.56	0.30
	50	4.20	17.57	0.36
	25	5.41	26.35	0.44
	bottom	9.66	38.76	0.86

3.4 Results and Discussion

3.4.1 Comparison of 3D Temperature Profiles during Thawing

The SDD represents the 2 L bottle by achieving an equivalent cumulative thermal history, although the number of control volumes in the CFD simulations was different. Consequently, temperature measurements at equivalent specific positions do not necessarily match. Nonetheless, temperature measurements are important to understand the influence of the SDD during thawing and to characterise the thawing behaviour in comparison to the 2 L and the 125 mL PharmaTainer™ bottles. Within this work, the term thawing time is used and defined as the time needed until a TC, placed inside the bottle, reaches 1 °C after the beginning of heating. At this point in time, ice is completely melted at this location and the intermediate plateau ends as no further heat of melting is needed. The term process time is used to describe the time required to reach 17 °C after the beginning of heating.

Temperature profiles during thawing were recorded at six positions. In the 125 mL bottle the TCs in the edges (TC 1 and TC 3 – 6) recorded similar profiles (Figure 3). The thawing and process times at these positions were 1.4 h to 1.9 h and 4.1 h to 4.6 h, respectively. The LPTT was the geometrical centre of the bottle (TC 2). Thawing time at this position was 3.4 h, process time was comparable to the TCs in the edges with 4.5 h.

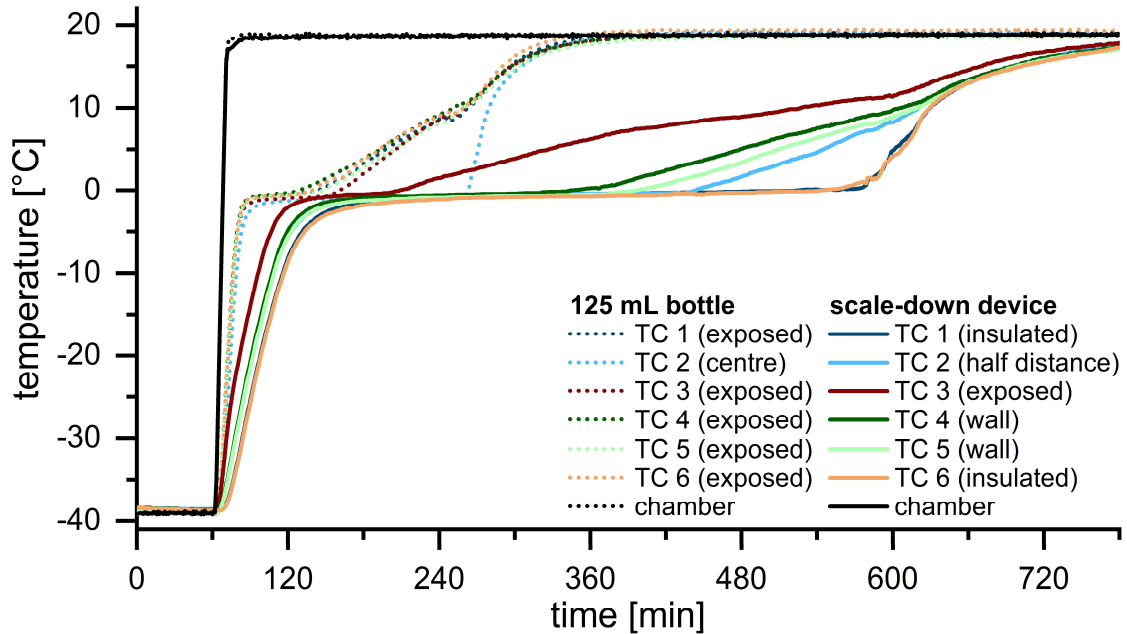


Figure 3 Temperature profiles during thawing in the SDD (solid lines) and the 125 mL bottle (dotted lines).

The time needed for thawing was significantly prolonged by the use of the SDD. In addition, the direction of thawing was changed. Thawing started at the exposed edge (TC 3) after 2.8 h and proceeded towards the geometrical centre (TC 2), where the material was thawed after 6.7 h. Similar thawing profiles were recorded for TC 4 and TC 5 near the walls of the SDD with slightly faster thawing within 5.4 h and 6.1 h, respectively. The LPTT was no longer the geometrical centre of the bottle but instead the insulated region (TC 1 and TC 6). After 8.7 h the ice completely melted at both positions. The difference in height between TC 1 and TC 6 did not influence the outcome. The process time was similar for all mapped positions with approximately 12 h.

The results for the 2 L bottle in comparison to the SDD are shown in Figure 4. Thawing started at the exposed edge (TC 3) and took 1.6 h. At the walls thawing needed 2.3 h (TC 4) and 4.0 h (TC 5) and thereby already exceeded the maximum thawing time at the LPTT in the 125 mL bottle. At half height and half distance thawing was completed after 7.2 h (TC 2). The LPTT was the centre of the 2 L bottle, where complete thawing took 9.3 h

(TC 6) and 10.0 h (TC 1). In contrast to the SDD, the difference in height between TC 1 and TC 6 changed thawing time by about 40 min. In agreement with the 125 mL bottle and the SDD, temperature profiles at the various locations merged after complete thawing. Therefore, process times were similar for all position with approximately 13 h.

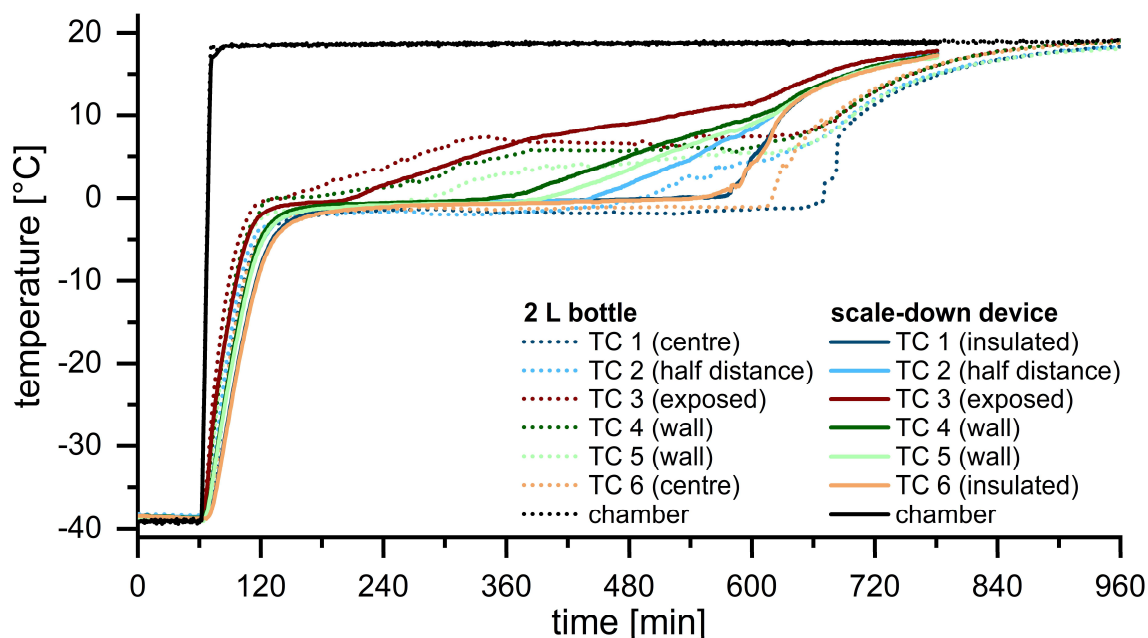


Figure 4 Temperature profiles during thawing in the SDD (solid lines) and the 2 L bottle (dotted lines).

In the 125 mL bottle, thawing started simultaneously at the exposed edges. The walls were heated by the air in the chamber and consequently the edges experienced heat exchange from both adjacent walls. The LPTT was the geometrical centre, the region furthest away from the walls. The latent heat of melting led to a plateau in the observed profiles. As long as the ice was not completely melted, energy was removed from the system to thaw the remaining ice. As soon as no ice was left, the different profiles started to merge. In comparison to the 2 L bottle, thawing time was significantly shorter due to the smaller volume.

The 2 L bottle also started to thaw in the region with highest heat exchange, the exposed edge, followed by the walls. Thawing proceeded towards the geometrical centre. The significantly higher volume increased the time for complete thawing at the LPTT by a factor of three in comparison to the smaller bottle. While the absolute difference in height between TC 1 and TC 6 is small in the SDD and the 125 mL bottle, the higher positioning of TC 6 led to a reduced thawing time in the 2 L bottle. Though more or less stagnant air

in the bottle's headspace provides insulation, heat exchange was still high enough to thaw the bottle also from top towards the centre.

Thawing the same volume in the SDD took significantly longer than in the 125 mL bottle. The SDD provided sufficient insulation to reach adiabatic conditions at two walls. The thawing direction and the heat exchange could be controlled through the exposed window. Consequently, the LPTT was no longer the geometric centre but instead the insulated edge. The temperature profiles were overall similar to those of the 2 L bottle. It took more time to thaw in the exposed regions in the edges and near the walls in the SDD compared to large-scale, whereas there was no difference at half distance. Only slightly less time was needed to completely thaw and fully process the mAb solution in the SDD despite the enormous difference in fill volume by a factor of 16. As the SDD is designed to match the overall thermal history, we expected some regions to thaw slightly faster and others more slowly.

In the SDD thawing was strongly delayed as compared to the 125 mL bottle. Furthermore, the SDD changed the thawing direction so that the LPTT was found in the insulated region and no longer in the geometrical centre. Although thawing and process time were marginally reduced in the SDD, we consider the SDD as representative for the thawing process in large-scale 2 L bottles. In contrast to material consuming large-scale experiments, the SDD needs only a fraction of the volume.

3.4.2 Comparison of Concentration Gradients after Thawing

Significant changes in concentration throughout the container can be expected after large-scale FT of mAb solutions, potentially affecting mAb stability (17–19). A screening study revealed marginal relative concentration gradients upon thawing highly concentrated mAb solution. Thus, higher mAb concentrations would level off changes in concentration upon thawing and impede the validation of the SDD. Consequently, we used a diluted solution to validate the SDD under maximally challenging conditions. We quantified the mAb, the buffering agent histidine, and the surfactant PS80 to picture the distribution of the protein versus its stabilisers. Changes in concentration were expressed as the concentration factor (CF), which is the ratio of the concentration of the sample to the initial concentration.

For the mAb CF values between 0.53 and 3.17 were found in the 2 L bottle (Figure 5). These results are in good agreement with previous studies, showing a highly diluted top region and a strongly increased protein concentration at the bottom (18,19). The CF steadily

decreased with increasing height. In contrast to the three-dimensional cryoconcentration after freezing (26), changes in concentration after thawing can be reduced to a two-dimensional behaviour. CF values were reproducible within each layer. The only exception was the bottom layer with CF values up to 3.17 in the edges, while the centre was significantly less concentrated (CF 2.15). This deviation in the centre is due to the shape of the bottle's bottom. The bottom is slightly elevated in the centre and reflects a region between the bottom layer and the layer directly above. Because of this deviation, centre samples were excluded from further data evaluation.

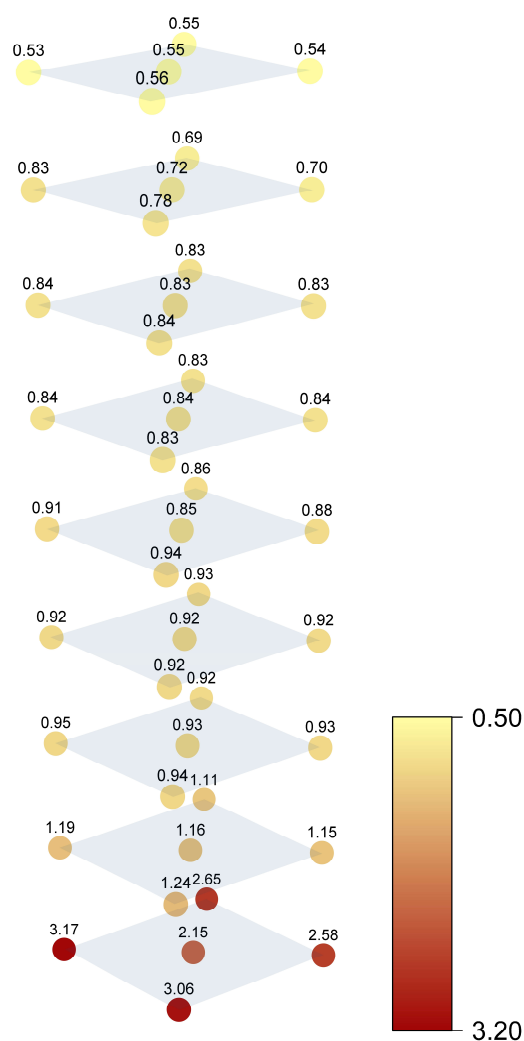


Figure 5 Concentration gradients of the mAb in a 2 L bottle after FT. CF values indicate the change in concentration relatively to the initial mAb concentration of 5 mg/mL.

Figure 6 shows mean and standard deviation of the CF values detected in the edges of the 2 L bottle. The CF values ranged between 0.54 and 2.86 for mAb, 0.61 and 2.79 for PS80 and 0.58 and 2.54 for histidine. All three components behaved similarly in the top and middle region. Near the bottom, maximum mAb and PS80 concentrations were identical.

The histidine CF was slightly higher at the 200 mL liquid level and slightly lower at the bottom compared to the mAb and PS80 CF values.

In the 125 mL bottle, CF values between 0.62 and 1.93 for mAb, 0.65 and 1.99 for PS80 and 0.61 and 1.86 for histidine were found (Figure 6b). For all three components dilution in the top region was only slightly less in comparison to the 2 L bottle. In contrast, the maximum concentrations at the bottom were significantly underestimated. In the second last layer deviations in histidine concentration compared to mAb and PS80 were still noticeable but less pronounced.

CF values between 0.24 and 3.22 for mAb, 0.26 and 3.23 for PS80 and 0.30 and 2.26 for histidine were detected in the SDD (Figure 6c). As previously shown, mAb and PS80 concentrations changed identically throughout the entity. Near the top, similar CF values for mAb, histidine and PS80 were detected. In contrast, histidine concentration was lower at the bottom and higher at 25 mL liquid level. In comparison to the 125 mL bottle, the SDD had a significant impact on concentration changes. The SDD increased the concentration gradient for all three components. Compared to the 2 L bottle, the dilution in the SDD was enhanced. The maximum mAb and PS80 concentrations at the bottom were insignificantly higher, revealing a good predictive power for this critical region. Deviations between the buffer and the remaining components were emphasized in the SDD.

Maity et al. studied the mechanism of gradient formation during thawing and concluded that the FCM, containing proteins and excipients, melts out of the ice, leaving more or less pure ice behind (19). Due to its lower density, this ice floats on top and dilutes the top region during melting. At the same time, fractions with higher solute concentrations exhibit increased densities and sink to the bottom of the bottle. The supplementary information illustrates this draining of the FCM out of the ice during thawing of a dyed sucrose solution in a video.

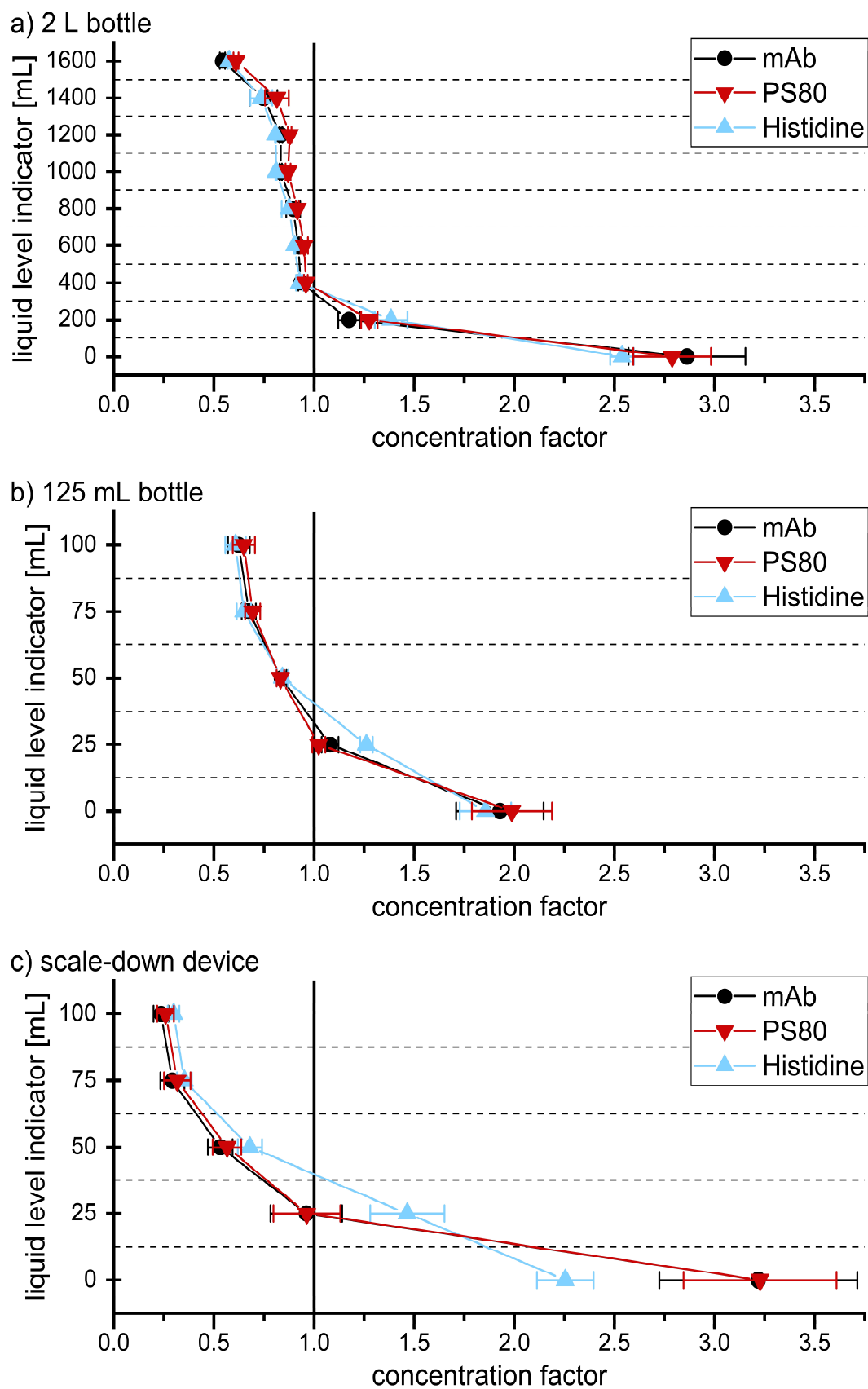


Figure 6 Concentration changes expressed as the CF values after FT of 5 mg/mL mAb, 20 mM histidine and 0.4 mg/mL PS80 in the 2 L bottle, 125 mL bottle and the SDD.

The difference between histidine CF and both the PS80 and the mAb CF in the second last and the bottom layer may be related to the difference in diffusion between the small histidine molecules and the larger mAb and PS80 micelles during and after thawing. The diffusion coefficients of mAb and PS80 micelles with $4.7 \cdot 10^{-11} \text{ m}^2/\text{s}$ and $5.0 \cdot 10^{-11} \text{ m}^2/\text{s}$ are significantly lower compared to that of histidine with $7.3 \cdot 10^{-10} \text{ m}^2/\text{s}$ (28). In order to substantiate this effect, we compared the mAb and histidine concentration in the SDD directly after a thawing period of 16 h and an additional 24 h and 48 h storage period at 20 °C (Figure 7).

After 16 h of thawing a strong concentration gradient was evident for the mAb with CF values between 0.36 and 3.32. This outcome is in good agreement with the results described previously. After additional 24 h and 48 h at 20 °C, the gradient only minimally diminished and showed CF values between 0.39 and 3.00 (+24 h) and between 0.41 and 2.49 (+48 h), indicating that the significant changes of mAb concentration compared to the initial CF value of 1 (representing 5 mg/mL mAb) sustain for more than two days. The dilution of histidine in the top region was similar after 16 h of thawing (CF 0.40), but, as described, the maximum CF was lower (CF 2.26). CF values between 0.60 and 1.58 as well as 0.78 and 1.24 after 24 h and 48 h, respectively, emphasized that the concentration gradient of histidine constantly declined.

The results demonstrate that the larger mAb diffuses much slower into the top region of the SDD than the smaller histidine. This is substantiated by the mAb to histidine ratio. Immediately after thawing, slight differences were already detectable and the ratio progressively shifted towards histidine near the top and towards mAb near the bottom (Figure 7). In the 125 mL bottle similar diffusion as in the SDD can be assumed. In the larger 2 L bottle, histidine diffusion, as described previously, only became noticeable in the two layers near the bottom due to significantly larger height.

Strong changes in concentration of mAb, histidine and PS80 were detected in the 2 L bottle after thawing with a diluted top region and a concentrated bottom region. Faster diffusion of histidine during and after thawing was the driving force for the different behaviour of mAb and PS80 in comparison to the buffering agent. The 125 mL bottle matched concentrations in the top region, but it significantly underestimated the maximum concentrations at the bottom. This outcome can be deduced from a faster thawing in the smaller bottle. Faster thawing allows less time for the FCM to melt out of the ice. Thus, the ice floating on top incorporates a larger fraction of solutes, resulting in a less diluted top

and consequently a less concentrated bottom region. In contrast, the thawing behaviour in the SDD is very similar to the 2 L bottle, enabling the release of the solutes from the ice. The slightly stronger gradient that developed in the SDD reflects a worst-case scenario in respect of changes in concentration after FT in the 2 L bottle.

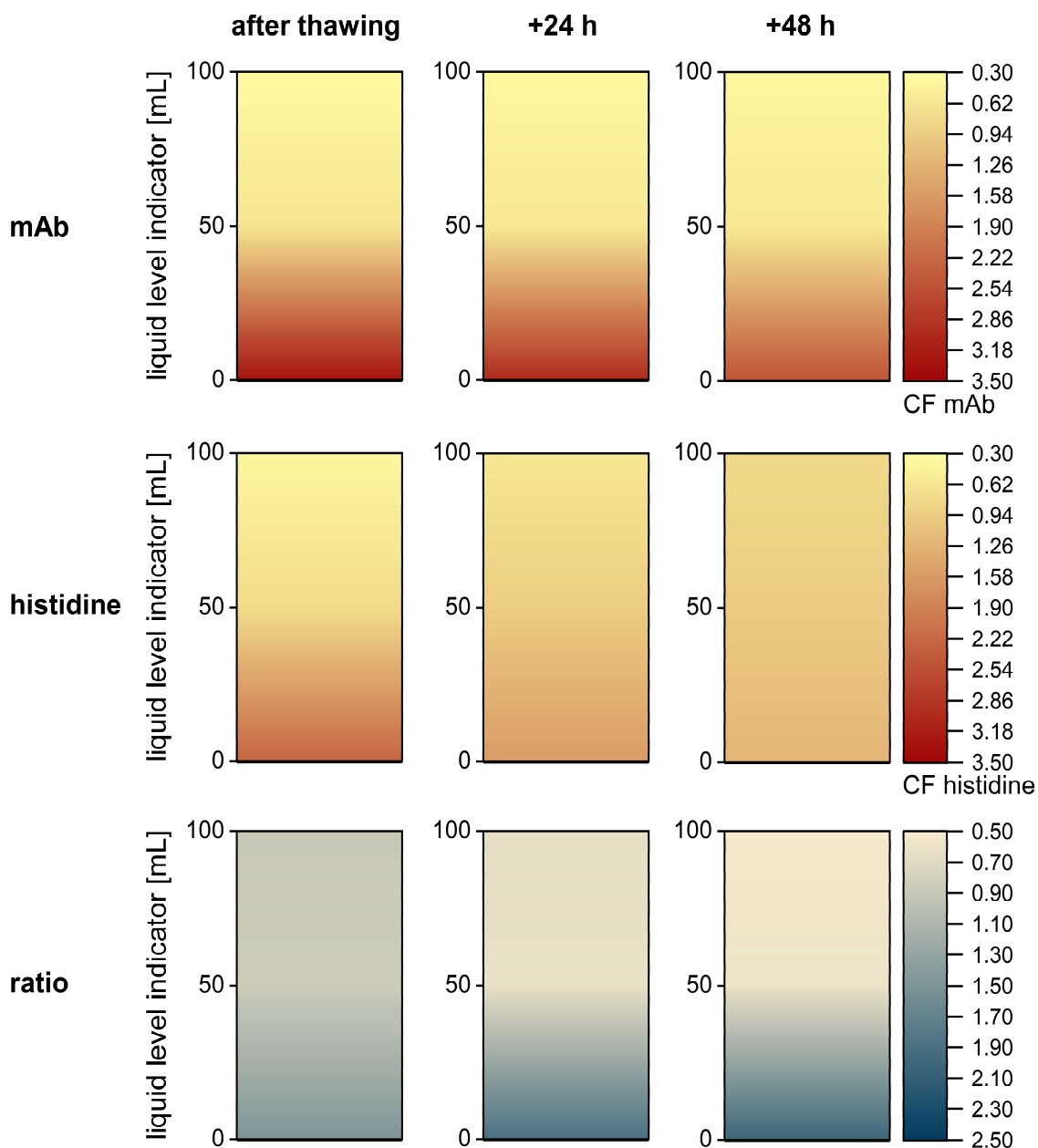


Figure 7 Diffusion of mAb and histidine in the SDD after thawing (16 hours) and additional 24 h and 48 h. Colours of the contour plots indicate changes in CF values of mAb and histidine and the mAb to histidine ratio.

3.4.3 Comparison of Density Gradients after Thawing

During thawing the solutes melt out of the ice, leaving ice behind that floats on top (19). At the same time, fractions with higher solute concentrations and increased density sink to the bottom. Although changes in density are often mentioned as an important factor for cryoconcentration after freezing (9,18), to our knowledge density gradients after thawing in large-scale bottles have not been analysed yet. Therefore, we assessed density gradients in the 2 L bottle, the SDD and the 125 mL bottle. The large volume that is needed for density measurements would inevitably entail interference and mixing of the different layers in the containers. Consequently, we did not take samples directly from the bottle, but prepared samples according to the concentrations found after thawing in the different devices (Table 1).

In the 2 L bottle the density steadily increased with each layer from 1.0003 g/cm^3 at the top to 1.0066 g/cm^3 at the bottom (Figure 8). In the 125 mL bottle the density was 1.0005 g/cm^3 at the top and 1.0042 g/cm^3 at the bottom. The density values in the SDD ranged between 0.9995 g/cm^3 and 1.0066 g/cm^3 . The slight density differences between the three systems reflect the differences in the concentrations of the different components. The minimum density in the 2 L bottle was mimicked by the 125 mL bottle, which had a similarly diluted top region. Density near the bottom was markedly underestimated in the 125 mL bottle, reflecting the lower CF values. The SDD showed a more diluted top layer of lower density. Although mAb and PS80 concentrations in the SDD were slightly higher at the bottom, the densities of the bottom layers were identical in the 2 L bottle and the SDD. We assume that the lower histidine concentration balanced the impact of the increased protein and surfactant concentrations in respect of the density.

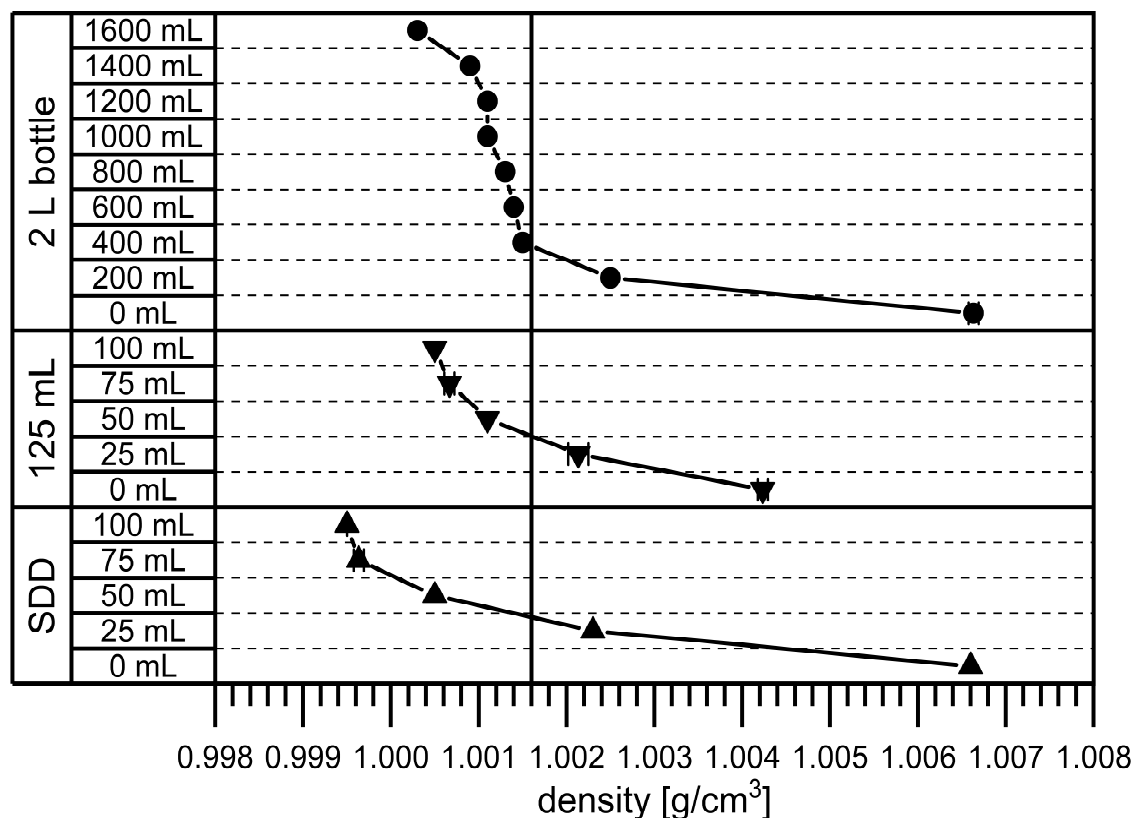


Figure 8 Density gradients in the 2 L bottle, the 125 mL bottle and the SDD. Samples were prepared according to concentrations found in the respective layer indicated by the liquid level indicator. The reference line highlights the initial density of a solution with 5 mg/mL mAb, 20 mM histidine and 0.4 mg/mL PS80.

3.4.4 Perspective

The SDD used in this study was designed to be universally utilised, regardless of the applied FT process. While our previous study validated the performance of the SDD in respect of freezing (26), the presented study proved the reliability of the SDD during thawing in an air-blast chamber. However, further studies are needed to validate that the SDD can be used regardless of the thawing method.

The design of the specific SDD led to a match of the thermal history compared to a large-scale 2 L bottle. The heat exchange can be adapted by a manipulation of the insulation via adaptation of the window of the SDD. SmartFreeZ used this to generate SDDs for rectangular 5 L, 10 L, and 20 L bottles. Studies similar to ours with the 2 L bottle are necessary to proof the reliability of the CFD based concept for the larger bottles.

3.5 Conclusion

In a previous study, we characterised the performance of an innovative SDD during freezing, which requires only a fraction of material in order to mimic and understand the large-scale freezing behaviour of mAb solutions in widely used disposable bottles (26). In this work, we focused on the validation of the SDD in respect of the subsequently following thawing process of mAb solutions. We compared thawing and process times and quantified concentration gradients of mAb, histidine and PS80 in the SDD to 2 L and 125 mL PharmaTainer™ PET bottles. Furthermore, we assessed changes in density.

Temperature profiles in the 2 L bottle revealed a directed thawing towards the centre of the bottle. LPTT was determined in the geometrical centre with 10.0 h for complete thawing. The 125 mL bottle showed significantly reduced thawing times due to the smaller volume, also progressing towards the centre. The SDD changed the direction of thawing so that no longer the centre, but the insulated edge was the LPTT. Hereby, the overall thawing time was strongly increased to 8.7 h. Thus, we consider the SDD as representative for thawing profiles in large-scale 2 L bottles.

Strong changes in concentration built up during thawing of the large-scale 2 L bottle. The top layer displayed a dilution of approximately 50% compared to the initial mAb, PS80 and histidine concentrations, whereas the concentrations near the bottom increased by a factor of 2.8. The concentration gradients in the 125 mL bottle were significantly smaller for all three components. In contrast, the SDD showed a slightly more pronounced concentration gradient. For mAb and PS80, this gradient persisted for days after thawing due to their slow diffusion. In contrast, the gradient significantly levelled off for the smaller histidine, which can rapidly diffuse into the top region. The density gradients reflected the concentration gradients. The SDD showed an identical density at the bottom and an only slightly lower density near the top compared to the large-scale 2 L bottle. Thus, the SDD can predict thawing processes in large-scale 2 L bottles using only a fraction of the material.

Acknowledgements

The Novartis Pharma AG provided us with the mAb stock solution. We give thanks to Miguel A. Rodrigues and Vitor Geraldes from SmartFreeZ who developed and printed the SDD. Eva Lacroix proved a steady hand during taking samples in the SDD and we especially thank her for her help with the diffusion experiment.

References

1. Miller MA, Rodrigues MA, Glass MA, Singh SK, Johnston KP, Maynard JA. Frozen-State Storage Stability of a Monoclonal Antibody: Aggregation is Impacted by Freezing Rate and Solute Distribution. *J Pharm Sci.* 2013 Apr;102(4):1194–208.
2. Roessl U, Leitgeb S, Nidetzky B. Protein freeze concentration and micro-segregation analysed in a temperature-controlled freeze container. *Biotechnol Reports.* 2015 Jun;6:108–11.
3. Hauptmann A, Hoelzl G, Loerting T. Distribution of Protein Content and Number of Aggregates in Monoclonal Antibody Formulation After Large-Scale Freezing. *AAPS PharmSciTech.* 2019 Feb 10;20(2):72.
4. Padala C, Jameel F, Rathore N, Gupta K, Sethuraman A. Impact of Uncontrolled vs Controlled Rate Freeze-Thaw Technologies on Process Performance and Product Quality. *PDA J Pharm Sci Technol.* 2010;64(4):290–8.
5. Rodrigues MA, Miller MA, Glass MA, Singh SK, Johnston KP. Effect of Freezing Rate and Dendritic Ice Formation on Concentration Profiles of Proteins Frozen in Cylindrical Vessels. *J Pharm Sci.* 2011 Apr;100(4):1316–29.
6. Roessl U, Jajcevic D, Leitgeb S, Khinast JG, Nidetzky B. Characterization of a Laboratory-Scale Container for Freezing Protein Solutions with Detailed Evaluation of a Freezing Process Simulation. *J Pharm Sci.* 2014 Feb;103(2):417–26.
7. Rathore N, Rajan RS. Current Perspectives on Stability of Protein Drug Products during Formulation, Fill and Finish Operations. *Biotechnol Prog.* 2008 Jun 6;24(3):504–14.
8. Arsiccio A, McCarty J, Pisano R, Shea J-E. Heightened Cold-Denaturation of Proteins at the Ice–Water Interface. *J Am Chem Soc.* 2020 Mar 25;142(12):5722–30.
9. Kolhe P, Mehta AP, Lary AL, Chico SC, Singh SK. Large-Scale Freezing of Biologics (Part III). *BioPharm Int.* 2012;25(October):40–8.
10. Connolly BD, Le L, Patapoff TW, Cromwell MEM, Moore JMR, Lam P. Protein Aggregation in Frozen Trehalose Formulations: Effects of Composition, Cooling Rate, and Storage Temperature. *J Pharm Sci.* 2015 Dec;104(12):4170–84.
11. Singh SK, Kolhe P, Mehta AP, Chico SC, Lary AL, Huang M. Frozen State Storage Instability of a Monoclonal Antibody: Aggregation as a Consequence of Trehalose Crystallization and Protein Unfolding. *Pharm Res.* 2011 Apr 7;28(4):873–85.
12. Pikal-Cleland KA, Rodríguez-Hornedo N, Amidon GL, Carpenter JF. Protein Denaturation during Freezing and Thawing in Phosphate Buffer Systems: Monomeric and Tetrameric β -Galactosidase. *Arch Biochem Biophys.* 2000 Dec;384(2):398–406.

13. Bhatnagar BS, Pikal MJ, Bogner RH. Study of the Individual Contributions of Ice Formation and Freeze-Concentration on Isothermal Stability of Lactate Dehydrogenase during Freezing. *J Pharm Sci.* 2008 Feb;97(2):798–814.
14. Kueltzo LA, Wang W e. i., Randolph TW, Carpenter JF. Effects of Solution Conditions, Processing Parameters, and Container Materials on Aggregation of a Monoclonal Antibody during Freeze-Thawing. *J Pharm Sci.* 2008 May;97(5):1801–12.
15. Authelin J-R, Rodrigues MA, Tchessalov S, Singh SK, McCoy T, Wang S, et al. Freezing of Biologicals Revisited: Scale, Stability, Excipients, and Degradation Stresses. *J Pharm Sci.* 2020 Jan;109(1):44–61.
16. Hauptmann A, Podgoršek K, Kuzman D, Srčić S, Hoelzl G, Loerting T. Impact of Buffer, Protein Concentration and Sucrose Addition on the Aggregation and Particle Formation during Freezing and Thawing. *Pharm Res.* 2018 May 19;35(5):101.
17. Mehta SB, Subramanian S, D’Mello R, Brisbane C, Roy S. Effect of protein cryoconcentration and processing conditions on kinetics of dimer formation for a monoclonal antibody: A case study on bioprocessing. *Biotechnol Prog.* 2019 Jul 15;35(4):1–7.
18. Kolhe P, Badkar A. Protein and solute distribution in drug substance containers during frozen storage and post-thawing: A tool to understand and define freezing-thawing parameters in biotechnology process development. *Biotechnol Prog.* 2011 Mar;27(2):494–504.
19. Maity H, Karkaria C, Davagnino J. Mapping of solution components, pH changes, protein stability and the elimination of protein precipitation during freeze–thawing of fibroblast growth factor 20. *Int J Pharm.* 2009 Aug;378(1–2):122–35.
20. Rodrigues MA, Balzan G, Rosa M, Gomes D, de Azevedo EG, Singh SK, et al. The importance of heat flow direction for reproducible and homogeneous freezing of bulk protein solutions. *Biotechnol Prog.* 2013 Sep;29(5):1212–21.
21. Zhang A, Singh SK, Shirts MR, Kumar S, Fernandez EJ. Distinct Aggregation Mechanisms of Monoclonal Antibody Under Thermal and Freeze-Thaw Stresses Revealed by Hydrogen Exchange. *Pharm Res.* 2012 Jan 30;29(1):236–50.
22. Wöll AK, Hubbuch J. Investigation of the reversibility of freeze/thaw stress-induced protein instability using heat cycling as a function of different cryoprotectants. *Bioprocess Biosyst Eng.* 2020 Jul 20;43(7):1309–27.
23. Shamlou PA, Breen LH, Bell W V., Pollo M, Thomas BA. A new scaleable freeze–thaw technology for bulk protein solutions. *Biotechnol Appl Biochem.* 2007 Jan 1;46(1):13.
24. Geraldés V, Gomes DC, Rego P, Fegley D, Rodrigues MA. A New Perspective on Scale-Down Strategies for Freezing of Biopharmaceuticals by Means of Computational Fluid Dynamics. *J Pharm Sci.* 2020 Jun;109(6):1978–89.
25. Pansare SK, Patel SM. Practical Considerations for Determination of Glass Transition Temperature of a Maximally Freeze Concentrated Solution. *AAPS PharmSciTech.* 2016 Aug 18;17(4):805–19.

26. Bluemel O, Buecheler JW, Rodrigues MA, Geraldes V, Hoelzl G, Bechtold-Peters K, et al. Cryoconcentration and 3D Temperature Profiles During Freezing of mAb Solutions in Large-Scale PET Bottles and a Novel Scale-Down Device. *Pharm Res.* 2020 Sep 30;37(9):179.
27. Zheng S, Smith P, Burton L, Adams ML. Sensitive fluorescence-based method for the rapid determination of polysorbate-80 content in therapeutic monoclonal antibody products. *Pharm Dev Technol.* 2015 Oct 3;20(7):872–6.
28. Winkelmann J. Diffusion coefficient of L-histidine in water. In: *Diffusion in Gases, Liquids and Electrolytes* [Internet]. Berlin, Heidelberg: Springer Berlin Heidelberg; 2018. p. 864–864. Available from: https://materials.springer.com/lb/docs/sm_lbs_978-3-662-54089-3_537

Chapter 4 The Effect of mAb and Excipient Cryoconcentration on Long-Term Frozen Storage Stability – Part 1: Higher Molecular Weight Species and Subvisible Particle Formation

Oliver Bluemel¹, Moritz Anuschek^{1,2}, Jakob W. Buecheler³, Georg Hoelzl⁴, Karoline Bechtold-Peters³, Wolfgang Friess¹

1 Pharmaceutical Technology and Biopharmaceutics, Department of Pharmacy, Ludwig-Maximilians-Universitaet Muenchen, 81377 Munich, Germany

2 Currently: Oral Pilot and Process Development, Novo Nordisk A/S, 2760 Måløv, Denmark and Department of Pharmacy, Københavns Universitet, 1165 Copenhagen, Denmark

3 Technical Research and Development, Novartis Pharma AG, 4002 Basel, Switzerland

4 Sandoz GmbH, 6336 Langkampfen, Austria

Author contributions:

O.B., M.A., W.F., and K.B.P. conceived the study. O.B. prepared long-term storage experiments, performed size-exclusion chromatography and subvisible particle analysis, and evaluated the data. M.A. performed lyophilisation and differential scanning calorimetry measurements. O.B. wrote the paper. W.F., M.A., J.W.B., K.B.P., and G.H. contributed to the discussion of the results and revised the manuscript. W.F. and K.B.P. supervised the work.

4.1 Abstract

Purpose: Cryoconcentration upon large-scale freezing of monoclonal antibody (mAb) solutions leads to regions of different ratios of low molecular weight excipients, like buffer species or sugars, to protein. This study focused on the impact of the buffer species to mAb ratio on aggregate formation after frozen storage at -80 °C, -20 °C, and -10 °C after 6 weeks, 6 months, and 12 months.

Methods: An optimised sample preparation was established to measure T_g' of samples with different mAb to histidine ratios via differential scanning calorimetry (DSC). After storage higher molecular weight species (HMWS) and subvisible particles (SVPs) were detected using size-exclusion chromatography (SEC) and FlowCam, respectively.

Results: For all samples, sigmoidal curves in DSC thermograms allowed to precisely determine T_g' in formulations without glass forming sugars. Storage below T_g' did not lead to mAb aggregation. Above T_g' , at -20 °C and -10 °C, small changes in mAb and buffer concentration markedly impacted stability. Samples with lower mAb concentration showed increased formation of HMWS. In contrast, higher concentrated samples led to more SVPs. A shift in the mAb to histidine ratio towards mAb significantly increased overall stability.

Conclusion: Cryoconcentration upon large-scale freezing affects mAb stability, although relative changes compared to the initial concentration are small. Storage below T_g' completely prevents mAb aggregation and particle formation.

Keywords: cryoconcentration, frozen storage, large-scale freezing, monoclonal antibody, stability

Abbreviations: DSC – Differential scanning calorimetry, FCM - Freeze-concentrated matrix, HMWS – Higher molecular weight species, HPLC - High-performance liquid chromatography, mAb – Monoclonal antibody, PES – Polyethersulfone, SEC – Size-exclusion chromatography, SVP – Subvisible particle, T_g' – Glass transition temperature of the maximally freeze-concentrated solution

4.2 Introduction

Therapeutic monoclonal antibodies (mAbs) are essential in the treatment of numerous diseases and part of a rapidly growing market (1–3). A common processing step to enhance chemical and physical stability and to minimise the risk of microbial growth is to freeze bulk drug substance (4–6). Frozen storage and transportation offer flexibility during manufacturing and eliminates the risk of shaking and foaming (4–7). Besides sustainability concerns, mechanical stress, local pressure, the formation of air bubbles, and oxidation are considerable drawbacks as recently highlighted (8). Others, such as the destabilising effect of the cold temperature itself (9), crystallisation of buffer components or cryoprotectants (10–12), interfaces (2,13), and cryoconcentration on a microscopic and macroscopic scale (3,14,15) are well known but still not completely understood. Thereby, freezing, which seems to be a simple and easily controllable process, becomes complex and the contribution of each stress on the overall stability nearly impossible to assess.

Often small-scale studies, typically performed in vials or tubes, are used to find the optimal formulation and ideal freezing and thawing conditions or to unveil unforeseen events (11,16–18). Connolly et al. highlighted the effects of formulation composition, cooling rate and storage temperature on mAb stability (11). They found that trehalose crystallisation is a considerable event during storage above the glass transition temperature of the maximally freeze concentrated solution (T_g') at -8 °C, -14 °C and -20 °C. Storage below T_g' at -40 °C prevented crystallisation and consequently protein aggregation. These outcomes can be associated with the negligible molecular mobility below T_g' . Hauptmann et al. examined the particle formation caused by multiple freeze-thaw cycles with the focus on processing rates, mAb concentration and buffer formulation, but did not investigate the effect on storage stability (17).

In a previous study, we examined cryoconcentration in a rectangular 2 L bottle after freezing of mAb in pure histidine buffer (19). Microscopically, ice crystals grow into unfrozen regions and exclude other formulation components. The mAb and excipients form a freeze-concentrated matrix (FCM) in between these ice crystals. Macroscopically, at the freezing front the solutes are transported away by natural convection and diffusion. This creates a heterogeneous distribution of solutes. In contrast to the previous scientific consensus that proteins and excipients freeze-concentrate to the same extent (20), recent studies show that large proteins are entrapped in the ice to a larger extent than small

excipients (15,21). This is in accordance with our study, where significant shifts in the mAb to histidine ratio were observed (19). As the ion concentration respectively the mAb to low molecular weight excipient ratio in the FCM vary throughout the container, also self-interaction of the mAb and colloidal stability vary. In addition, T_g' as the temperature at which the highly viscous FCM forms a glass will differ with solution composition (8,11,22,23). Ultimately, the mAb stability at different spots of large containers can vary.

To our knowledge, no study has connected the cryoconcentration associated with a change in mAb to excipient ratio after freezing in large-scale containers to long-term frozen storage. To assess the impact of this cryoconcentration and the shifted ratios of mAb and histidine, we prepared samples according to the concentrations found previously (Figure 1). In the current study, we focused on the areas with minimum and maximum mAb and histidine concentrations. We stored these formulations small-scale at $-80\text{ }^\circ\text{C}$, $-20\text{ }^\circ\text{C}$, or $-10\text{ }^\circ\text{C}$ for up to 12 months and analysed mAb aggregation. Storage below T_g' at $-80\text{ }^\circ\text{C}$ completely prevented any formation of higher molecular weight species (HMWS) and subvisible particles (SVPs). Storage above T_g' at $-20\text{ }^\circ\text{C}$ led to significant aggregation and SVP levels after 6 months and 12 months. This effect was boosted at $-10\text{ }^\circ\text{C}$. Long-term storage stability above T_g' was affected by ΔT between T_g' and the storage temperature, the ionic strength in the non-solidified FCM, and mAb concentration. Significant differences in mAb stability resulted in the samples reflecting the solute concentration variants as a consequence of cryoconcentration. Transferred to regions in a 2 L bottle the small-scale experiments indicate that highly concentrated areas in the centre and the top region in a 2 L bottle can be associated with significant formation of SVPs. In contrast, the diluted core in the geometrical centre is more prone to formation of soluble mAb aggregates. The samples containing minimum histidine, representative for the areas at the wall, showed the highest stability.

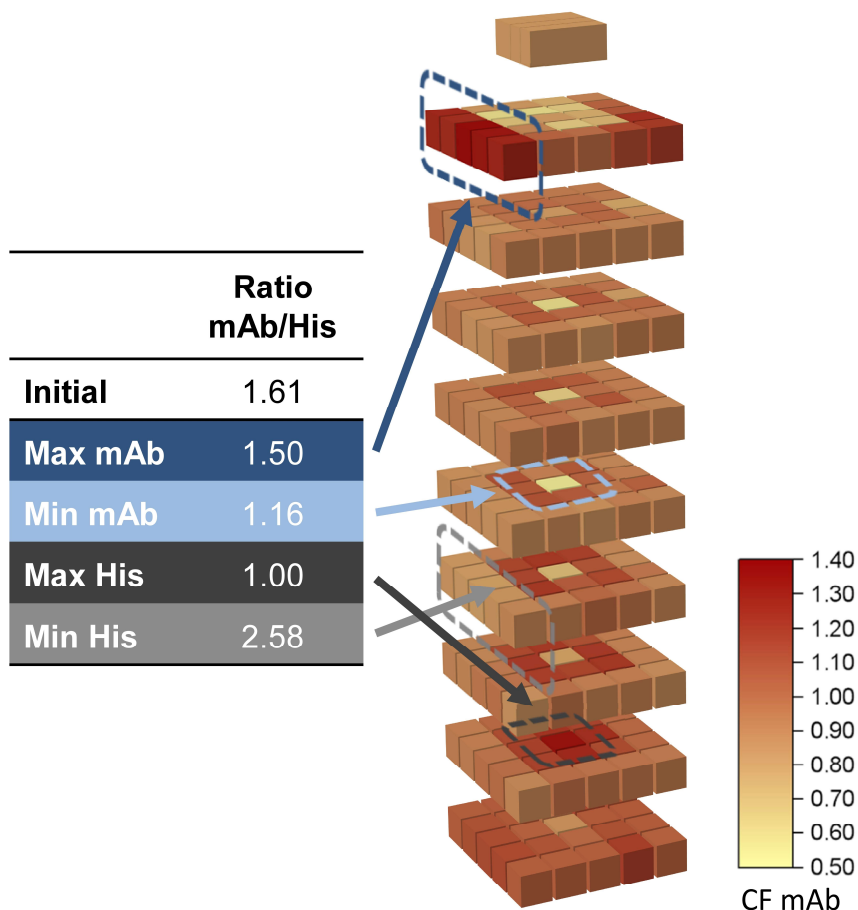


Figure 1 Changes in mAb concentration after freezing a mAb solution in histidine in a 2 L bottle. Details were published and discussed previously (19). The legend highlights the cryoconcentration factor, which is the ratio of the mAb concentration of the sample to the initial mAb concentration. The mAb to histidine ratios for selected samples are given in the table. Corresponding areas are highlighted for visualisation.

4.3 Materials and Methods

4.3.1 Materials

An IgG1 mAb stock solution in histidine buffer at pH 5.5 was provided by Novartis AG (Basel, Switzerland). L-histidine and L-histidine monochloride monohydrate were obtained from Merck KGaA (Darmstadt, Germany).

Potassium dihydrogen phosphate and dipotassium hydrogen phosphate were purchased from Merck KGaA (Darmstadt, Germany).

Sucrose was obtained from Sigma-Aldrich (Steinheim am Albuch, Germany).

VWR International GmbH (Darmstadt, Germany) provided 0.2 µm polyethersulfone (PES) membrane syringe filters. 2R glass vials were purchased from SCHOTT AG (Mainz,

Germany). FluroTec® lyophilisation stoppers from West Pharmaceuticals (Eschweiler, Germany) were used.

4.3.2 Sample Preparation

The mAb stock solution was diluted to mAb to histidine ratios given in Figure 1. Different histidine buffers at pH 5.5 were prepared to reach the final histidine concentrations. Due to confidentiality, the exact composition of the samples may not be revealed. The mAb concentration was controlled with a NanoDrop One (Thermo Fisher Scientific Inc., Waltham, Massachusetts, USA) via UV absorption at 280 nm. Samples were filtered through 0.2 µm PES membrane filters. Three 2R glass vials for each formulation and each time point were filled with 1 mL and semi-stoppered.

All vials were frozen in a Christ Epsilon 2-6D LSCplus (Martin Christ Gefriertrocknungsanlagen GmbH, Osterode am Harz, Germany). Samples were arranged in the centre of lyophilisation trays surrounded by two rows of vials filled with 10% (w/V) sucrose. Vials were cooled with 1 K/min to -5 °C and this temperature held for 60 min. During this temperature plateau, controlled nucleation was induced using the LyoCoN ice fog technology (Martin Christ Gefriertrocknungsanlagen GmbH, Osterode am Harz, Germany). This technique introduces ice crystals for seeding of vials by aeration through the condenser. Subsequently, samples were cooled to -40 °C with 1 K/min. Thereby similar ice morphology should be achieved in all samples. Afterwards, the vials were transferred to precooled -10 °C (Köttermann GmbH, Uetze, Germany), -20 °C (Liebherr, Bulle, Switzerland) and -80 °C freezers (LAUDA-GFL GmbH, Burgwedel, Germany).

4.3.3 Stability Analysis

After 12 h of acclimatisation triplicates of each formulation were thawed at room temperature on the laboratory bench and analysed as t₀. After 6 weeks, 6 months and 12 months further samples (n = 3) were thawed and analysed.

4.3.3.1 Flow Imaging Microscopy

SVPs were characterised with a FlowCam 8100 (Fluid Imaging Technologies, Inc., Scarborough, Maine, USA) equipped with a 10x magnification cell. Particles were counted using 160 µL sample volume, a flow rate of 0.15 mL/min, an auto image frame rate of 28 frames/s and a sampling time of 60 s. Distance to the nearest neighbour for particle identification was set to 3 µm. Particle segmentation thresholds of 10 for light and 13 for

dark pixels were defined. Particle size was reported as the equivalent spherical diameter. The VisualSpreadsheet® 4.7.6 software was used for measuring and processing.

4.3.3.2 Size-Exclusion Chromatography

Size-exclusion chromatography (SEC) on an Agilent 1200 high-performance liquid chromatography (HPLC) system equipped with a diode array detector (Agilent Technologies, Santa Clara, California, USA) set to 220 nm was used to quantify HMWS. A TSKgel G3000 SWxl column (Tosoh Bioscience GmbH, Griesheim, Germany) as stationary phase, a 150 mM potassium phosphate buffer pH 6.5 at a flow rate of 0.4 mL/min as mobile phase, and 5 µl injection volume were used. Prior to injection all samples were centrifuged 2 min at 25.700 x g with a Heraeus™ Megafuge™ 16R (Thermo Fisher Scientific Inc., Waltham, Massachusetts, USA). Agilent OpenLAB Data Analysis Software 2.1 was used to analyse the chromatograms.

4.3.4 Determination of T_g'

Samples of different mAb to histidine ratios were prepared as described in 4.3.2. 2 mL of each solution was filled into 2R glass vials and arranged in the centre of a lyophilisation tray surrounded by vials filled with 10% (w/V) sucrose. Lyophilisation was carried out with the Christ Epsilon 2-6D LSCplus (Martin Christ Gefriertrocknungsanlagen GmbH, Osterode am Harz, Germany). Samples were frozen to -40 °C with a ramp of 1 K/min. Temperature was increased to -20 °C with 1 K/min and primary drying carried out for 35 h at a pressure of 0.09 mbar. For secondary drying a 0.3 K/min ramp to 30 °C was applied and shelf temperature held for 4 h at 0.09 mbar. Afterwards, samples were stoppered at 600 mbar in a nitrogen atmosphere. Lyophilisates were reconstituted with highly purified water to 100 mg/mL mAb and after 24 h, to ensure complete dissolution, differential scanning calorimetry (DSC) measurements were carried out.

DSC thermograms were acquired with the DSC821® (METTLER TOLEDO, Columbus, Ohio, USA). Aluminium crucibles (METTLER TOLEDO, Columbus, Ohio, USA) were filled with 20 µL. An empty crucible of the same type was used as reference. Samples were cooled from 25 °C to -60 °C with a rate of 10 K/min. After isothermal hold for 1 min, samples were analysed while heated to 25 °C at 3 K/min. T_g' was determined as the inflection point of the sigmoidal glass transition. Data analysis was carried out with the STARE-Software (METTLER TOLEDO, Columbus, Ohio, USA).

4.4 Results

4.4.1 Long-Term Storage at -80 °C

The formation of HMWS as well as SVPs was analysed at the start and after storage for 6 weeks, 6 months, and 12 months. The results for storage at -80 °C are displayed in Figure 2. All samples contained approximately 1.5% HMWS at the start of the experiment. This level did not increase during storage, regardless of the sample composition.

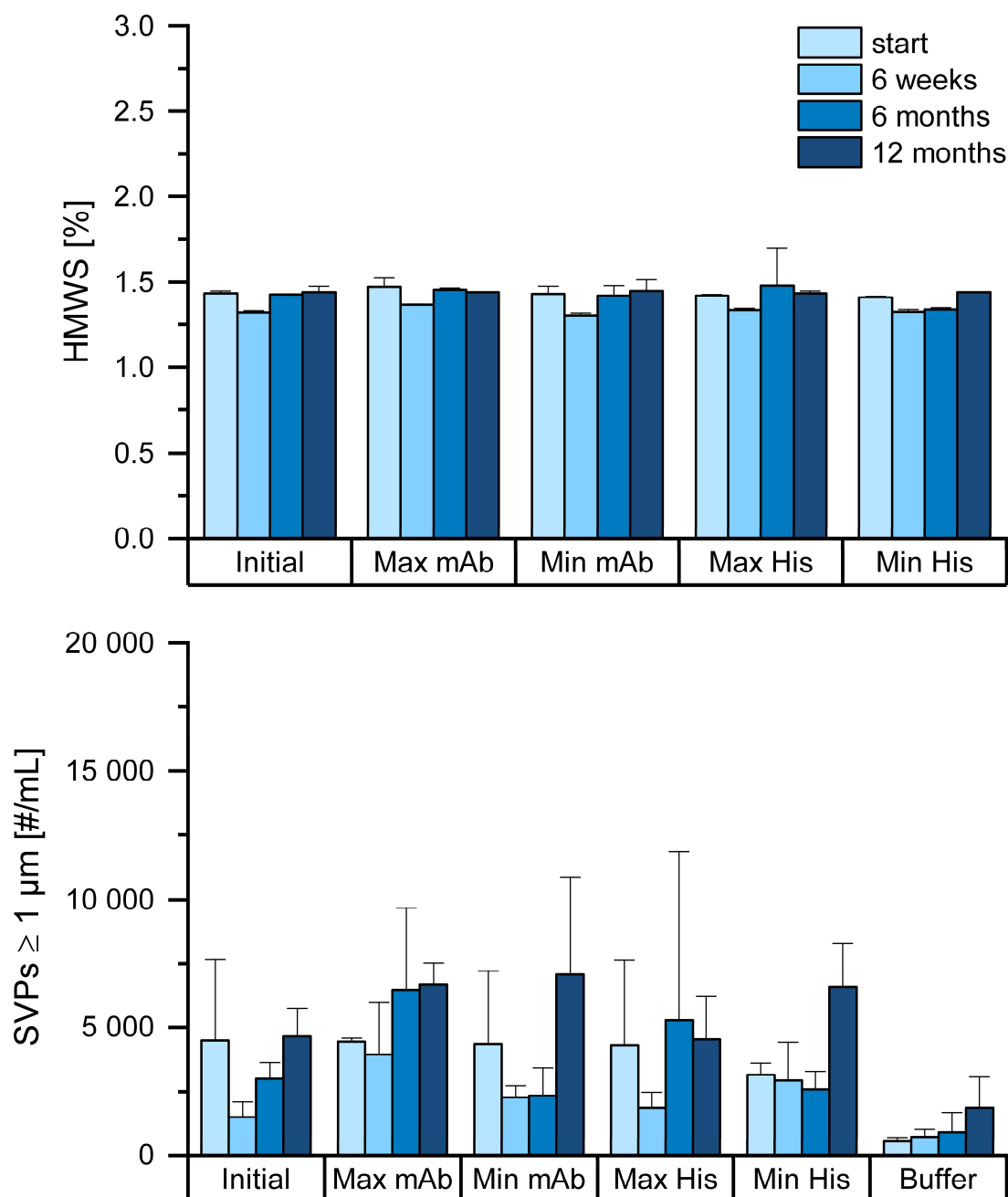


Figure 2 HMWS and SVPs after storage at -80 °C up to 12 months.

The histidine buffer control sample showed 500 SVPs $\geq 1 \mu\text{m}$ per mL at the start and only a minor increase to 1 900 after 12 months. All mAb containing samples displayed approximately 4 000 SVPs at t0. These t0 samples had been frozen, stored at the intended temperature for 12 h, and thawed. No significant increase in SVP level could be detected during long-term storage at -80 °C.

4.4.2 Long-Term Storage at -20 °C

All samples stored at -20 °C again started with approximately 1.5% HMWS (Figure 3). After 6 weeks, the soluble aggregate levels did not increase in any of the samples. In general, the increase after 6 months was still moderate, considering the following 12 months point and the changes observed after storage at -10 °C (see 4.4.3). After 6 months, the HMWS reached 2.2% in samples with the initial composition (mAb to histidine ratio 1.61), while samples representing maximum (ratio 1.50) and minimum mAb (ratio 1.16) concentration regions in the 2 L bottle displayed 1.5% and 2.0%, respectively. The highest aggregation level of 2.7% was observed in maximum histidine samples (ratio 1.00), whereas minimum histidine samples (ratio 2.58) did not show an increase in HMWS. After 12 months at -20 °C, samples with the initial concentrations contained 2.8% HMWS. Maximum mAb (2.1%), minimum histidine (1.8%), and maximum histidine (2.4%) showed less increase. The highest HMWS levels were found for minimum mAb samples (3.4%).

After 6 months, SVP levels did not increase significantly and remained below 10 000 particles per mL in all cases. The buffer control stored at -20 °C displayed 1 700 SVPs per mL after 12 months compared to 900 at t0. Also, after 12 months the total particle count stayed low for the initial concentrations (12 700), the minimum mAb (7 000), and the minimum histidine samples (9 800). In contrast, approximately 230 000 SVPs were counted in maximum mAb and 570 000 in maximum histidine samples, both containing the highest absolute mAb concentration.

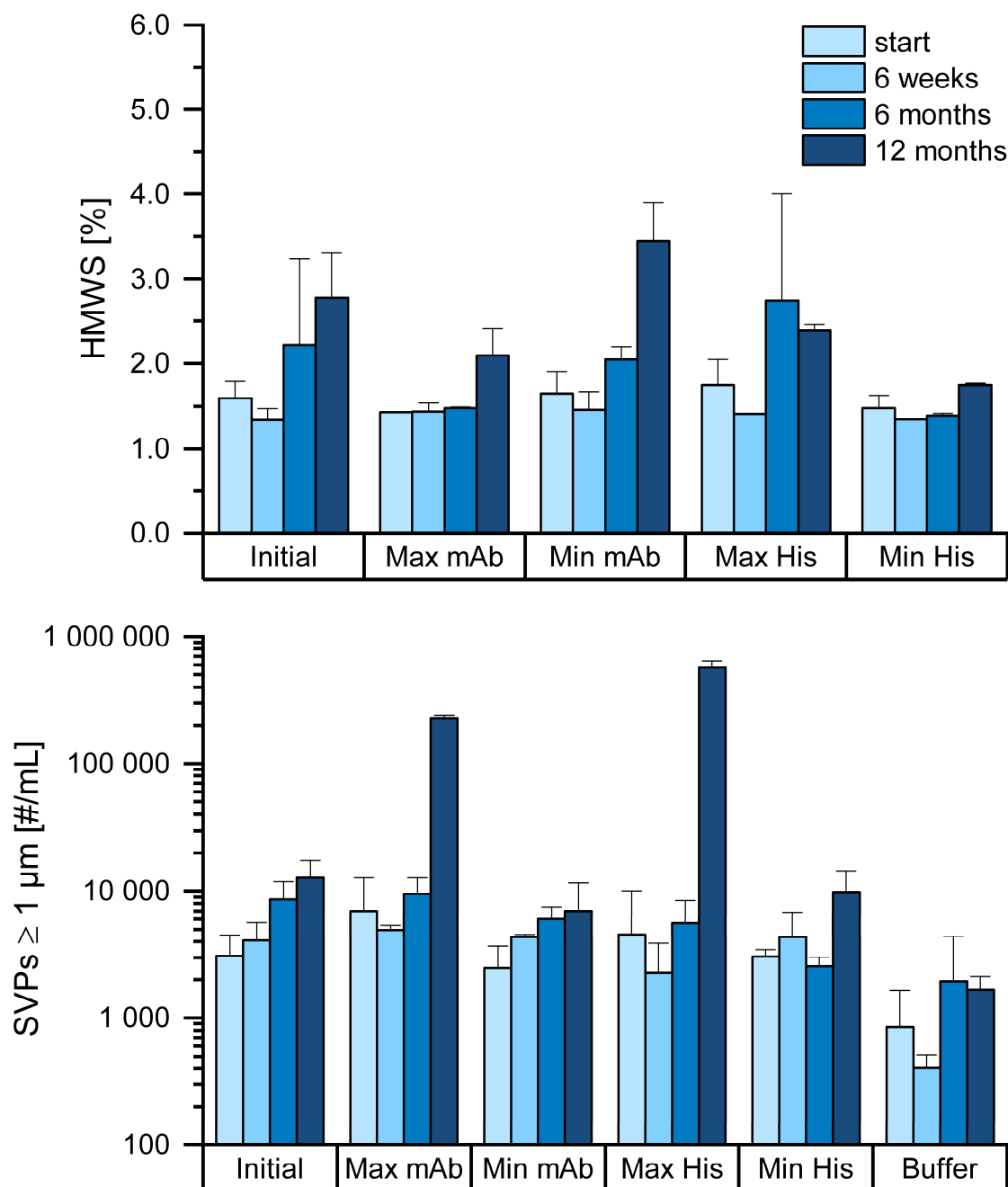


Figure 3 HMWS and SVPs after storage at $-20\text{ }^{\circ}\text{C}$ up to 12 months.

4.4.3 Long-Term Storage at $-10\text{ }^{\circ}\text{C}$

Figure 4 shows that HMWS did not form over 6 weeks storage at $-10\text{ }^{\circ}\text{C}$. After 6 months and 12 months, the HMWS increase for the different formulations was similar to the change at $-20\text{ }^{\circ}\text{C}$, but aggregation was much more pronounced. After 6 months storage, samples with the initial concentrations displayed 3.5% HMWS. The numbers were lower in maximum mAb (2.7%), maximum histidine (2.3%), and minimum histidine (1.6%), but higher in the minimum mAb (4.1%) sample. Similar trends were seen after 12 months.

The Effect of mAb and Excipient Cryoconcentration on Long-Term Frozen Storage Stability – Part 1: Higher Molecular Weight Species and Subvisible Particle Formation

Samples being representative for the initial formulation conditions displayed 4.0% HMWS. Maximum mAb (3.6%), maximum histidine (2.7%), and minimum histidine (1.8%) again contained less soluble aggregates, whereas minimum mAb (5.1%) samples were least stable.

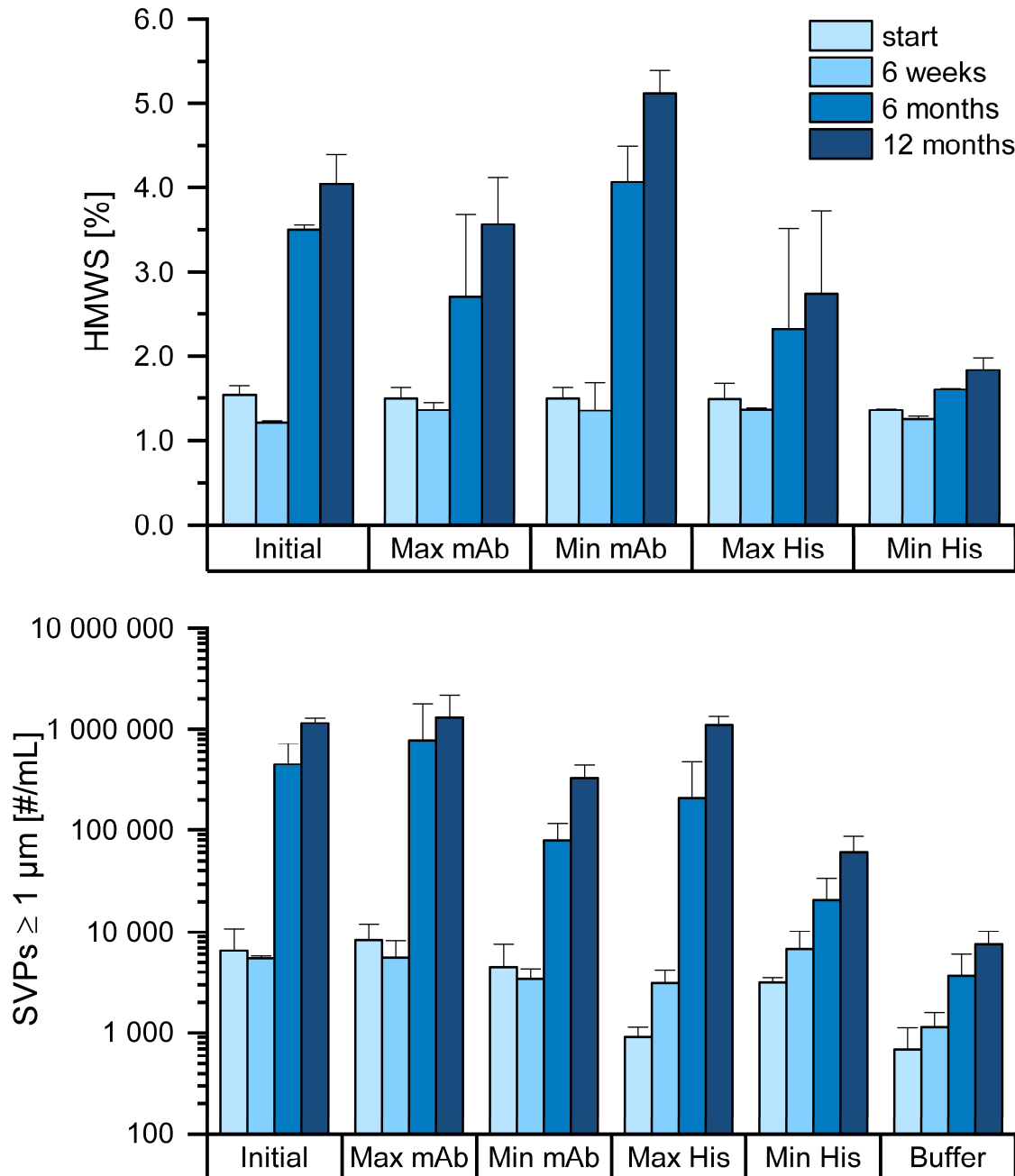


Figure 4 HMWS and SVPs after storage at $-10 \text{ }^\circ\text{C}$ up to 12 months.

In the histidine buffer control SVP levels increased to 7 500 SVPs $\geq 1 \mu\text{m}$ per mL after 12 months. For all samples, SVPs remained low after 6 weeks storage at $-10 \text{ }^\circ\text{C}$. In contrast, particle levels were increased in mAb containing samples after 6 months. Samples with the

initial concentration showed approximately 450 000 SVPs. Minimum mAb and minimum histidine samples displayed only 79 300 and 20 700 SVPs, respectively. Maximum histidine (207 400) and maximum mAb (777 200), both containing the highest absolute mAb concentration, led to similar particle levels as the formulation representing the initial mAb concentration. Substantial SVP formation was seen after twelve-month storage at -10 °C. The trends were the same as after 6 months. In samples representing the initial concentrations 1 150 800 SVPs \geq 1 μ m per mL were detected. Maximum mAb (1 316 000) and maximum histidine (1 092 200) gave similar counts. In contrast, samples with minimum mAb and minimum histidine showed tremendously less SVPs \geq 1 μ m per mL with only 330 100 and 60 400, respectively.

4.4.4 Determination of T_g'

After lyophilisation and subsequent reconstitution with less water, inflection points could automatically be detected by the DSC software in all DSC thermograms (Figure 5). The highest T_g' (-30.9 °C) was measured for samples containing minimum histidine and consequently the highest mAb to histidine ratio of 2.58. T_g' shifted towards lower temperatures the more the ratio shifted towards histidine. At the initial ratio of 1.61 a T_g' at -35.3 °C resulted and the maximum mAb (ratio 1.50) sample value was only minimally lower at -35.6 °C. Minimum mAb (ratio 1.16) and maximum histidine (ratio 1.00) samples showed the lowest T_g' values of -36.3 °C and -37.1 °C, respectively.

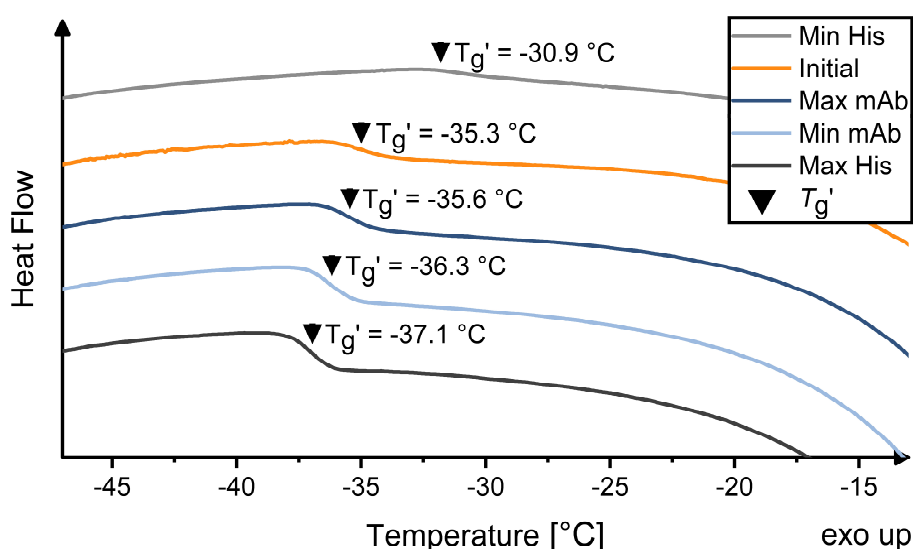


Figure 5 DSC thermograms of samples with different mAb to histidine ratios. The ratio of the samples was: Min His (2.58), Initial (1.61), Max mAb (1.50), Min mAb (1.16), Max His (1.00).

4.5 Discussion

Our aim was to close a gap in knowledge about the stability of biologics, specifically proteins exemplarily studied using a mAb, as frozen bulk material. During industrial production of mAb solutions, bulk drug substance that is not fully formulated is regularly frozen. Hence, we characterised cryoconcentration after large-scale freezing of a mAb in pure histidine buffer without further excipients (19). In the recent study, we connected the cryoconcentration, which comes with a change in protein to solute ratio after freezing, to the T_g' and long-term frozen storage stability. At first, we developed a method to analyse the T_g' of pure mAb/histidine mixtures at different concentrations found previously upon freezing in large-scale containers (Figure 1). The focus was on minimum and maximum mAb and histidine concentrations. DSC thermograms of protein samples that do not contain glass formers such as sugars often do not show a sharp sigmoidal change in heat flow signal (24). In such cases, the onset of T_g' can be determined using the first derivative plot. However, this inevitably leads to a deviation between the obtained T_g' and the commonly reported midpoint T_g' (24). Therefore, we optimised the sample preparation in order to directly measure the midpoint T_g' , based on the inflection point, of samples that only consist of a mAb and the buffer component. Increasing the sample concentration via lyophilisation and subsequent reconstitution with less water resulted in distinct glass transition signals. This enabled us to determine T_g' as the inflection point. By keeping the mAb to histidine ratio, the T_g' of the solutions was not influenced (22,24). The T_g' of a solution depends on the sample composition, but is independent of the initial concentration (22,23). Additionally, higher histidine concentrations than expected from its solubility product could be reached via this method. Histidine is known to form an amorphous phase upon freezing of aqueous solutions and to keep its glassy state throughout lyophilisation (25). In combination with the high mAb concentration, which is preventing buffer crystallisation (26), this may support to reach such high histidine concentrations by lyophilisation and reconstitution with less volume (27). By reducing the heating rate to 3 K/min we could avoid an interference of the ice melting endotherm with the glass transition endotherm. The samples significantly differed in T_g' between approximately -31 °C (minimum histidine) for the highest and -37 °C (maximum histidine) for the lowest mAb to histidine ratio. In comparison, the pure mAb shows a T_g' of -18 °C. It has been shown that higher salt concentrations lower the overall T_g' of the formulation matrix (16,24).

None of the samples showed aggregate formation when stored well below T_g' at $-80\text{ }^\circ\text{C}$. After storage at $-20\text{ }^\circ\text{C}$, both HMWS and SVPs levels were increased. This effect, already discernible after 6 months, was boosted after 12 months. Similar trends, but even more pronounced, were detected at $-10\text{ }^\circ\text{C}$. Relative aggregation, assessed via SEC, was highest in samples with the lowest mAb concentration. Maximum mAb but also maximum histidine samples displayed considerably lower HMWS levels. In contrast, when focusing on the absolute aggregation level assessed via SVPs, increasing mAb concentration negatively affected colloidal stability. At $-20\text{ }^\circ\text{C}$, maximum mAb and maximum histidine samples in particular formed insoluble aggregates. At $-10\text{ }^\circ\text{C}$, SVPs counts were still highest for samples with the highest absolute mAb concentration (maximum mAb and maximum histidine), but also in mAb samples representing the initial composition significant SVP formation occurred. At the lowest absolute mAb concentration significantly less SVPs were found. It appears that the mAb concentration affects the stability, however the mAb to histidine ratio was not kept constant. The change in mAb concentration comes with a shift of the mAb to excipient ratio and consequently of T_g' as well as ionic strength in the FCM. This might explain why minimum histidine samples with a moderate mAb concentration showed highest stability in all cases.

The solution T_g' is a key parameter for frozen storage stability (10,28). Below T_g' , the unfrozen FCM forms a glassy state, a solid solution of cryoconcentrated solutes and unfrozen, amorphous water (29). The viscosity of this glass is in the order of 10^{14} Pas, so that motion is in the range of mm/year (22,24). Ultimately, molecular mobility is greatly reduced and mAb aggregation prevented (21). Consequently, neither soluble nor insoluble aggregates were detected, when samples were stored at $-80\text{ }^\circ\text{C}$, more than $40\text{ }^\circ\text{C}$ below T_g' . It has been shown for lyophilisates that storage at temperatures slightly below the glass transition T_g does not necessarily result in complete prevention of aggregation (30). Assuming that these finding can be transferred to T_g' , we propose that a safety margin should be considered when choosing the appropriate storage temperature for frozen protein solutions. Alhalaweh et al. highlighted that ΔT of $20\text{ }^\circ\text{C}$ between T_g and storage temperature of lyophilisates is sufficient to essentially reduce mobility to a level that aggregation becomes minimal (28). In contrast, when samples are stored above T_g' , the viscosity drops, facilitating irreversible denaturation and aggregation (23). Above T_g' , the viscosity of the FCM decreases exponentially with increasing temperature (31). The lower viscosity is associated with increased molecular mobility and consequently accelerated

physical and chemical instability (24). Correspondingly, we saw marked mAb aggregation upon storage at temperatures above T_g' , which was much more pronounced at $-10\text{ }^{\circ}\text{C}$ compared to $-20\text{ }^{\circ}\text{C}$. Nevertheless, it took several months until the stability was markedly impacted. Lim et al. investigated the influence of glass transition and storage temperature of frozen peas on quality attributes (29). They found that the loss of quality is relative to ΔT between T_g' and storage temperature. Transferring these findings to the mAb samples, reflecting different regions within a frozen large bottle, the sample stability would decrease according to their T_g' , which is defined by their mAb to histidine ratio (Figure 5): minimum histidine \gg initial $>$ maximum mAb $>$ minimum mAb $>$ maximum histidine. This can explain why samples containing minimum histidine showed the highest stability during storage above T_g' , whereas maximum histidine displayed significantly less colloidal stability at both temperatures. These differences in T_g' , driven by the composition of the FCM but not by the initial concentration (8,11,22,23), clearly affected stability.

In addition, not only T_g' but also the ionic strength in the FCM is impacted by the mAb to histidine ratio. The ionic strength of a solution affects mAb aggregation (32). Though the net effect of ionic strength on aggregation is dependent on the specific mAb, its protein-protein interactions, and the salt type, the ionic strength is undeniably a key parameter. Ions interact electrostatically with mAbs and thereby influence protein-protein interactions and the conformational state. In addition, electrostatic interactions between the FCM and the ice surface were hypothesized (2). In the recent study, lower ionic strength in the non-solidified FCM increased stability. Most likely protein-protein interactions and electrostatic interactions with the ice surface were enhanced by higher salt concentrations. Not necessarily all results can be explained by T_g' and ionic strength effects alone. While the colloidal stability for samples with the lowest mAb to histidine ratio was reduced, the formation of soluble aggregates was decreased. Maximum mAb samples displayed equivalent low HMWS levels. Both samples contain the highest absolute mAb concentration. In contrast, minimum mAb concentration led to the highest relative HMWS fraction. Several studies highlighted that surface-induced local enrichment and denaturation play an important role in mAb aggregation (13,20,33). Possible mechanisms of ice-induced denaturation at the interface are discussed, such as adsorption, pH shifts, accumulation of air bubbles, increased pressure, and enhanced cold denaturation (2). To reduce dissimilarity in ice morphology in the samples, we used controlled nucleation during sample preparation. Thereby, we aimed to focus on the influence of the sample composition

on storage stability and eliminate any interface related influence. But Ostwald ripening may occur upon storage at $-20\text{ }^{\circ}\text{C}$ as well as $-10\text{ }^{\circ}\text{C}$. It has been highlighted before, that the number of protein molecules that adsorb to the interface is limited by the total interface area. (2,34). Consequently, the relative adsorbed fraction decreases with increasing absolute mAb concentration (2,35). Our results suggest that the formation of HMWS is also driven by the enrichment of protein molecules and their aggregation at the FCM/ice interface. In respect of SVPs, levels remained low in the histidine buffer control. A miniscule increase upon storage at $-10\text{ }^{\circ}\text{C}$ up to 12 months might be due to the laboratory environment and potential oxidation processes (36). For mAb containing samples, increasing absolute mAb concentration had a negative impact on the formation of insoluble aggregates. While surface-induced denaturation is limited, the SVPs levels, which are not measured relatively, increased with mAb concentration. The formation of SVPs detected via flow imaging microscopy might result from hundredth of a percent of the total protein in solution (37). Thus, samples that showed low relative aggregation because of their high mAb concentration, displayed highest absolute SVPs levels. Protein-protein interactions in the unfrozen FCM might facilitate the formation of SVPs at higher mAb concentration. It should be noted that insoluble particles are not covered by SEC measurement and flow imaging microscopy via Flowcam® detects insoluble particles $\geq 1\text{ }\mu\text{m}$. Insoluble aggregates in the nanometre range were not tracked by these methods. Dynamic light scattering measurements could have closed that gap and should be considered for future studies that examine long-term frozen storage stability of proteins as a qualitative method.

When these small-scale results are transferred to the cryoconcentration that we found in a 2 L bottle after large-scale freezing (19), marked differences in stability can be associated with the apparently small changes in concentration. The highly concentrated top region of the bottle with maximum mAb concentration and the highly concentrated area with maximum histidine tend to form less HMWS compared to samples with the initial concentration, but significantly contribute to the formation of SVPs. In contrast, the diluted core of the bottle with minimum mAb can be associated with moderate SVPs formation but increased HMWS. The minimum histidine region at the bottle wall is characterised by highest stability.

Thus, the study highlights that a shift in the ratio of protein to small excipient molecules in different regions of large-scale frozen containers of bulk drug substance can substantially impact the quality of the product. Storage at -80°C can level off the effect. We studied the

effect over one-year storage at temperatures 10 °C to 20 °C above T_g' to enhance the effect. Frequently drug substance is stored for much longer times. Future studies have to focus on temperatures slightly below T_g' as it would be an enormous contribution to sustainability if storage of frozen drug substance would not require -80 °C but e.g. -40 °C would be sufficiently low.

Overall, many other effects have to be considered before generalising the conclusion of our study. The regions in a large-scale freezing container significantly differ in freezing time and therefore ice morphology, which could affect local mAb stability. Furthermore, local pressure or air bubbles and consequently oxidation could be affected by the position. Cryoconcentration can be reduced by faster freezing rates, which would additionally reduce the exposure time of the protein to a non-solidified FCM above T_g' (20), but would also result in smaller ice crystals and consequently larger interfaces. Another way to reduce cryoconcentration is directed freezing from bottom to top. Thereby, natural convection, the main driving force for cryoconcentration, can be prevented (38). In addition, optimisation of the formulation can decrease the risk of aggregation. In that respect, we highlight in our study that the interplay of the mAb to histidine ratio, determining T_g' and the ionic strength in the FCM, and the absolute mAb concentration has to be considered. ΔT between T_g' and the storage temperature can be optimised by avoiding excipients forming cryoconcentrates with low T_g' . The ionic strength can be reduced by using minimal salt and buffer concentrations. By increasing the initial mAb concentration, the relative fractions that aggregate upon long-term frozen storage can be decreased.

4.6 Conclusion

In a previous study, we characterised the cryoconcentration in a 2 L bottle after large-scale freezing of mAb in pure histidine buffer (19). We found significant changes in mAb concentration that were associated with shifts in mAb to histidine ratio. In this work, we characterised long-term frozen storage stability of respective samples with focus on mAb aggregation.

We analysed the T_g' of samples, which do not contain a glass forming sugar and which reflect the different regions in the bottle, via an optimised DSC method. Samples were lyophilised and subsequently reconstituted in less volume to increase signal strength in DSC thermograms. T_g' of samples ranged between -31 °C and -37 °C and was defined by the mAb to histidine ratio. MAb stability was not affected when samples were stored below

T_g' at $-80\text{ }^\circ\text{C}$. Long-term mAb stability upon storage above T_g' , at $-20\text{ }^\circ\text{C}$ or $-10\text{ }^\circ\text{C}$, was found to be an interplay of T_g' , the ionic strength in the non-solidified FCM, and the mAb concentration. ΔT between T_g' and the storage temperature had a marked impact on stability. Consequently, stability was higher at $-20\text{ }^\circ\text{C}$ than at $-10\text{ }^\circ\text{C}$. Samples with the highest mAb to histidine ratio and thus highest T_g' and lowest ionic strength in the FCM displayed least formation of soluble and insoluble aggregates. In addition, the absolute mAb concentration affected storage stability. The relative aggregated fraction, assessed via SEC, decreased with increasing mAb concentration. In contrast, absolute aggregation in respect of SVPs was negatively affected, pointing to an additional protein-protein interaction effect.

Transferred to cryoconcentration in a 2 L bottle, apparently small changes in mAb and excipient concentration and shifts in mAb to histidine ratio have a marked impact on long-term frozen storage stability. Regions with increased mAb concentration, in case of a 2 L bottle the centre near the bottom and the top region, tend to form SVPs, while a lower mAb concentration, in case of a 2 L bottle in the core, leads to enhanced formation of HMWS. The highest stability can be expected for the areas with lowest histidine concentration at the wall.

Further studies will focus on possible correlations between mAb and buffer concentration that are systematically varied and long-term stability during frozen storage. In addition, storage at intermediate temperatures below T_g' , e.g. $-40\text{ }^\circ\text{C}$, could contribute to the sustainability of long-term frozen storage, but requires detailed studies of the cryoconcentration effects and formulation impacts. Frozen storage stability will be impacted if a cryoprotectant is added, which increases viscosity and provides spacing between mAb molecules in the freeze concentrate decreasing mAb aggregation.

Acknowledgements

The authors thank the Novartis Pharma AG for providing mAb stock solutions.

References

1. Mehta SB, Subramanian S, D'Mello R, Brisbane C, Roy S. Effect of protein cryoconcentration and processing conditions on kinetics of dimer formation for a monoclonal antibody: A case study on bioprocessing. *Biotechnol Prog.* 2019 Jul 15;35(4):1–7.
2. Arsiccio A, Pisano R. The Ice-Water Interface and Protein Stability: A Review. *J Pharm Sci.* 2020 Jul;109(7):2116–30.
3. Roessl U, Leitgeb S, Nidetzky B. Protein freeze concentration and micro-segregation analysed in a temperature-controlled freeze container. *Biotechnol Reports.* 2015 Jun;6:108–11.
4. Padala C, Jameel F, Rathore N, Gupta K, Sethuraman A. Impact of Uncontrolled vs Controlled Rate Freeze-Thaw Technologies on Process Performance and Product Quality. *PDA J Pharm Sci Technol.* 2010;64(4):290–8.
5. Rodrigues MA, Miller MA, Glass MA, Singh SK, Johnston KP. Effect of Freezing Rate and Dendritic Ice Formation on Concentration Profiles of Proteins Frozen in Cylindrical Vessels. *J Pharm Sci.* 2011 Apr;100(4):1316–29.
6. Rathore N, Rajan RS. Current Perspectives on Stability of Protein Drug Products during Formulation, Fill and Finish Operations. *Biotechnol Prog.* 2008 Jun 6;24(3):504–14.
7. Roessl U, Jajcevic D, Leitgeb S, Khinast JG, Nidetzky B. Characterization of a Laboratory-Scale Container for Freezing Protein Solutions with Detailed Evaluation of a Freezing Process Simulation. *J Pharm Sci.* 2014 Feb;103(2):417–26.
8. Authelin J-R, Rodrigues MA, Tchessalov S, Singh SK, McCoy T, Wang S, et al. Freezing of Biologicals Revisited: Scale, Stability, Excipients, and Degradation Stresses. *J Pharm Sci.* 2020 Jan;109(1):44–61.
9. Arsiccio A, McCarty J, Pisano R, Shea J-E. Heightened Cold-Denaturation of Proteins at the Ice–Water Interface. *J Am Chem Soc.* 2020 Mar 25;142(12):5722–30.
10. Kolhe P, Amend E, K. Singh S. Impact of freezing on pH of buffered solutions and consequences for monoclonal antibody aggregation. *Biotechnol Prog.* 2009 Dec 28;26(3):727–33.
11. Connolly BD, Le L, Patapoff TW, Cromwell MEM, Moore JMR, Lam P. Protein Aggregation in Frozen Trehalose Formulations: Effects of Composition, Cooling Rate, and Storage Temperature. *J Pharm Sci.* 2015 Dec;104(12):4170–84.
12. Singh SK, Kolhe P, Mehta AP, Chico SC, Lary AL, Huang M. Frozen State Storage Instability of a Monoclonal Antibody: Aggregation as a Consequence of Trehalose Crystallization and Protein Unfolding. *Pharm Res.* 2011 Apr 7;28(4):873–85.
13. Duarte A, Rego P, Ferreira A, Dias P, Geraldes V, Rodrigues MA. Interfacial Stress and Container Failure During Freezing of Bulk Protein Solutions Can Be Prevented by Local Heating. *AAPS PharmSciTech.* 2020 Oct 1;21(7):251.

14. Hauptmann A, Hoelzl G, Loerting T. Distribution of Protein Content and Number of Aggregates in Monoclonal Antibody Formulation After Large-Scale Freezing. *AAPS PharmSciTech*. 2019 Feb 10;20(2):72.
15. Kolhe P, Mehta AP, Lary AL, Chico SC, Singh SK. Large-Scale Freezing of Biologics (Part III). *BioPharm Int*. 2012;25(October):40–8.
16. Kuelzto LA, Wang W e. i., Randolph TW, Carpenter JF. Effects of Solution Conditions, Processing Parameters, and Container Materials on Aggregation of a Monoclonal Antibody during Freeze-Thawing. *J Pharm Sci*. 2008 May;97(5):1801–12.
17. Hauptmann A, Podgoršek K, Kuzman D, Srčić S, Hoelzl G, Loerting T. Impact of Buffer, Protein Concentration and Sucrose Addition on the Aggregation and Particle Formation during Freezing and Thawing. *Pharm Res*. 2018 May 19;35(5):101.
18. Zhang A, Singh SK, Shirts MR, Kumar S, Fernandez EJ. Distinct Aggregation Mechanisms of Monoclonal Antibody Under Thermal and Freeze-Thaw Stresses Revealed by Hydrogen Exchange. *Pharm Res*. 2012 Jan 30;29(1):236–50.
19. Bluemel O, Buecheler JW, Rodrigues MA, Geraldes V, Hoelzl G, Bechtold-Peters K, et al. Cryoconcentration and 3D Temperature Profiles During Freezing of mAb Solutions in Large-Scale PET Bottles and a Novel Scale-Down Device. *Pharm Res*. 2020 Sep 30;37(9):179.
20. Singh SK, Kolhe P, Wang W, Nema S. Large-Scale Freezing of Biologics A Practitioner’s Review, Part One: Fundamental Aspects. *Bioprocess Int*. 2009;7(9):32–44.
21. Miller MA, Rodrigues MA, Glass MA, Singh SK, Johnston KP, Maynard JA. Frozen-State Storage Stability of a Monoclonal Antibody: Aggregation is Impacted by Freezing Rate and Solute Distribution. *J Pharm Sci*. 2013 Apr;102(4):1194–208.
22. Kasper JC, Friess W. The freezing step in lyophilization: Physico-chemical fundamentals, freezing methods and consequences on process performance and quality attributes of biopharmaceuticals. *Eur J Pharm Biopharm*. 2011 Jun;78(2):248–63.
23. Franks F. Freeze-drying of bioproducts: Putting principles into practice. *Eur J Pharm Biopharm*. 1998;45(3):221–9.
24. Pansare SK, Patel SM. Practical Considerations for Determination of Glass Transition Temperature of a Maximally Freeze Concentrated Solution. *AAPS PharmSciTech*. 2016 Aug 18;17(4):805–19.
25. Österberg T, Wadsten T. Physical state of l-histidine after freeze-drying and long-term storage. *Eur J Pharm Sci*. 1999 Aug 1;8(4):301–8.
26. Thorat AA, Munjal B, Geders TW, Suryanarayanan R. Freezing-induced protein aggregation - Role of pH shift and potential mitigation strategies. *J Control Release*. 2020 Jul;323(April):591–9.
27. Wlodarski K, Sawicki W, Paluch KJ, Tajber L, Grembecka M, Hawelek L, et al. The influence of amorphization methods on the apparent solubility and dissolution rate of tadalafil. *Eur J Pharm Sci*. 2014 Oct 1;62:132–40.

The Effect of mAb and Excipient Cryoconcentration on Long-Term Frozen Storage Stability – Part 1: Higher Molecular Weight Species and Subvisible Particle Formation

28. Alhalaweh A, Alzghoul A, Mahlin D, Bergström CAS. Physical stability of drugs after storage above and below the glass transition temperature: Relationship to glass-forming ability. *Int J Pharm.* 2015 Nov;495(1):312–7.
29. Lim M, Wu H, Breckell M, Birch J. Influence of the glass transition and storage temperature of frozen peas on the loss of quality attributes. *Int J Food Sci Technol.* 2006 May;41(5):507–12.
30. Chang BS, Beauvais RM, Dong A, Carpenter JF. Physical Factors Affecting the Storage Stability of Freeze-Dried Interleukin-1 Receptor Antagonist: Glass Transition and Protein Conformation. *Arch Biochem Biophys.* 1996 Jul;331(2):249–58.
31. Seifert I, Friess W. Freeze concentration during freezing: How does the maximally freeze concentrated solution influence protein stability? *Int J Pharm.* 2020 Nov;589(June):119810.
32. Wang W, Nema S, Teagarden D. Protein aggregation—Pathways and influencing factors. *Int J Pharm.* 2010 May;390(2):89–99.
33. Sarciaux J-M, Mansour S, Hageman MJ, Nail SL. Effects of buffer composition and processing conditions on aggregation of bovine IgG during freeze-drying. *J Pharm Sci.* 1999 Dec;88(12):1354–61.
34. Wang W. Lyophilization and development of solid protein pharmaceuticals. *Int J Pharm.* 2000 Aug;203(1–2):1–60.
35. Jiang S, Nail SL. Effect of process conditions on recovery of protein activity after freezing and freeze-drying. *Eur J Pharm Biopharm.* 1998 May;45(3):249–57.
36. Mason BD, McCracken M, Bures EJ, Kerwin BA. Oxidation of Free L-histidine by tert-Butylhydroperoxide. *Pharm Res.* 2010 Mar 2;27(3):447–56.
37. Barnard JG, Singh S, Randolph TW, Carpenter JF. Subvisible Particle Counting Provides a Sensitive Method of Detecting and Quantifying Aggregation of Monoclonal Antibody Caused by Freeze-Thawing: Insights Into the Roles of Particles in the Protein Aggregation Pathway. *J Pharm Sci.* 2011 Feb;100(2):492–503.
38. Rodrigues MA, Balzan G, Rosa M, Gomes D, de Azevedo EG, Singh SK, et al. The importance of heat flow direction for reproducible and homogeneous freezing of bulk protein solutions. *Biotechnol Prog.* 2013 Sep;29(5):1212–21.

Chapter 5 The Effect of mAb and Excipient Cryoconcentration on Long-Term Frozen Storage Stability – Part 2: Aggregate Formation and Oxidation

Oliver Bluemel¹, Jakob W. Buecheler², Astrid Hauptmann³, Georg Hoelzl³,
Karoline Bechtold-Peters², Wolfgang Friess¹

1 Pharmaceutical Technology and Biopharmaceutics, Department of Pharmacy, Ludwig-Maximilians-
Universitaet Muenchen, 81377 Munich, Germany

2 Technical Research and Development, Novartis Pharma AG, 4002 Basel, Switzerland

3 Sandoz GmbH, 6336 Langkampfen, Austria

Author contributions:

O.B., W.F., and K.B.P. conceived the study. O.B. performed the experiments and evaluated the data. O.B. wrote the paper. W.F., K.B.P., J.W.B., A.H., and G.H. contributed to the discussion of the results and revised the manuscript. W.F. and K.B.P. supervised the work.

5.1 Abstract

Purpose: We examined the impact of monoclonal antibody (mAb) and buffer concentration, mimicking the cryoconcentration found upon freezing in a 2 L bottle, on mAb stability during frozen storage. Upon cryoconcentration, larger protein molecules and small excipient molecules freeze-concentrate differently, resulting in different protein to stabiliser ratios within a container. Understanding the impact of these shifted ratios on protein stability is essential.

Methods: For two mAbs a set of samples with constant mAb (5 mg/mL) or buffer concentration (medium histidine/adipic acid) was prepared and stored for 6 months at -10 °C. Stability was evaluated via size-exclusion chromatography, flow imaging microscopy, UV/Vis spectroscopy at 350 nm, and protein A chromatography. Dynamic light scattering was used to determine k_D values.

Results: Soluble aggregate levels were unaffected by mAb concentration, but increased with histidine concentration. No trend in optical density could be identified. In contrast, increasing mAb or buffer concentration facilitated the formation of subvisible particles. A trend towards attractive protein-protein interactions was seen with higher ionic strength. MAb oxidation levels were negatively affected by increasing histidine concentration, but became less with higher mAb concentration.

Conclusion: Small changes in mAb and buffer composition had a significant impact on stability during six-month frozen storage. Thus, preventing cryoconcentration effects in larger freezing containers may improve long-term stability.

Keywords: cryoconcentration, frozen storage, large-scale freezing, monoclonal antibody, stability

Abbreviations: DLS – Dynamic light scattering, FCM - Freeze-concentrated matrix, HMWS – Higher molecular weight species, HPLC - High-performance liquid chromatography, HPW – Highly purified water, mAb – Monoclonal antibody, OD350 – Optical density at 350 nm, PES – Polyethersulfone, SEC – Size-exclusion chromatography, SVP – Subvisible particle, T_g' – Glass transition temperature of the maximally freeze-concentrated solution

5.2 Introduction

Therapeutic proteins, especially monoclonal antibodies (mAbs), are high-value biotechnological products and gained importance in the treatment of a variety of diseases (1–4). Numerous technical challenges have to be considered during production, storage, and transportation (5). Freezing of bulk protein solution is commonly used to increase chemical and physical stability (6). By decoupling drug substance and drug product processing, frozen storage and transportation offers manufacturing flexibility (7,8). Additionally, freezing eliminates the risk of shaking and foaming and minimises microbial growth (6,7). While controlled freezing and thawing are intentionally performed during production, mishandling may lead to unintentional uncontrolled freezing of drug product. Although freezing is associated with numerous advantages, it also comes with several drawbacks. Detrimental effects from cold denaturation (9), denaturation at the ice-liquid interface (4,10), crystallisation of excipients and buffers (11,12), potentially coming with marked pH shifts (8,13), and especially cryoconcentration (5,14,15) are well described. Growing ice only partially includes solutes (3). Most of the solutes are excluded by growing ice crystals and consequently form a freeze-concentrated matrix (FCM), which composition is described by phase or state diagrams (3,16). The glass transition temperature of the maximally freeze-concentrated solution (T_g') determines the vitrification of this FCM. In practical terms not only this microscopic cryoconcentration is of interest, but also macroscopic freeze-concentration plays an important role. During freezing, natural convection and diffusion transport proteins and excipients away from the freezing front (3). Recent studies outline differences in cryoconcentration of large proteins and small excipients, mainly attributed to differences in diffusivity (3,15,17). Consequently, a spatial heterogeneity builds up that is mainly driven by the processing conditions. Beside colloidal and conformation instability, the importance of protein oxidation has recently been highlighted (16). Often small-scale studies in tubes, vials or vessels are used to optimise processing conditions, formulation composition, unveil aggregation mechanisms, and examine long-term storage stability (3,11,18–20). Miller et al. examined the frozen-state storage stability of a mAb in 50 mL stainless steel cylindrical vessels (3). They found that changes in concentration persist over time, regardless of the storage temperature. Furthermore, long-term storage stability is mainly impacted by the solution's T_g' . Storage below T_g' completely inhibits aggregation, whereas storage above T_g' may result in marked aggregation.

Previously, we highlighted significant changes in concentration upon large-scale freezing of mAb solutions and different ratios of mAb to histidine buffer in larger containers due to differences in diffusivity (17). Miller et al. connected cryoconcentration and long-term stability of frozen mAb solutions (3). However, they focused on the freezing conditions rather than the impact of freeze-concentration and shifted protein to excipient ratio.

In the current study, we examine the influence of changes in mAb and buffer concentration on higher molecular weight species (HMWS) levels, subvisible particles (SVPs), optical density at 350 nm (OD₃₅₀) as well as mAb oxidation. MAb to buffer concentrations and ratios were adjusted in the similar range that evolves during large-scale freezing (17). All samples were frozen identically to minimise the effect of processing conditions and stored for 6 months at -10 °C. A temperature above T_g' was selected to generate a stress model. Thereby, we directly connect cryoconcentration and long-term storage stability. For two human IgG1 mAbs two sets of samples were prepared; one set with fixed mAb concentration (5 mg/mL) and varying buffer concentration (zero to maximum histidine/adipic acid) and a second set that covered variations in mAb concentration (0 mg/mL to 10 mg/mL) at a given buffer concentration (medium histidine/adipic acid).

Increasing mAb concentration did not alter HMWS levels after six-month storage, but led to a higher SVP count. Higher buffer concentrations weakened repulsive protein-protein interactions and decreased mAb storage stability. Both mAbs formulated in highly purified water (HPW) showed highest levels of soluble aggregates, but lowest levels of SVPs. Higher levels of partially oxidised mAb fractions were detected in samples with lower mAb concentration. Oxidation of proteins is most likely induced at the surface of air bubbles that form during freezing (16). In addition, histidine facilitated mAb1 oxidation.

Our study reveals that the little changes in mAb and buffer concentration at the different positions in a large container with frozen drug substance can affect long-term storage stability. Therefore, cryoconcentration should be avoided and the initial formulation composition optimised. In addition to the formation of soluble and insoluble aggregates, mAb oxidation is an important parameter during frozen storage, which should receive more attention in future stability studies.

5.3 Materials and Methods

5.3.1 Materials

Novartis AG (Basel, Switzerland) provided IgG1 mAb1 in medium histidine buffer at pH 5.5 and IgG1 mAb2 in medium adipic acid at pH 5.2 stock solutions. L-histidine monochloride and L-histidine monohydrate were both purchased from Merck KGaA (Darmstadt, Germany). Adipic acid 99% was obtained from Sigma-Aldrich Produktions GmbH (Steinheim am Albuch, Germany).

Dipotassium phosphate, monopotassium phosphate, and disodium phosphate dihydrate were acquired from Merck KGaA (Darmstadt, Germany). Acetic acid and potassium chloride were purchased from VWR International GmbH (Darmstadt, Germany), sodium chloride from Bernd Kraft GmbH (Duisburg, Germany).

Uncoated 2R glass vials from SCHOTT AG (Mainz, Germany) were used. West Pharmaceuticals (Eschweiler, Germany) provided FluroTec® lyophilisation stoppers. Sucrose was obtained from Sigma-Aldrich Produktions GmbH (Steinheim am Albuch, Germany).

Colourless 1.5 mL Eppendorf Tubes® 3810X (Eppendorf AG, Hamburg, Germany) were used for centrifugation.

0.2 µm Polyethersulfone (PES) membrane syringe filters were purchased from VWR International GmbH (Darmstadt, Germany).

Either Slide-A-Lyzer® 12 mL - 30 mL dialysis cassettes (Thermo Fisher Scientific Inc., Waltham, Massachusetts, USA) or Vivaspin® 6 centrifugal concentrators (Sartorius AG, Göttingen, Germany) with a 10K MWCO were used for dialysis.

5.3.2 Sample Preparation

Samples were adjusted as given in Table 1. For the set of samples with constant buffer concentration, mAb1 and mAb2 stock solutions were diluted with a medium histidine buffer pH 5.5 and a medium adipic acid buffer pH 5.2, respectively. Samples with varying buffer concentrations but constant mAb concentration were prepared by diluting stock solutions with differently concentrated buffer solutions. The contribution of the stock solution to the final buffer concentration was considered. For samples with zero buffer, 30 mL of each stock solution was dialysed against HPW using Slide-A-Lyzer® dialysis cassettes. 6 L HPW for each dialysis step were needed to assure complete buffer exchange.

Subsequently, these solutions were diluted to 5 mg/mL mAb with HPW. The pH of these samples was measured but not adjusted. The final mAb concentration of all samples was controlled via UV absorption at 280 nm using a NanoDrop™ One (Thermo Fisher Scientific Inc., Waltham, Massachusetts, USA) prior to filtration through 0.2 µm PES syringe filters. For each formulation six 2R glass vials were filled with 1 mL aliquots and semi-stoppered with FluroTec® lyophilisation stoppers. Samples were arranged in the centre of lyophilisation trays surrounded by two rows of vials filled with 10% (w/V) sucrose. These rows were added to minimise variations in heat transfer in the samples due to radiation, known as the edge effect during lyophilisation. Subsequently, all vials were frozen in a Christ Epsilon 2-6D LSCplus (Martin Christ Gefriertrocknungsanlagen GmbH, Osterode am Harz, Germany). Samples were cooled to -5 °C with a rate of 1 K/min. During a 60 min plateau at -5 °C the ice fog technology induced controlled nucleation. After nucleation a 1 K/min ramp was applied to -40 °C. Immediately after the freezing run all samples were transferred to a precooled -10 °C tritec® TC 231 freezer (tritec® Gesellschaft für Labortechnik und Umweltsimulation mbH, Hannover, Germany). To compensate any temperature fluctuations in the freezer, samples were placed inside a polystyrene thermobox. The t0 samples were kept for 12 h at -10 °C.

Table 1 Samples overview; for both mAbs a set of samples with constant buffer and constant mAb concentration was prepared.

mAb1										
Histidine	medium					zero	low	medium	high	max
mAb [mg/mL]	0	2.5	5	7.5	10	5				
mAb2										
Adipic Acid	medium					zero	low	medium	high	max
mAb [mg/mL]	0	2.5	5	7.5	10	5				

5.3.3 Stability Analysis

Triplicates were thawed at room temperature on the laboratory bench prior to characterisation.

5.3.3.1 Flow Imaging Microscopy

SVPs were analysed using a FlowCam® 8100 (Fluid Imaging Technologies, Inc., Scarborough, Maine, USA) equipped with a 10x magnification cell with 160 µL sample volume and a 0.15 mL/min flow rate. Distance to the nearest neighbour for particle identification was 3 µm. Particle segmentation thresholds were 10 for light and 13 for dark pixels. The auto image frame rate was set to 28 frames/s and sampling time to 60 s. Particle size was reported as the equivalent spherical diameter. For measurements and analysis, the VisualSpreadsheet® 4.7.6 software was used.

5.3.3.2 Size-Exclusion Chromatography

An Agilent 1200 high performance liquid chromatography (HPLC) system equipped with a diode array detector (Agilent Technologies, Santa Clara, California, USA) was used to quantify HMWS via size-exclusion chromatography (SEC). A TSKgel G3000 SWxl column (Tosoh Bioscience GmbH, Griesheim, Germany) at 30 °C served as stationary phase, 150 mM potassium phosphate buffer pH 6.5 as mobile phase at a flow rate of 0.4 mL/min. All samples were diluted to 0.75 mg/mL with mobile phase and 100 µL diluted sample were centrifuged 2 min in 1.5 mL tubes at 25 700 x g with a Heraeus™ Megafuge™ 16R (Thermo Fisher Scientific Inc., Waltham, Massachusetts, USA). 10 µL of the supernatant were analysed at 210 nm. Chromatograms were evaluated with the Agilent OpenLAB Data Analysis Software version 2.1.

5.3.3.3 Optical Density at 350 nm

The OD₃₅₀ of 200 µl sample was measured using a FLUOstar® Omega microplate reader (BMG LABTECH GmbH, Ortenberg, Germany) in a quartz 96 microwell plate (Hellma Holding GmbH, Müllheim, Germany).

5.3.3.4 Protein A Analytical Chromatography

MAb oxidation was evaluated via Protein A chromatography with an Agilent 1200 HPLC system (Agilent Technologies, Santa Clara, California, USA) detecting at 280 nm. The method was adapted from Loew et al. (21). Briefly, the stationary phase, an Applied Biosystems™ POROS™ A (4.6 mmD x 50 mmL) column (Thermo Fisher Scientific Inc., Waltham, Massachusetts, USA), was kept at 23 °C and 250 µg mAb were injected. Elution was performed at 2.0 mL/min in a gradient mode with buffer A (Dulbecco's phosphate buffered saline 1X in HPW at pH 7.4) and buffer B (100 mM acetic acid with 150 mM

sodium chloride in HPW at pH 2.8) at 0:0, 40:60, 41:100, 51:100, 52:0, 62:0 (time [minutes]:buffer B [percentage]). 200 μ L samples were centrifuged with a Heraeus™ Megafuge™ 16R (Thermo Fisher Scientific Inc., Waltham, MA, USA) at 25 700 x g in 1.5 mL tubes.

5.3.4 Determination of the Interaction Parameter k_D

mAb1 and mAb2 stock solutions were dialysed against histidine and adipic acid buffers (low – maximum), respectively. Therefore, 1 mL stock solution was diluted 1:5 with the respective buffer and spun in a Vivaspin® 6 at 4 000 x g until approximately 1 mL diluted sample was left. This process was repeated three times to assure sufficient buffer exchange. Finally, samples were diluted to concentrations between 1 mg/mL and 8 mg/mL and filtered through 0.2 μ m PES syringe filters.

Dynamic light scattering (DLS) measurements were performed on a DynaPro Plate Reader III (Wyatt Technology, Dernbach, Germany) with 25 μ L sample in a 384-well plate (Corning Inc., Corning, New York, USA), centrifuged at 2 000 rpm for 2 min using the Heraeus™ Megafuge™ 16R (Thermo Fisher Scientific Inc., Waltham, Massachusetts, USA) with an M-20 microplate swinging-bucket rotor (Thermo Fisher Scientific Inc., Waltham, Massachusetts, USA). Each well was sealed with 5 μ L silicon oil and the plate was centrifuged again. All samples were analysed in triplicates with 20 acquisitions of 5 s at 25 °C. The Dynamics V7.8.2.18 software was used to analyse recorded autocorrelation functions and to calculate diffusion coefficients. The linear fit of diffusion coefficient versus protein concentration allows to calculate the interaction parameter k_D (22–24).

5.4 Results

The formation of HMWS and SVPs, changes in OD350, and mAb oxidation upon six-month storage at -10 °C were analysed to evaluate the long-term stability of two mAbs in either histidine or adipic acid buffer. Our main objective was to highlight the contribution of mAb as well as buffer concentration on stability during frozen storage. Two sets of samples were prepared for each mAb (Table 1) reflecting the concentration range found upon large-scale freezing of drug substance in 2 L bottles (17). Additionally, protein-protein interactions in the formulations were assessed via the interaction parameter k_D .

5.4.1 Formation of HMWS

The formation of HMWS for both set of samples and both mAbs are shown in Figure 1. The mAb1 samples showed 1.6% HMWS at the start of the experiment except for samples in HPW with 2.0%. It is important to note that also the t0 samples were subject to freezing and thawing. After 6 months storage, samples with varying mAb1 concentration displayed only marginally increased aggregate levels between 1.7% and 1.9%, independent of the mAb concentration. Overall, the aggregate formation indicates a general mobility in the given formulations at -10 °C as expected upon storage above T_g' (25); differential scanning calorimetry showed T_g' values between -38 °C and -30 °C and between -59 °C and -45 °C for formulations with histidine and adipic acid, respectively. With increasing histidine concentration aggregation levels after 6 months at -10 °C increased from 1.9% (low histidine) to 6.4% (maximum histidine). The highest HMWS level of 7.6% was detected for mAb1 samples without any histidine, which had a slightly higher pH value of 5.9 compared to the histidine samples buffered to pH 5.5.

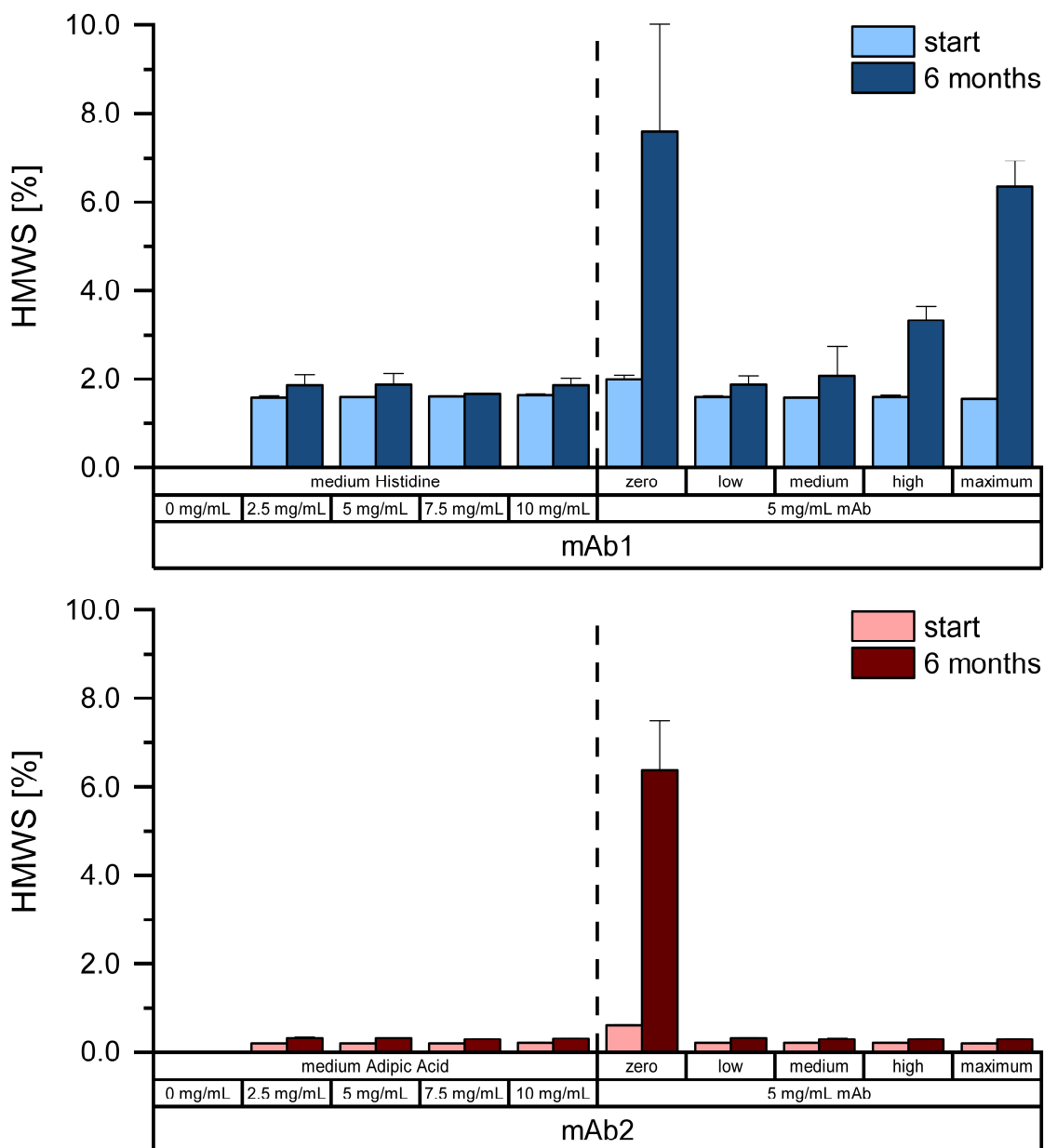


Figure 1 HMWS levels at the start and after six-month storage at -10 °C.

The mAb2 samples showed 0.2% soluble aggregates at the start of the experiment, except for the buffer-free sample with 0.6% HMWS. After 6 months frozen storage, HMWS levels were only slightly increased to 0.3%, regardless of the mAb or adipic acid concentration. Marked aggregation was detected for the buffer-free formulation with 6.4% HMWS. These samples had a pH of 5.7 compared to the formulations buffered with adipic acid at 5.2.

5.4.2 Formation of Subvisible Particles

In the medium histidine buffer control less than 1 200 SVPs $\geq 1 \mu\text{m}$ at the start and after 6 months at -10°C were detected (Figure 2). At the start, up to 10 200 SVPs $\geq 1 \mu\text{m}$ were detected in mAb1 samples without a trend with increasing histidine concentration. However, an increase in protein concentration from 2.5 mg/mL to 10 mg/mL mAb1 resulted in an increase in SVPs from 2 400 to 8 300. After six months storage at -10°C , clear trends in SVPs were seen. With increasing mAb1 concentration from 2.5 mg/mL to 10 mg/mL the SVP count rose from 40 300 to 101 300 SVPs. Higher histidine concentrations decreased the colloidal stability. Samples without histidine displayed only 13 800 insoluble aggregates, but particle levels steadily increased to 22 000 (low histidine), 45 200 (medium histidine), 83 600 (high histidine), and 166 100 (maximum histidine). In both sample sets, samples with 5 mg/mL mAb1 in medium histidine buffer did not differ significantly in respect of SVP count.

The medium adipic acid buffer control sample showed less than 1 000 SVPs $\geq 1 \mu\text{m}$ at the start and after 6 months. At t_0 , SVPs were low and independent of the adipic acid concentration, but increasing with mAb2 concentration from 2 300 to 6 300. The negative impact of mAb and buffer concentration on colloidal stability during long-term storage seen for mAb1 in histidine buffer was confirmed by the results for mAb2 in adipic acid buffer. SVP formation was more pronounced at higher mAb concentration increasing from 52 300 at 2.5 mg/mL mAb2 to 166 700 at 10 mg/mL mAb2. Similarly, the adipic acid concentration had a negative impact with 45 800 SVPs at low adipic acid to 95 200 at maximum adipic acid concentration. Samples without adipic acid showed 24 300 SVPs at the start without further SVP formation upon storage.

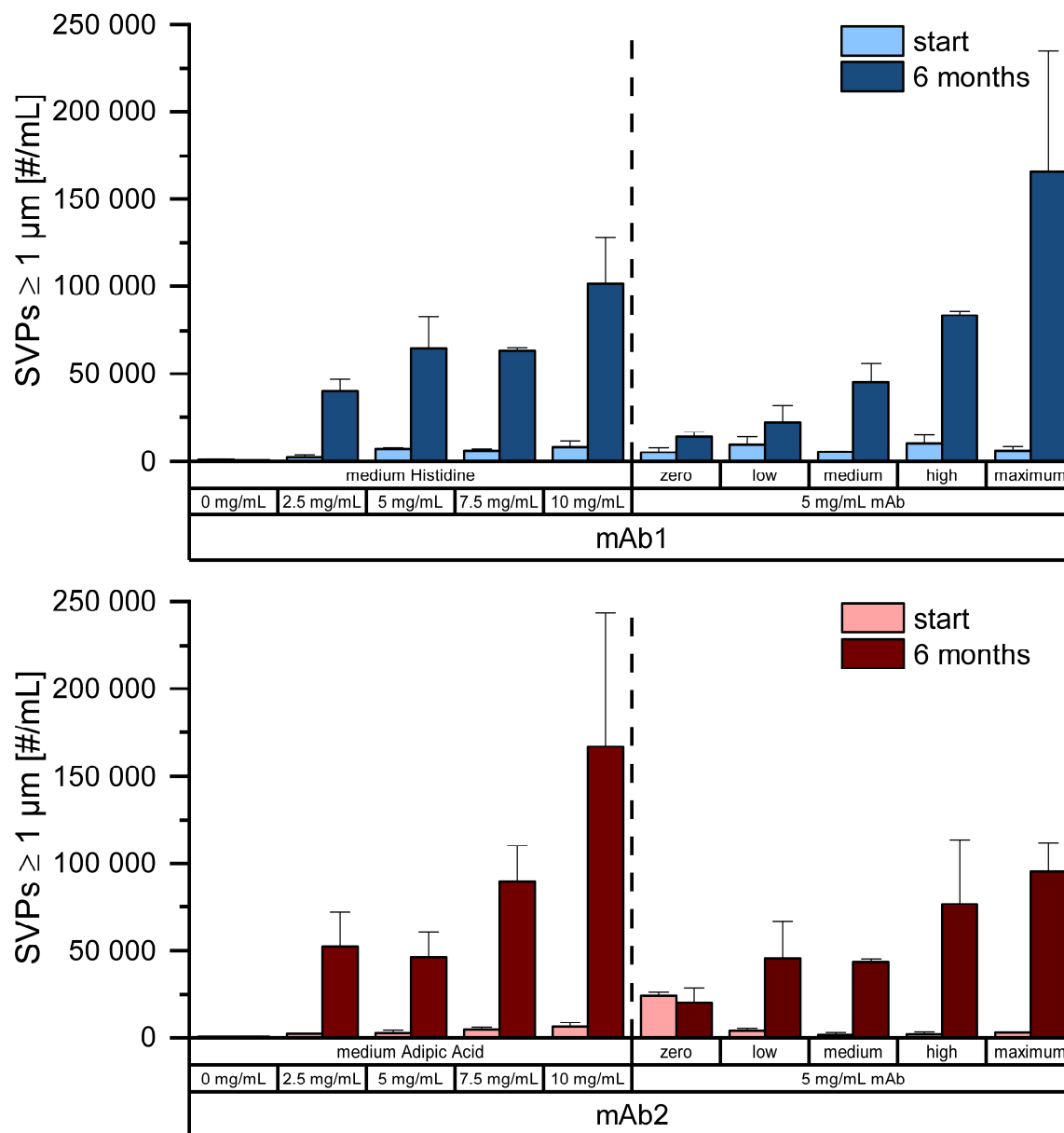


Figure 2 SVPs $\geq 1 \mu\text{m}$ at the start and after six-month storage at $-10 \text{ }^\circ\text{C}$.

5.4.3 Optical Density at 350 nm

Aggregate formation affecting turbidity was covered by analysis of OD350. At t_0 the OD350 was between 0.039 and 0.054, increasing slightly with mAb concentration (Figure 3). There was no clear trend in the change in OD350 after six-month frozen storage and in many samples no change was detectable.

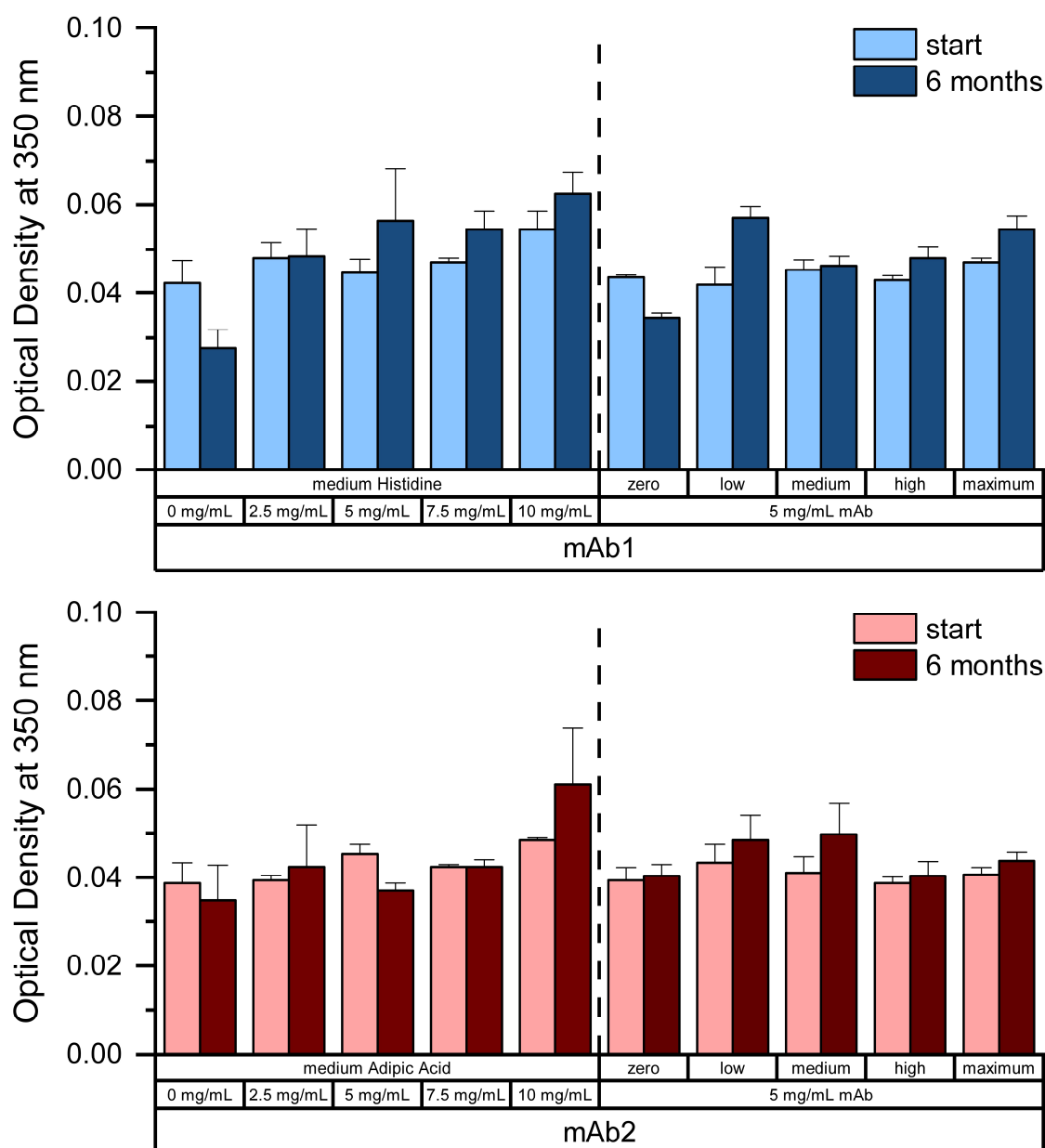


Figure 3 Optical density at 350 nm at the start and after six-month storage at $-10\text{ }^{\circ}\text{C}$.

5.4.4 MAb Oxidation

Additionally, mAb oxidation was analysed by protein A chromatography. Three peaks for different degrees of methionine oxidation in the Fc part can occur (21). We did not observe the peak reflecting full oxidation of Met252 and strongly oxidised Met428, but detected partially oxidised species. Oxidation of mAb1 was between 3.3% and 4.5% at t_0 (Figure 4). Upon six-month storage, samples with lowest mAb1 concentration showed 7.7% oxidised species. With increasing mAb1 concentration the oxidised fraction became less and at 10 mg/mL mAb1 only 5.0% oxidised species were detected. Mab oxidation increased with higher histidine concentration respectively mAb storage stability slightly

decreased, as only 4.9% partially oxidised mAb1 were detected in the histidine free formulation, while 7.4% were observed at maximum histidine.

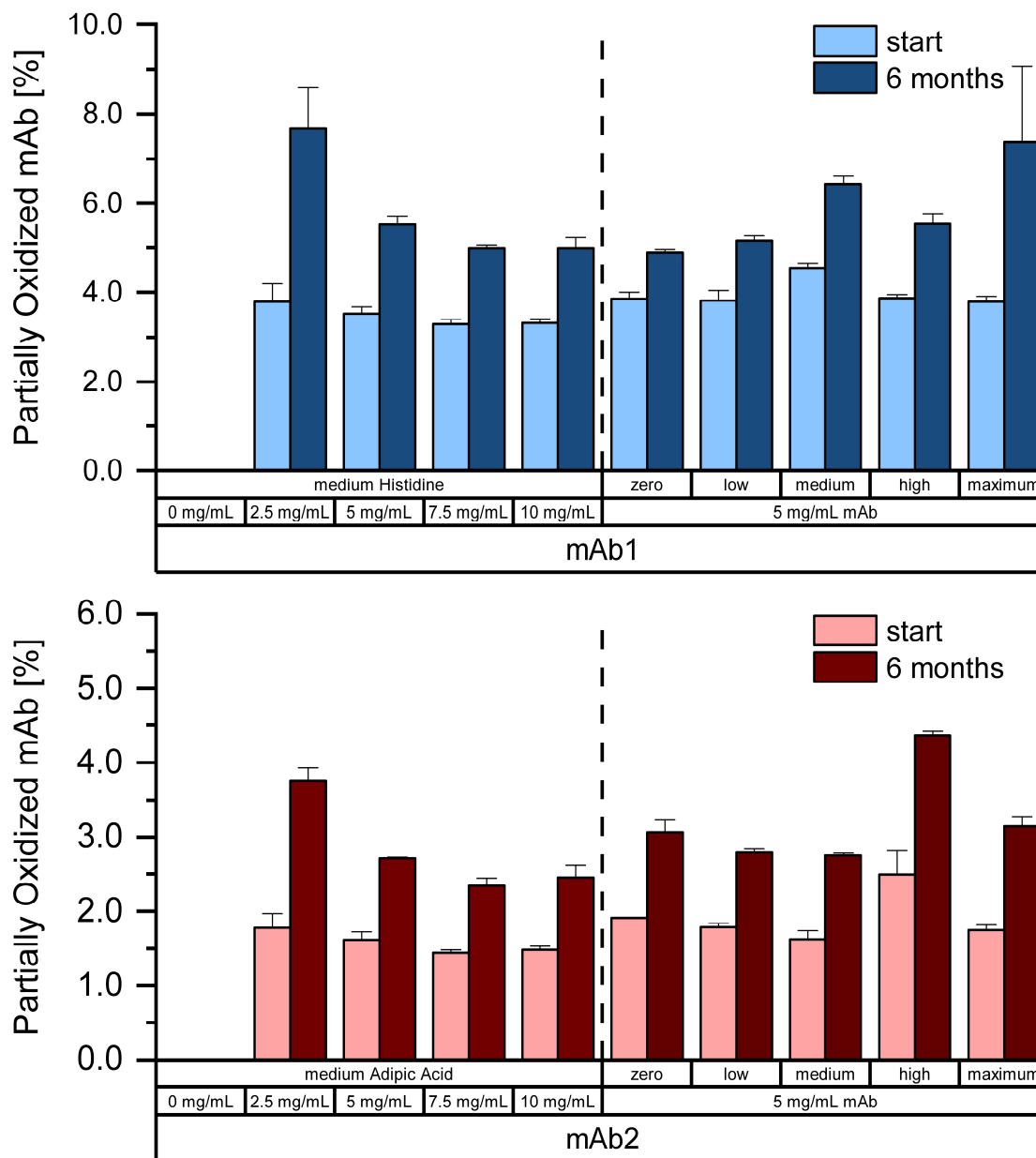


Figure 4 mAb oxidation levels at the start and after six-month storage at -10 °C.

Initially, mAb2 samples in adipic acid showed between 1.4% and 2.5% oxidation. During frozen storage, the partially oxidised fraction increased but less than for mAb1 in histidine. The mAb concentration again had a positive impact with 3.8% oxidised species at 2.5 mg/mL mAb2 compared to 2.5% at 10 mg/mL. The increase in oxidised species by approximately 1.2% upon storage was independent of the adipic acid concentrations (samples with high adipic acid concentration displayed the highest oxidised fraction after 6 months with 4.4%, but also had the highest level at t0).

5.4.5 Interaction Parameter k_D

The linear fit of mutual diffusion coefficients versus mAb concentration allows to calculate the interaction parameter k_D (22–24). While it was possible to evaluate the effect of histidine and adipic acid on mAb self-interaction, k_D analysis at low ionic strength has to be carefully interpreted because of nonlinearity of the experimental data (23,24). We therefore excluded buffer-free formulations. Increasing histidine concentration reduced mAb1 k_D values from 24.6 mL/g to 1.8 mL/g (Figure 5). The k_D value of mAb2 decreased from 3.0 mL/g in low adipic acid to a negative value of -4.2 mL/g in maximum adipic acid.

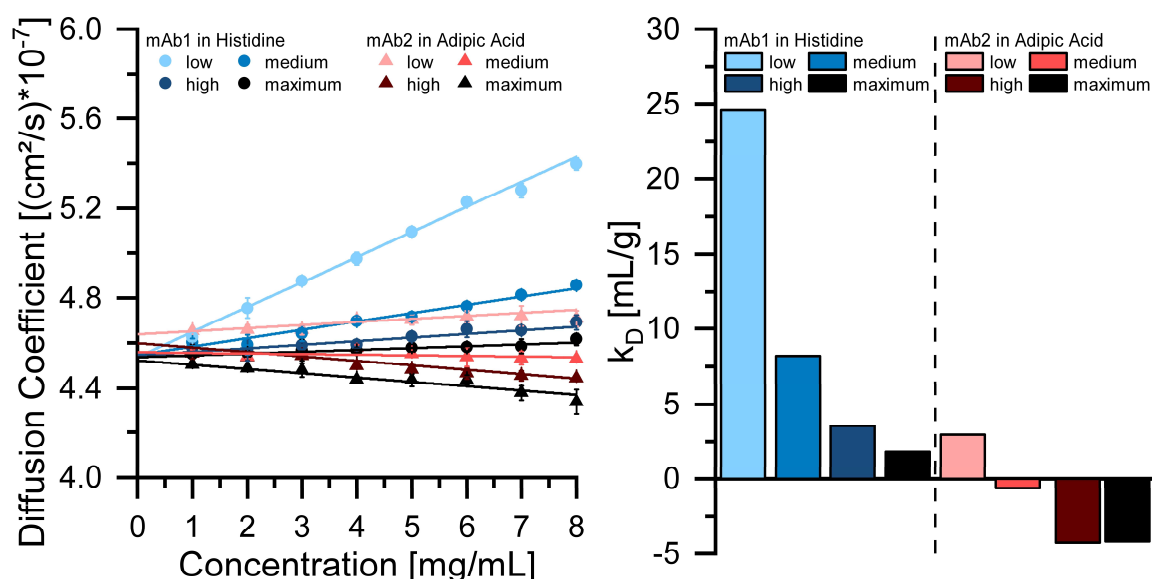


Figure 5 Linear regression fit of diffusion coefficient versus protein concentration (left) and calculated k_D (right).

5.5 Discussion

Our aim was to close the knowledge gap about the stability of frozen bulk drug substance, which is regularly utilised in production of protein pharmaceuticals. Due to differences in diffusivity, large-scale freezing is not only associated with cryoconcentration (5,14,15), but can come with spatial shifts in the mAb to excipient ratio (3,15,17). In the present study, we connected freeze-concentration with frozen storage stability of mAbs. We examined aggregation and oxidation of two mAbs formulated in histidine (mAb1) or adipic acid (mAb2). Samples were adjusted in the similar concentration range that evolves during cryoconcentration upon large-scale freezing (17). Two sets of samples were prepared for each mAb, one at a given mAb concentration and varying the buffer concentration and a

second one with fixed buffer concentration but variation of the mAb concentration. Samples were stored at $-10\text{ }^{\circ}\text{C}$, significantly above T_g , to generate a stress model.

Formation of small soluble aggregates was analysed via SEC. Upon frozen storage, samples with varying mAb concentration showed only a marginal increase in HMWS levels of approximately 0.2%. Several studies emphasize a positive effect of protein concentration on stability (4,26,27). During freezing, mAbs adsorb at the ice/FCM interface. This interface area is finite and the relative adsorbed fraction decreases when mAb concentration is increased (4,26). However, the sensitivity for denaturation and aggregation during freezing/thawing or freeze-drying is protein dependent (26,27). Furthermore, these studies focussed on the process conditions, whereas the recent study examines the storage stability of mAbs. While the mAb concentration did not affect HMWS levels upon frozen storage, an increase in histidine concentration increased the HMWS level by up to 4.8%. Protein-protein interactions highly depend on ionic strength (28) and can be correlated to the protein interaction parameter k_D . Positive k_D values are associated with net repulsive interactions (22–24). We found less repulsive interactions with higher buffer concentration, which can increase aggregation tendency in solution but also at the interface, where the adsorbed layer reflects a phase of high protein concentration with molecules fixed in close vicinity. Soluble aggregates in buffer-free samples increased by 5.6% and 5.8% upon six-month frozen storage of mAb1 and mAb2, respectively. This may be due to the pH of these samples that was not adjusted and differed from the histidine or adipic acid buffered solutions. This pH difference might also explain the higher HMWS levels at t_0 . Due to the nonlinearity of the data under buffer-free conditions, k_D values cannot be reliably assessed to evaluate protein-protein interactions at the given pH and ionic strength (23,24).

Larger aggregates were analysed via OD350 (3,29,30). No clear trends upon storage could be identified and no effects of mAb or buffer concentration. The negative impact of higher histidine concentrations on mAb1 stability, which was seen in SEC, was not reflected on this nanometre-size level, but was additionally pronounced at the micrometre level (see discussion on SVPs below). An influence of adipic acid concentration on mAb2 stability could not be detected via OD350. It has been shown previously that an increase in HMWS is not necessarily connected to an increase in turbidity (12).

Particles in the micrometre range were evaluated via flow imaging microscopy. Increasing mAb concentration led to higher SVPs counts up to approximately 100 000 SVPs for mAb1 and 170 000 SVPs for mAb2 upon six-month frozen storage. SVP formation steadily

increased with mAb concentration for both mAbs, already seen at t₀, which included freeze-thaw stress. The significant increase in SVPs with mAb concentration presumably resulted from hundredth of a percent of the total protein in solution and is therefore not reflected in the HMWS levels (30). Increasing the buffer concentration and consequently the ionic strength resulted in more pronounced formation of SVPs. Highest counts were detected for the maximum histidine (for mAb1 formulations) and maximum adipic acid concentration (for mAb2 formulations) with approximately 170 000 SVPs and 100 000 SVPs, respectively. During storage, protein-protein interactions contribute substantially to the overall stability, while especially surface-induced denaturation drives aggregation during the freezing and the thawing process (10,27,31). The decrease in k_D values with increasing histidine concentration showed a trend towards more attractive protein-protein interactions that was similarly observed for higher adipic acid concentration. While in buffer-free samples highest levels of soluble aggregates were detected, OD350 and SVPs remained on the initial level. Repulsive interactions between mAb aggregates presumably prevented the formation of large particles. Additionally performed dynamic light scattering measurements of buffer-free samples proved the general absence of particles in the micrometre range.

To our knowledge, no study examined the possible oxidation during frozen storage of proteins or mAbs. Authelin et al. emphasized the possible importance of mAb oxidation upon freezing (16). Samples at lower temperatures per se contain high concentrations of oxygen due to an increase in oxygen solubility with decreasing temperature. In addition, dissolved gases freeze-concentrate as other solutes. As soon as the solubility limit is reached, gases, predominantly oxygen and nitrogen, can form air bubbles. This process is facilitated by cryoconcentration of other solutes, such as sugars or salts, which further reduce the solubility of gases. The practical relevance of freeze-concentration of oxygen has been shown by Takenaka et al. (32). In our study, we saw marked mAb oxidation as well as a significant impact of mAb concentration on oxidation. In particular, at the lowest concentration of 2.5 mg/mL mAb1 or mAb2 the oxidation level after storage was substantially increased, whereas the different samples with a protein concentration between 5 mg/mL and 10 mg/mL showed a rather similar increase. At this point we could only speculate on rate limiting effects setting in at high protein concentration or enhancing effects at low protein concentration. No clear trend was observed for increasing adipic acid concentration, whereas higher histidine concentrations promoted mAb1 oxidation. Mason

et al. have demonstrated that histidine oxidises, accompanied by multiple byproducts, and that even pure histidine contains catalytic amounts of metal cations (33). The rapid oxidation of polysorbate 80 has been connected to the use of histidine buffer (34); addition of a mAb completely prevented surfactant oxidation with the mAb potentially acting like a scavenger, which itself might get oxidised. Our experiment highlighted the need for a routine check of mAb oxidation during long-term frozen storage.

Transferred to cryoconcentration that we found upon large-scale freezing in a 2 L bottle (17), our small-scale experiments suggest a marked impact of little changes in mAb and buffer concentration on mAb aggregation and oxidation. Depending on the position in the bottle, the stability significantly differs in comparison to the solution's initial nominal composition. Areas with the highest mAb concentration, found in the top region of the bottle, significantly contribute to the formation of SVPs. However, mAb oxidation is reduced in these regions. Due to differences in diffusivity, the mAb to buffer ratio is shifted towards the buffer component in the centre region near the bottom (17). This region can be associated with substantial formation of SVPs and, in case of the mAb1 formulation containing histidine, with higher HMWS levels and an increased partially oxidised mAb fraction. In contrast, the areas near the wall of the bottle, containing minimum buffer concentration, are characterised by highest stability. Overall, cryoconcentration should be avoided. One option is faster freezing, which could in addition reduce the exposure time of proteins to detrimental factors but may render smaller ice crystals and thus larger critical ice/FCM interface (3,7). Alternatively, natural convection, which is thought to be the main driving force for freeze-concentration, could be reduced e.g. by freezing from bottom to top if the liquid level is low (35). However, this would inevitably imply a new bottle and freezer design. Freezing solutions with lower mAb concentration may help to reduce SVP formation, but at the same time may increase the risk of mAb oxidation. The buffer concentration should be sufficient to stabilise the pH, but unnecessarily high concentrations coming with reduced repulsive mAb self-interaction should be avoided.

5.6 Conclusion

In this work, we examined the effects that changes in mAb and buffer concentration due to cryoconcentration have on long-term frozen storage stability. Two set of samples were prepared, one with constant mAb concentration (5 mg/mL mAb1 and mAb2, respectively) and a second one with constant buffer concentration (medium histidine/adipic acid).

Concentrations were adjusted similarly to the position-dependent cryoconcentration that was found after large-scale freezing in a 2 L bottle (17). All samples were processed equally and subsequently stored for 6 months at $-10\text{ }^{\circ}\text{C}$, significantly above T_g' .

Increasing mAb concentration did not affect the formation of HMWS upon long-term frozen storage, while higher histidine concentration facilitated the formation of HMWS. No effects of mAb or buffer species and concentrations on larger aggregates assessed via OD350 could be identified. The SVP count steadily increased for both mAbs with protein as well as buffer concentration. The protein-protein interaction parameter k_D revealed a trend towards more attractive interactions with higher ionic strength, i.e. buffer concentration. MAb oxidation upon frozen storage was found to be an important parameter, which was negatively affected by increasing histidine concentration, but became less with increasing mAb concentration. Transferred to spatial cryoconcentration in a large-scale 2 L bottle upon freezing (17), apparently small position-dependent changes in mAb and buffer concentration have a substantial impact on storage stability. Areas with higher mAb concentration, found in the top region, are prone to form SVPs, but show reduced levels of oxidised species. Regions with increased buffer concentration, in case of a 2 L bottle in the centre near the bottom, are associated with marked SVP levels. In case of mAb1 formulated in histidine, these areas additionally tend to form HMWS and oxidised mAb species. The highest stability is expected in regions near the wall that represent lowest buffer concentrations.

These findings suggest that reducing cryoconcentration, e.g. by accelerating freezing or directed freezing from bottom to top, can improve the long-term frozen storage stability of mAb solutions. Additionally, reducing the initial mAb concentration may help to decrease the formation of SVPs. However, this might increase the risk mAb oxidation. High buffer concentrations that reduce repulsive protein-protein interactions should be avoided, but sufficiently high concentration assured to stabilise the formulation pH.

Acknowledgements

The authors thank the Novartis Pharma AG for providing mAb stock solutions and Leonie Kainz for a helping hand during the sample preparation.

References

1. Maity H, Karkaria C, Davagnino J. Mapping of solution components, pH changes, protein stability and the elimination of protein precipitation during freeze–thawing of fibroblast growth factor 20. *Int J Pharm.* 2009 Aug;378(1–2):122–35.
2. Gervasi V, Dall Agnol R, Cullen S, McCoy T, Vucen S, Crean A. Parenteral protein formulations: An overview of approved products within the European Union. *Eur J Pharm Biopharm.* 2018 Oct;131(July):8–24.
3. Miller MA, Rodrigues MA, Glass MA, Singh SK, Johnston KP, Maynard JA. Frozen-State Storage Stability of a Monoclonal Antibody: Aggregation is Impacted by Freezing Rate and Solute Distribution. *J Pharm Sci.* 2013 Apr;102(4):1194–208.
4. Arsiccio A, Pisano R. The Ice-Water Interface and Protein Stability: A Review. *J Pharm Sci.* 2020 Jul;109(7):2116–30.
5. Hauptmann A, Hoelzl G, Loerting T. Distribution of Protein Content and Number of Aggregates in Monoclonal Antibody Formulation After Large-Scale Freezing. *AAPS PharmSciTech.* 2019 Feb 10;20(2):72.
6. Padala C, Jameel F, Rathore N, Gupta K, Sethuraman A. Impact of Uncontrolled vs Controlled Rate Freeze-Thaw Technologies on Process Performance and Product Quality. *PDA J Pharm Sci Technol.* 2010;64(4):290–8.
7. Rodrigues MA, Miller MA, Glass MA, Singh SK, Johnston KP. Effect of Freezing Rate and Dendritic Ice Formation on Concentration Profiles of Proteins Frozen in Cylindrical Vessels. *J Pharm Sci.* 2011 Apr;100(4):1316–29.
8. Kolhe P, Amend E, K. Singh S. Impact of freezing on pH of buffered solutions and consequences for monoclonal antibody aggregation. *Biotechnol Prog.* 2009 Dec 28;26(3):727–33.
9. Arsiccio A, McCarty J, Pisano R, Shea J-E. Heightened Cold-Denaturation of Proteins at the Ice–Water Interface. *J Am Chem Soc.* 2020 Mar 25;142(12):5722–30.
10. Duarte A, Rego P, Ferreira A, Dias P, Geraldes V, Rodrigues MA. Interfacial Stress and Container Failure During Freezing of Bulk Protein Solutions Can Be Prevented by Local Heating. *AAPS PharmSciTech.* 2020 Oct 1;21(7):251.
11. Connolly BD, Le L, Patapoff TW, Cromwell MEM, Moore JMR, Lam P. Protein Aggregation in Frozen Trehalose Formulations: Effects of Composition, Cooling Rate, and Storage Temperature. *J Pharm Sci.* 2015 Dec;104(12):4170–84.
12. Singh SK, Kolhe P, Mehta AP, Chico SC, Lary AL, Huang M. Frozen State Storage Instability of a Monoclonal Antibody: Aggregation as a Consequence of Trehalose Crystallization and Protein Unfolding. *Pharm Res.* 2011 Apr 7;28(4):873–85.

13. Pikal-Cleland KA, Rodríguez-Hornedo N, Amidon GL, Carpenter JF. Protein Denaturation during Freezing and Thawing in Phosphate Buffer Systems: Monomeric and Tetrameric β -Galactosidase. *Arch Biochem Biophys*. 2000 Dec;384(2):398–406.
14. Roessl U, Leitgeb S, Nidetzky B. Protein freeze concentration and micro-segregation analysed in a temperature-controlled freeze container. *Biotechnol Reports*. 2015 Jun;6:108–11.
15. Kolhe P, Mehta AP, Lary AL, Chico SC, Singh SK. Large-Scale Freezing of Biologics (Part III). *BioPharm Int*. 2012;25(October):40–8.
16. Authelin J-R, Rodrigues MA, Tchessalov S, Singh SK, McCoy T, Wang S, et al. Freezing of Biologics Revisited: Scale, Stability, Excipients, and Degradation Stresses. *J Pharm Sci*. 2020 Jan;109(1):44–61.
17. Bluemel O, Buecheler JW, Rodrigues MA, Geraldes V, Hoelzl G, Bechtold-Peters K, et al. Cryoconcentration and 3D Temperature Profiles During Freezing of mAb Solutions in Large-Scale PET Bottles and a Novel Scale-Down Device. *Pharm Res*. 2020 Sep 30;37(9):179.
18. Kuelto LA, Wang W e. i., Randolph TW, Carpenter JF. Effects of Solution Conditions, Processing Parameters, and Container Materials on Aggregation of a Monoclonal Antibody during Freeze-Thawing. *J Pharm Sci*. 2008 May;97(5):1801–12.
19. Hauptmann A, Podgoršek K, Kuzman D, Srčić S, Hoelzl G, Loerting T. Impact of Buffer, Protein Concentration and Sucrose Addition on the Aggregation and Particle Formation during Freezing and Thawing. *Pharm Res*. 2018 May 19;35(5):101.
20. Zhang A, Singh SK, Shirts MR, Kumar S, Fernandez EJ. Distinct Aggregation Mechanisms of Monoclonal Antibody Under Thermal and Freeze-Thaw Stresses Revealed by Hydrogen Exchange. *Pharm Res*. 2012 Jan 30;29(1):236–50.
21. Loew C, Knoblich C, Fichtl J, Alt N, Diepold K, Bulau P, et al. Analytical Protein A Chromatography as a Quantitative Tool for the Screening of Methionine Oxidation in Monoclonal Antibodies. *J Pharm Sci*. 2012 Nov;101(11):4248–57.
22. Menzen T, Friess W. Temperature-Ramped Studies on the Aggregation, Unfolding, and Interaction of a Therapeutic Monoclonal Antibody. *J Pharm Sci*. 2014 Feb;103(2):445–55.
23. Pindrus MA, Shire SJ, Yadav S, Kalonia DS. The Effect of Low Ionic Strength on Diffusion and Viscosity of Monoclonal Antibodies. *Mol Pharm*. 2018;15(8):3133–42.
24. Sorret LL, DeWinter MA, Schwartz DK, Randolph TW. Challenges in Predicting Protein-Protein Interactions from Measurements of Molecular Diffusivity. *Biophys J*. 2016 Nov;111(9):1831–42.
25. Pansare SK, Patel SM. Practical Considerations for Determination of Glass Transition Temperature of a Maximally Freeze Concentrated Solution. *AAPS PharmSciTech*. 2016 Aug 18;17(4):805–19.
26. Jiang S, Nail SL. Effect of process conditions on recovery of protein activity after freezing and freeze-drying. *Eur J Pharm Biopharm*. 1998 May;45(3):249–57.

The Effect of mAb and Excipient Cryoconcentration on Long-Term Frozen Storage
Stability – Part 2: Aggregate Formation and Oxidation

27. Sarciaux J-M, Mansour S, Hageman MJ, Nail SL. Effects of buffer composition and processing conditions on aggregation of bovine IgG during freeze-drying. *J Pharm Sci.* 1999 Dec;88(12):1354–61.
28. Wang W, Nema S, Teagarden D. Protein aggregation—Pathways and influencing factors. *Int J Pharm.* 2010 May;390(2):89–99.
29. Jameel F, Hershenson S. Formulation and Process Development Strategies for Manufacturing Biopharmaceuticals. Jameel F, Hershenson S, editors. *Formulation and Process Development Strategies for Manufacturing Biopharmaceuticals.* Hoboken, NJ, USA: John Wiley & Sons, Inc.; 2010. 955 p.
30. Barnard JG, Singh S, Randolph TW, Carpenter JF. Subvisible Particle Counting Provides a Sensitive Method of Detecting and Quantifying Aggregation of Monoclonal Antibody Caused by Freeze-Thawing: Insights Into the Roles of Particles in the Protein Aggregation Pathway. *J Pharm Sci.* 2011 Feb;100(2):492–503.
31. Singh SK, Kolhe P, Wang W, Nema S. Large-Scale Freezing of Biologics A Practitioner’s Review, Part One: Fundamental Aspects. *Bioprocess Int.* 2009;7(9):32–44.
32. Takenaka N, Ueda A, Daimon T, Bandow H, Dohmaru T, Maeda Y. Acceleration Mechanism of Chemical Reaction by Freezing: The Reaction of Nitrous Acid with Dissolved Oxygen. *J Phys Chem.* 1996 Jan;100(32):13874–84.
33. Mason BD, McCracken M, Bures EJ, Kerwin BA. Oxidation of Free L-histidine by tert-Butylhydroperoxide. *Pharm Res.* 2010 Mar 2;27(3):447–56.
34. Gopalrathnam G, Sharma AN, Dodd SW, Huang L. Impact of Stainless Steel Exposure on the Oxidation of Polysorbate 80 in Histidine Placebo and Active Monoclonal Antibody Formulation. *PDA J Pharm Sci Technol.* 2018;72(2):163–75.
35. Rodrigues MA, Balzan G, Rosa M, Gomes D, de Azevedo EG, Singh SK, et al. The importance of heat flow direction for reproducible and homogeneous freezing of bulk protein solutions. *Biotechnol Prog.* 2013 Sep;29(5):1212–21.

Chapter 6 Evaluation of Two Novel Scale-Down Devices for Testing mAb Aggregation during Large-Scale Freezing

Oliver Bluemel¹, Miguel A. Rodrigues², Jakob W. Buecheler³, Vitor Geraldés⁴, Astrid Hauptmann⁵, Georg Hoelzl⁵, Karoline Bechtold-Peters³, Wolfgang Friess¹

1 Pharmaceutical Technology and Biopharmaceutics, Department of Pharmacy, Ludwig-Maximilians-Universität München, 81377 Munich, Germany

2 Centro de Química Estrutural, Department of Chemical Engineering, Instituto Superior Técnico, Lisboa 1049-001, Portugal

3 Technical Research and Development, Novartis Pharma AG, 4002 Basel, Switzerland

4 CeFEMA, Department of Chemical Engineering, Instituto Superior Técnico, Lisboa 1049-001, Portugal

5 Sandoz GmbH, 6336 Langkampfen, Austria

Author contributions:

O.B., W.F., and K.B.P. conceived the study. M.A.R. and V.G. developed the scale-down device and the micro scale-down device. O.B. performed the experiments and evaluated the data. O.B. wrote the paper. W.F., K.B.P., J.W.B., A.H., and G.H. contributed to the discussion of the results and revised the manuscript. W.F. and K.B.P. supervised the work.

6.1 Abstract

Purpose: Monoclonal antibody (mAb) aggregation during freezing and thawing of drug substance in large volumes cannot be scaled down simply by reducing the volume drastically. Thus, there is a need for representative scale-down devices (SDDs) that reflect the stress in large containers, but require only a fraction of the material. To this end we studied two novel SDDs.

Methods: We characterised mAb aggregation upon repeated freezing and thawing in two SDDs that aim to mimic the stress in a rectangular 2 L bottle. One SDD consists of a 3D printed cover that surrounds a 125 mL bottle and thereby manipulates heat exchange, whereas the micro SDD (mSDD) adapts cooling and heating of 10 mL vials to extend stress time. MAb aggregation was evaluated in respect of the formation of higher molecular weight species (HMWS), subvisible particles $\geq 1 \mu\text{m}$ per mL (SVPs), and the increase in hydrodynamic radius, polydispersity index (PDI), and optical density at 350 nm. Three different mAb solutions were processed.

Results: The SDD as well as the unshielded 125 mL bottle mimicked mAb aggregation in a 2 L bottle upon repeated freezing and thawing of a 5 mg/mL mAb1 or an 85 mg/mL mAb2 solution. Upon processing a 1 mg/mL mAb2 solution in a 2 L bottle, the increase in HMWS to 1.25%, in SVPs to 108 100 $\geq 1 \mu\text{m}$ per mL, in average hydrodynamic radius to 5.7 nm, and in PDI to 0.38 indicated significant aggregation. Both the SDD and the unshielded 125 mL bottle showed similar SVP levels, hydrodynamic radius, and PDI. However, in the SDD up to 1.55% soluble aggregates were detected, while the 125 mL bottle showed only 0.95%.

Aggregation in 10 mL vials was negligible. The utilisation of the mSDD led to 0.63% HMWS, 31 700 SVPs $\geq 1 \mu\text{m}$ per mL, and an average hydrodynamic radius and PDI of 5.2 nm and 0.14, respectively.

Conclusion: In general, both the unshielded 125 mL bottle and the SDD can be used to predict aggregation upon freezing and thawing in large-scale 2 L bottles. In specific cases the unshielded 125 mL bottle might underestimate soluble aggregates, whereas the SDD slightly overestimates HMWS levels. The mSDD significantly increases aggregation in comparison to 10 mL vials. Nevertheless, the results of the 2 L bottle were not matched.

Keywords: aggregation, freezing, monoclonal antibody, scale-down device, thawing

Abbreviations: CFD – Computational Fluid Dynamics, DLS – Dynamic light scattering, FCM - Freeze-concentrated matrix, FT – Freezing and Thawing, HMWS – Higher molecular weight species, HPLC - High-performance liquid chromatography, mAb – Monoclonal antibody, mSDD – Micro scale-down device, PDI – Polydispersity index, SDD Scale-down device, OD350 – Optical density at 350 nm, PES – Polyethersulfone, SEC – Size-exclusion chromatography, SVP – Subvisible particle, T_g' – Glass transition temperature of the maximally freeze-concentrated solution

6.2 Introduction

Therapeutic proteins, such as monoclonal antibodies (mAbs), are generally stored frozen during industrial production to increase shelf life (1–5). Freezing minimises the risk of microbial growth and slows down physical and chemical reactions (3,4,6). By decoupling drug substance and drug product processing, freezing offers flexibility during manufacturing while maintaining stability for an extended period of time (3,6,7). Frozen transportation reduces the risk of foaming, shaking, and agitation compared to liquid (5). In addition to intentional freezing and subsequent thawing operations during production, mishandling by operators or patients might lead to unintended freezing and thawing (FT) of drug substance or drug product (8). These benefits might be outbalanced by several undesirable effects. Microscopic and macroscopic cryoconcentration after freezing (9–12) and concentration gradients after thawing (5,13) are well examined. During freezing, solutes are mostly excluded from the growing ice phase, form a freeze-concentrated matrix (FCM) in between ice crystals, and define the protein microenvironment. The macroscopic spatial composition is determined by natural convection and diffusivity of solutes during freezing (2). This results in substantial heterogeneity in the frozen bulk (14). During thawing, the FCM melts out of the ice (1). Because of its significantly increased concentration and consequently higher density, nearly pure ice is left which starts to float and dilutes the top region (1). Thus, not only after freezing but also after thawing a substantial heterogeneity evolves (1,5,13). Additionally, conformational and colloidal stability during FT might be impacted by cold denaturation (15–17), (re)crystallisation (6,18–20), significant pH shifts (7,21), and degradation at the ice interface (12,22). Recently, the formation of air bubbles, local pressure, and mechanical stresses have been proposed (23) and add to the various possible stresses.

Typically, effects of solution conditions or processing parameters on the protein, specifically its physical stability as reflected by aggregate formation, are not performed at the production scale spending several litres of highly valuable material, but in small-scale studies (3,7,8,18,20,21,24,25). Such experiments support optimisation of the formulation or to unveil stability issues during storage. Nonetheless, processing and freezing rates, exposure times to critical effects, freeze-concentration, as well as the ice/FCM interface area are not preserved (2,14,26,27). Thus, the freeze-thaw stress at small scale does not reflect large-scale stress and the results have to be interpreted with care. SmartFreeZ developed a scale-down device (SDD) that tries to overcome this limitation (Figure 1). It

enables to mimic FT of 2 L bottles utilising 125 mL bottles. In short, Computational Fluid Dynamics (CFD) modelling was used to assess the stress time of each control volume, defined as the time after the beginning of freezing until the glass transition temperature of the maximally freeze-concentrated solution (T_g') is reached. The 3D printed SDD surrounds a 125 mL bottle, which footprint is one fourth of the 2 L bottle. By insulating two walls, heat exchange is controlled to match the cumulative stress time of a 2 L bottle. Thereby, the SDD significantly prolongs process time in comparison to an unshielded 125 mL bottle and mimics the cryoconcentration during freezing and the concentration gradients after thawing of a 2 L bottle (28). With this approach the material need can be reduced 16-fold from 1.6 L to 100 mL. The same CFD based approach of matching stress time was realised in a micro SDD (mSDD) to scale the volume further down (Figure 1). The mSDD operates with vials filled with 5.5 mL and thus minimises the volume nearly 300-fold. The significantly lower volume and different geometries do not allow to adapt cooling and heating rates by insulating the vials. Instead, heat exchange is controlled from the bottom through a stainless-steel plate.

Neither the 125 mL bottle nor the 10 mL vial based SDD have been evaluated concerning the question whether they can reflect the overall stress and physical instability of proteins in a 2 L bottle. To answer this question, we assessed aggregation of two mAbs during multiple freeze-thaw cycles comparing the 2 L bottle, the unshielded 125 mL bottle, the SDD, 10 mL vials, and the mSDD setup. We analysed the formation of higher molecular weight species (HMWS), subvisible particles $\geq 1 \mu\text{m}$ per mL (SVPs), the development of the average hydrodynamic radius R_h and the polydispersity index (PDI), as well as the optical density at 350 nm.

Upon five freeze-thaw cycles of 5 mg/mL mAb1 and 85 mg/mL mAb2 in the 2 L bottle with 1.6 L fill we observed only little changes. Both the unshielded 125 mL bottle and the SDD matched this outcome requiring only 100 mL. A 1 mg/mL mAb2 solution was much more sensitive and HMWS, SVPs, R_h , and PDI significantly increased with each freeze-thaw cycle in the 2 L bottle. The 125 mL bottle matched the development of insoluble aggregates, but markedly underestimated the formation of soluble aggregates. In contrast, the SDD led to more HMWS. 10 mL vials filled with 5.5 mL that were handled in the same freezer as the 2 L bottle significantly underestimated both soluble and insoluble aggregate formation. In contrast, the mSDD demonstrated more stress for the mAb, but still slightly less aggregation compared to the 2 L bottle was observed.

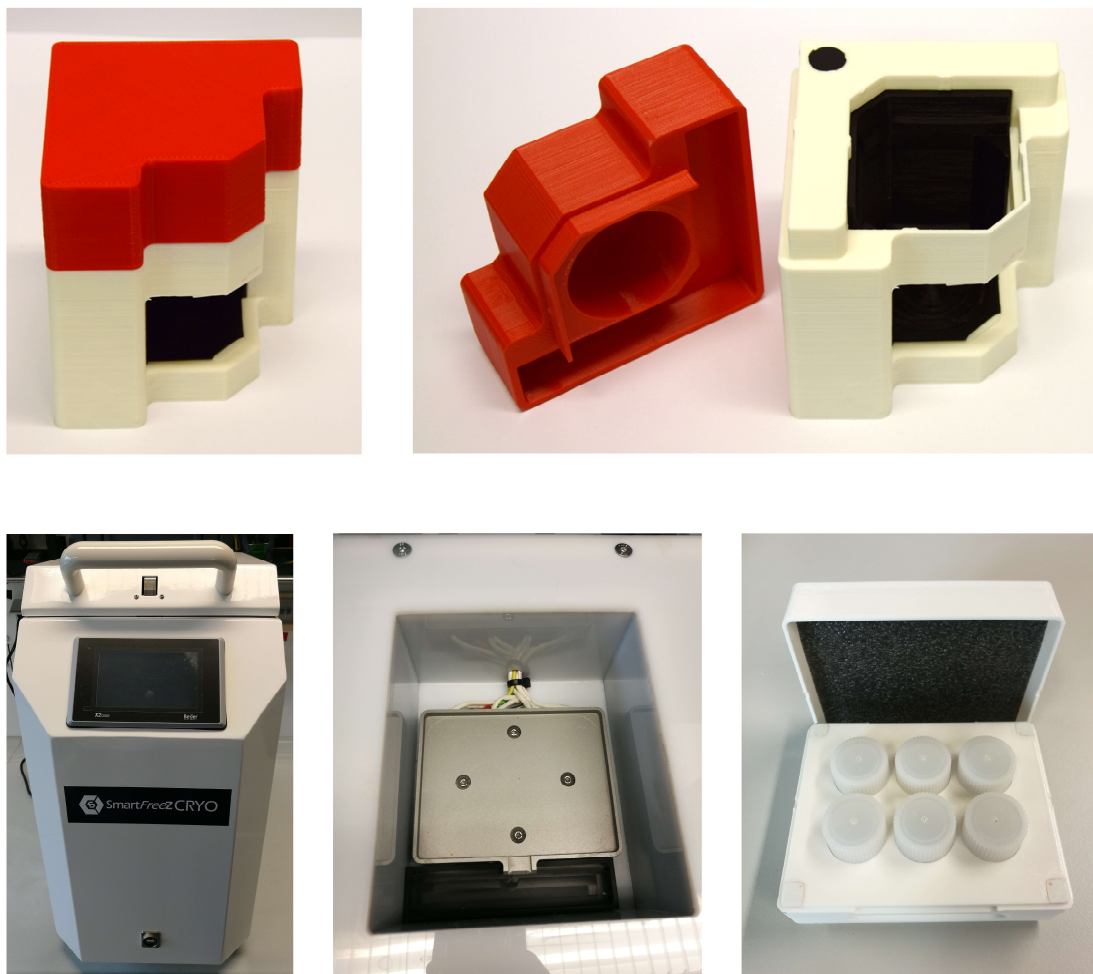


Figure 1 Top: SDD by SmartFreeZ that consists of a surrounding cover filled with 1% ethanol and a top cover. Bottom: The mSDD (left) controls heat exchange from the bottom via a plate filled with ethanol (centre). A 3D printed holder controls the positioning of six vials (right).

6.3 Materials and Methods

6.3.1 Materials

Novartis AG (Basel, Switzerland) provided two mAb stock solutions, a 185 mg/mL IgG1 mAb1 stock solution in 20 mM histidine buffer at pH 5.5 and an 85 mg/mL IgG1 mAb2 stock solution in 25 mM adipic acid buffer at pH 5.2. Adipic acid 99% was purchased from Sigma-Aldrich Produktions GmbH (Steinheim am Albuch, Germany). L-histidine monohydrate and L-histidine monochloride were both acquired from Merck KGaA (Darmstadt, Germany). Dipotassium phosphate and monopotassium phosphate were obtained from Merck KGaA (Darmstadt, Germany).

Cellon S.A. (Bascharage, Luxembourg) delivered 125 mL and 2 L PharmaTainer™ bottles as well as 10 mL PharmaTainer™ stability vials all made of polyethylene terephthalate. 0.2 µm polyethersulfone membrane syringe and bottle top filters were acquired from VWR International GmbH (Darmstadt, Germany). Colourless 1.5 mL Eppendorf Tubes® 3810X were obtained from Eppendorf AG (Hamburg, Germany).

6.3.2 Preparation of Protein Samples

The mAb1 stock solution was diluted to a final concentration of 5 mg/mL in 20 mM histidine buffer at pH 5.5. MAb2 stock solution was used as delivered at 85 mg/mL or diluted to 1 mg/mL mAb2 in 25 mM adipic acid buffer at pH 5.2. The final mAb concentrations were controlled using a NanoDrop™ One (Thermo Fisher Scientific Inc., Waltham, Massachusetts, USA) via UV absorption at 280 nm with baseline correction. Subsequently, samples were filtered through 0.2 µm bottle top or syringe filters. 2 L bottles were filled with 1.6 L, the 125 mL bottles and the SDD with 100 mL and the 10 mL vials as well as the mSDD with 5.5 mL mAb solution.

6.3.3 SDD and mSDD

The SDD and the mSDD were provided by SmartFreeZ (Porto Salvo, Portugal). A 125 mL PharmaTainer™ bottle is covered by the SDD (Figure 1). The SDD is filled with 1% ethanol to reach adiabatic conditions at two walls and thereby control heat exchange. Two SDDs were used in back-to-back orientation. One filled with 100 mL mAb solution was used for the experiment, a second one containing 100 mL highly purified water for shielding.

The mSDD (Figure 1) defines cooling and heating rates to control heat exchange during FT in the vial and thereby mimic the thermal history of a 2 L bottle that is frozen and thawed at constant external temperatures, namely -80 °C for freezing and 25 °C for thawing. The mSDD can generate temperature profiles to mimic FT under a user-selected average heat transfer coefficient. In this work, the average heat transfer coefficient during FT was set to 27 W/(m²K) and the calculated temperature profile is shown in Figure 5. To control the heat exchange from the bottom, a stainless steel plate was filled with high-performance liquid chromatography (HPLC) grade ethanol. Six vials at room temperature were manually transferred to the plate that was precooled to -80 °C. After 120 s the vials were placed in the 3D printed holder. To assure correct assembly of the holder, the cover was tightly

pressed on and the position fixed with 3M™ 5413 polyimide tape (3M Deutschland GmbH, Neuss, Germany). Finally, the holder was placed inside the mSDD to start the FT run.

6.3.4 Freezing and Thawing

The 2 L PharmaTainer™ bottle, the SDD and the 125 mL PharmaTainer™ bottle were processed simultaneously in an MKF 240 air-blast chamber (Binder GmbH, Tuttlingen, Germany). After 1 h acclimatisation at 20 °C in the air-blast chamber, the chamber was cooled at maximum rate to -40 °C and held for 10 h to assure complete freezing of all devices, followed by maximum heating of the air-blast chamber to 20 °C. This temperature was held for 16 h to assure complete thawing. The devices were gently homogenised by inverting the bottles five times and 1 mL triplicates collected. This process was repeated until five FT cycles were completed.

Additionally, aggregation in 10 mL PharmaTainer™ stability vials, which were equally processed in the MKF 240 air-blast chamber, was analysed. After acclimatisation at 20 °C for 1 h in the air-blast chamber, the chamber was cooled at maximum rate to -40 °C and held at this temperature for 1.5 h until the set temperature was reached in the vials. Afterwards, the chamber was heated to 20 °C with maximum speed and the temperature held for 2 h. Triplicates for each time point were prepared and homogenised before subsequent FT.

Six PharmaTainer™ stability vials were frozen and thawed in the mSDD. After each FT run, samples were gently homogenised and moved to the right to the next of the six positions to compensate possible inhomogeneities on the plate. Aggregation was evaluated at the start and after one, three, and five freeze-thaw cycles. The fill volume of 5.5 mL is mandatory for reproducible runs. Thus, for each time point six vials were processed separately until the intended number of freeze-thaw cycles was completed.

6.3.5 Stability Analysis

6.3.5.1 Flow Imaging Microscopy

SVPs $\geq 1 \mu\text{m}$ per mL were analysed using a FlowCam® 8100 (Fluid Imaging Technologies, Inc., Scarborough, Maine, USA) equipped with a 10x magnification cell. The sample volume was 160 μL . Sampling time and flow rate were set to 60 s and 0.15 mL/min, respectively. Particle segmentation thresholds were 10 for light and 13 for dark pixels and distance to the nearest neighbour 3 μm . An auto image frame rate of 28 frames/s was used.

The equivalent spherical diameter was reported with the VisualSpreadsheet® 4.7.6 software.

6.3.5.2 Size-Exclusion Chromatography

HMWS were detected via size-exclusion chromatography (SEC) on an Agilent 1200 series HPLC system equipped with a diode array detector (Agilent Technologies, Santa Clara, California, USA) detecting at 210 nm. As stationary phase a TSKgel G3000 SWxl column (Tosoh Bioscience GmbH, Griesheim, Germany) and as mobile phase 150 mM potassium phosphate buffer at pH 6.5 were used. The column temperature was kept at 30 °C and the flow rate set to 0.4 mL/min. Prior to analysis, samples were diluted to 1 mg/mL with mobile phase and centrifuged at 25 700 x g in a Heraeus™ Megafuge™ 16R (Thermo Fisher Scientific Inc., Waltham, Massachusetts, USA). 10 µL sample were injected. The Agilent OpenLAB Data Analysis Software version 2.1 was used to evaluate the relative percentage of HMWS based on the area under the curve.

6.3.5.3 Dynamic Light Scattering

Dynamic light scattering (DLS) measurements were performed on a DynaPro Plate Reader III (Wyatt Technology, Dernbach, Germany). 100 µL undiluted sample were filled in a 96-well clear bottom plate (Corning Inc., Corning, NY, USA). For each well five acquisitions of 5 s at 25 °C were taken. Data were processed via the Dynamics V7.8.2.18 software. The cumulant fit analysis was performed to derive the mutual diffusion coefficient and the PDI. The apparent hydrodynamic radius was calculated via the Stokes-Einstein equation.

6.3.5.4 Optical Density at 350 nm

The optical density of undiluted samples at 350 nm was determined using the FLUOstar® Omega microplate reader (BMG LABTECH GmbH, Ortenberg, Germany). 200 µL were pipetted into a 96 well quartz microplate (Hellma Holding GmbH, Müllheim, Germany).

6.3.6 Temperature Mapping in the mSDD

To compare the vial and the set temperature during FT in the mSDD, six 10 mL PharmaTainer™ vials were equipped with type T thermocouples fed through holes drilled into the vial caps and fixed with polyimide tape to be in direct contact with the bottom. HH520 handheld data logger thermometers (OMEGA Engineering GmbH, Deckenpfronn, Germany) recorded the temperature in 15 s intervals. Vials were filled with 5.5 mL freshly

filtered 1 mg/mL mAb2 solution in 25 mM adipic acid at pH 5.2. The experiment was performed in triplicate.

6.4 Results and Discussion

6.4.1 MAb Aggregation in the 2 L Bottle, 125 mL Bottle, and the SDD

Three different mAb solutions were frozen and thawed repeatedly to compare stress in the SDD to the large-scale 2 L bottle and an unshielded 125 mL bottle. A 5 mg/mL mAb1 solution in 20 mM histidine buffer as well as an 85 mg/mL and a 1 mg/mL mAb2 solution in 25 mM adipic acid buffer were studied. To evaluate protein aggregation, the formation of HMWS and SVPs $\geq 1 \mu\text{m}$ per mL, the increase in average hydrodynamic radius and PDI, and the optical density at 350 nm were determined.

Overall, the mAb1 solution at a moderate concentration of 5 mg/mL showed a high resistance against FT induced aggregation (Figure 2). The initial HMWS level of 1.7% did not increase in the 2 L bottle after five freeze-thaw cycles. The SDD as well as the 125 mL bottle matched this outcome. Flow imaging microscopy is a very sensitive method to detect protein aggregation as often only hundredths of a percent of the total protein content forming aggregates $\geq 1 \mu\text{m}$ result in clearly distinguishable differences in total SVP count (29). The initial SVP levels below 1 000 particles per mL increased by approximately 10 000 particles per mL each FT cycle in the 2 L bottle (53 100 SVPs $\geq 1 \mu\text{m}$ per mL after five freeze-thaw cycles). The total count in the SDD was marginally higher after the third cycle, but similar after the fifth (59 600 SVPs $\geq 1 \mu\text{m}$ per mL). SVP formation in the unshielded 125 mL bottle was less after the first, similar after the second, and slightly higher after the third to fifth FT cycle reaching 71 000 particles $\geq 1 \mu\text{m}$ per mL. During FT surface-induced denaturation plays a critical role (12,30,31). We previously demonstrated much faster freezing in the 125 mL bottle compared to the 2 L bottle and the SDD (28), which can result in more but smaller ice crystals (30). This may explain the higher SVP count in the 125 mL bottle assuming that mAb1 adsorption to the ice surface induces the formation of aggregates. However, considering the sensitivity of the method, these differences are not expected to have a practical relevance.

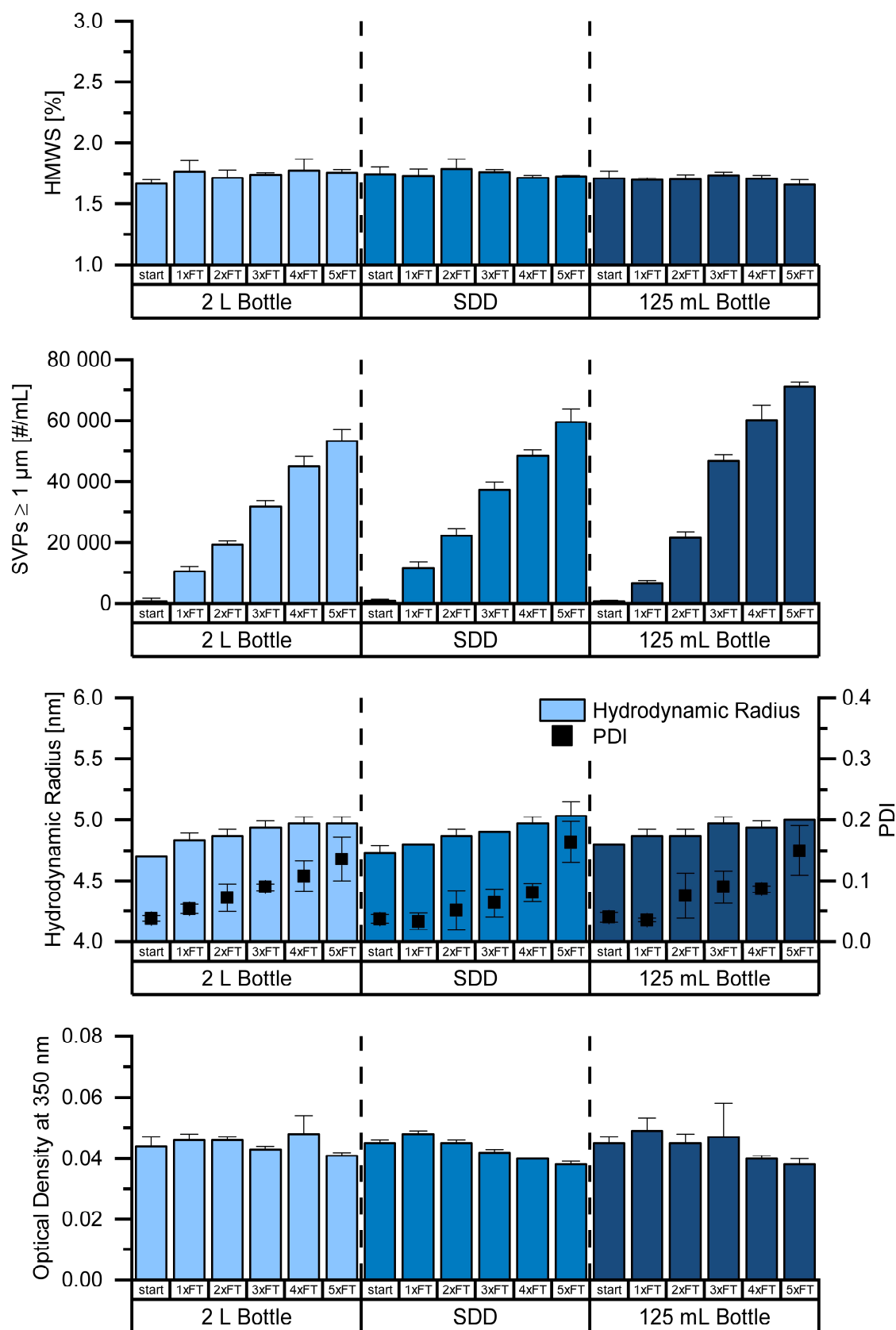


Figure 2 Comparison of mAb aggregation in the large-scale 2 L bottle, the SDD, and the unshielded 125 mL bottle upon repeated FT of a 5 mg/mL mAb1 solution in 20 mM histidine buffer at pH 5.5.

Several studies highlighted that DLS measurements can facilitate and accelerate the tracking of mAb aggregation (32–34). Even small quantities of aggregates, especially larger particles, can be detected with high sensitivity, because the intensity of the scattered light is proportional to the sixth power of the hydrodynamic radius (34). Therefore, we reported the average hydrodynamic radius and the PDI. An increase in hydrodynamic radius can be associated with the formation of aggregated particles (32,33). The PDI allows to estimate the heterogeneity of this sample. For monodisperse samples a $PDI \leq 0.1$ is expected (32,35). Consequently, a PDI larger than 0.1 indicates that more than a single species is present (32). At the beginning of the experiment, we observed an average hydrodynamic radius of 4.7 nm and a PDI of 0.04. The impact of FT was little, but hydrodynamic radius and PDI increased to 5.0 nm and 0.14 in the 2 L bottle, respectively, indicating aggregation. Both the SDD and the 125 mL bottles displayed the same extent of change. Finally, we measured optical density at 350 nm. The turbidity of initially 0.045 remained low in all devices even after the fifth FT cycle as it is a less sensitive measure for aggregate formation.

We additionally studied an 85 mg/mL mAb2 solution, which was expected to be more sensitive to FT stress, especially at high concentration. During FT in the 2 L bottle the soluble aggregate level indeed increased from 0.24% to 0.33% (Figure 3). The SDD as well as the 125 mL bottle generated similar HMWS levels upon repeated FT. The HMWS levels were marginally higher after four compared to five FT cycles pointing towards further aggregation of the HMWS forming larger insoluble aggregates with the last FT cycle. The mAb2 solution initially showed less than 1 000 SVPs $\geq 1 \mu\text{m}$ per mL. With each FT the levels increased up to 54 000, 63 600, and 112 200 SVPs $\geq 1 \mu\text{m}$ per mL in the 2 L bottle, the 125 mL bottle, and the SDD, respectively. DLS analysis of initial mAb2 samples revealed an average hydrodynamic radius of 5.2 nm and a PDI of 0.02. Even after the fifth FT cycle neither the hydrodynamic radius nor the PDI significantly increased in any of the three devices. Similarly, the initial optical density of 0.08 remained unaffected. The detection of insoluble aggregate formation by DLS and UV may be hampered by the high protein concentration of 85 mg/mL masking little changes.

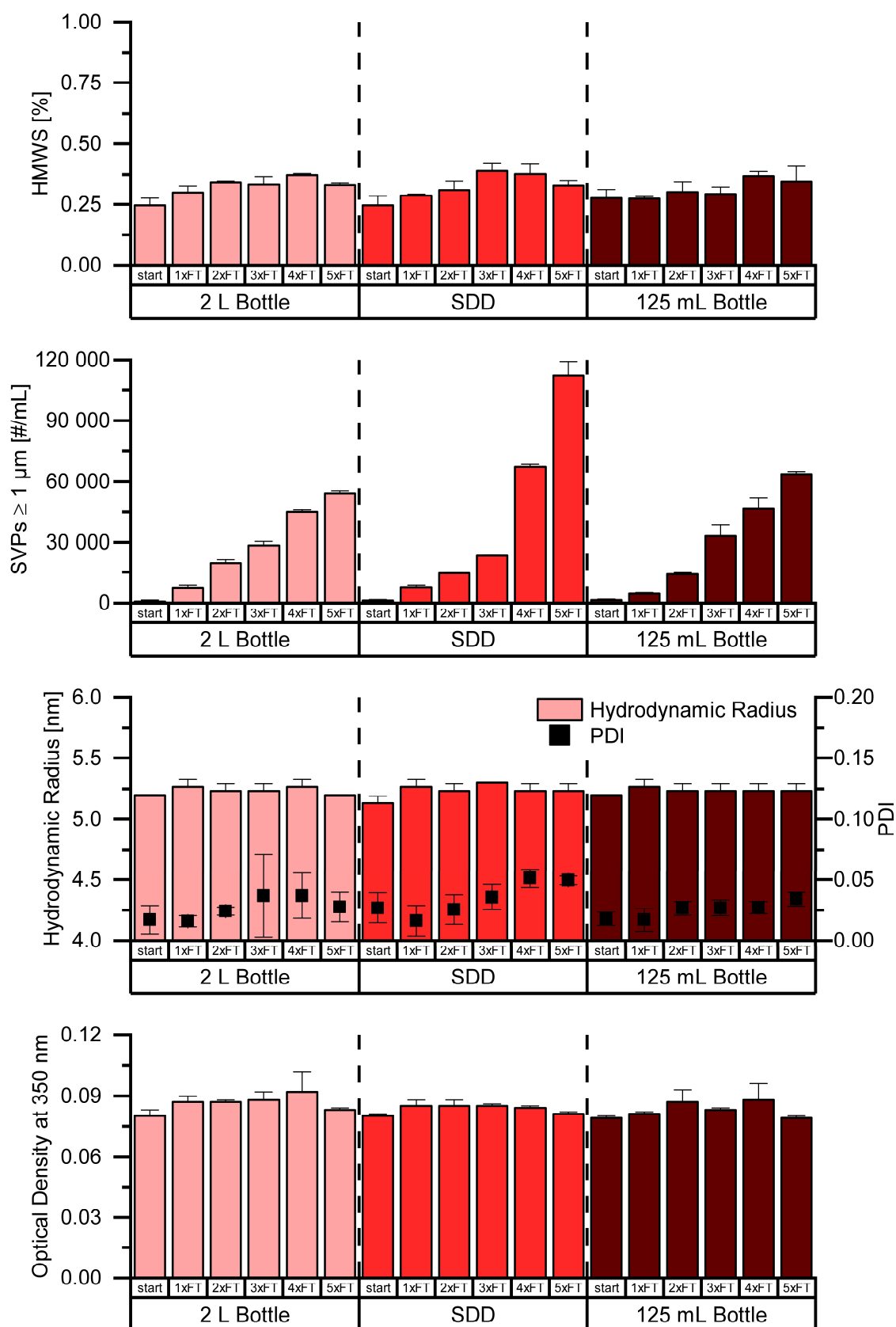


Figure 3 Comparison of mAb aggregation in the large-scale 2 L bottle, the SDD, and the unshielded 125 mL bottle upon repeated FT of an 85 mg/mL mAb2 solution in 25 mM adipic acid buffer at pH 5.2.

Several studies have highlighted that protein adsorption to the ice interface is limited (22,36) and consequently the relative adsorbed fraction increases, when mAb concentration is decreased (22,37). We therefore also investigated a 1 mg/mL mAb2 solution. As displayed in Figure 4 this solution showed enhanced sensitivity to FT. Initially displayed 0.24% HMWS steadily increased with FT cycles in all three devices up to 1.25%, 1.55% and 0.96% in the 2 L bottle, the SDD, and the unshielded 125 mL bottle. The insoluble particle levels increased as well with FT in the 2 L bottle up to 108 100 SVPs $\geq 1 \mu\text{m}$ per mL after the fifth cycle, which was overall well reflected in both the SDD and the unshielded 125 mL bottle. DLS analysis recorded a hydrodynamic radius of 4.9 nm and a PDI of 0.01 at the start. In comparison to the 85 mg/mL solution, dilution to 1 mg/mL diminished the hydrodynamic radius of the mAb2 monomer. This deviation can be explained by reversible self-association of mAbs at high concentrations (34). With FT in the 2 L bottle the average hydrodynamic radius as well as PDI drastically increased after the five cycles to 5.7 nm and 0.38, respectively, indicating substantial aggregate formation. Again, both SDD and unshielded 125 mL bottle showed a highly similar outcome. As with the 85 mg/mL solution, the optical density at 350 nm did not change with FT in any of the setups.

In summary, the SDD but also the unshielded 125 mL bottle showed mAb aggregation similar to the large-scale 2 L bottle upon repeated FT of a 5 mg/mL mAb1 or an 85 mg/mL mAb2 solution. Thus, both might be used to predict FT related aggregation in most of the cases. For a highly aggregation sensitive formulation such as the diluted mAb2, the formation of HMWS might be underrepresented in the unshielded 125 mL bottle, but the SDD might represent a worst-case scenario as it marginally overpredicts aggregation. Thereby, the material need is significantly reduced by the utilisation of the SDD. Additionally, the SDD can be used to assess long-term frozen storage stability. While the unshielded 125 mL bottle significantly underpredicts cryoconcentration in a 2 L bottle, the SDD mimics changes in mAb as well as buffer concentration (28). Thus, bottles frozen in the SDD could be used to examine the effect of cryoconcentration on frozen storage stability. Alternatively, small-scale studies in vials that represent the mAb and buffer concentrations found in the SDD could be prepared. However, further studies are necessary to proof the validity of this concept.

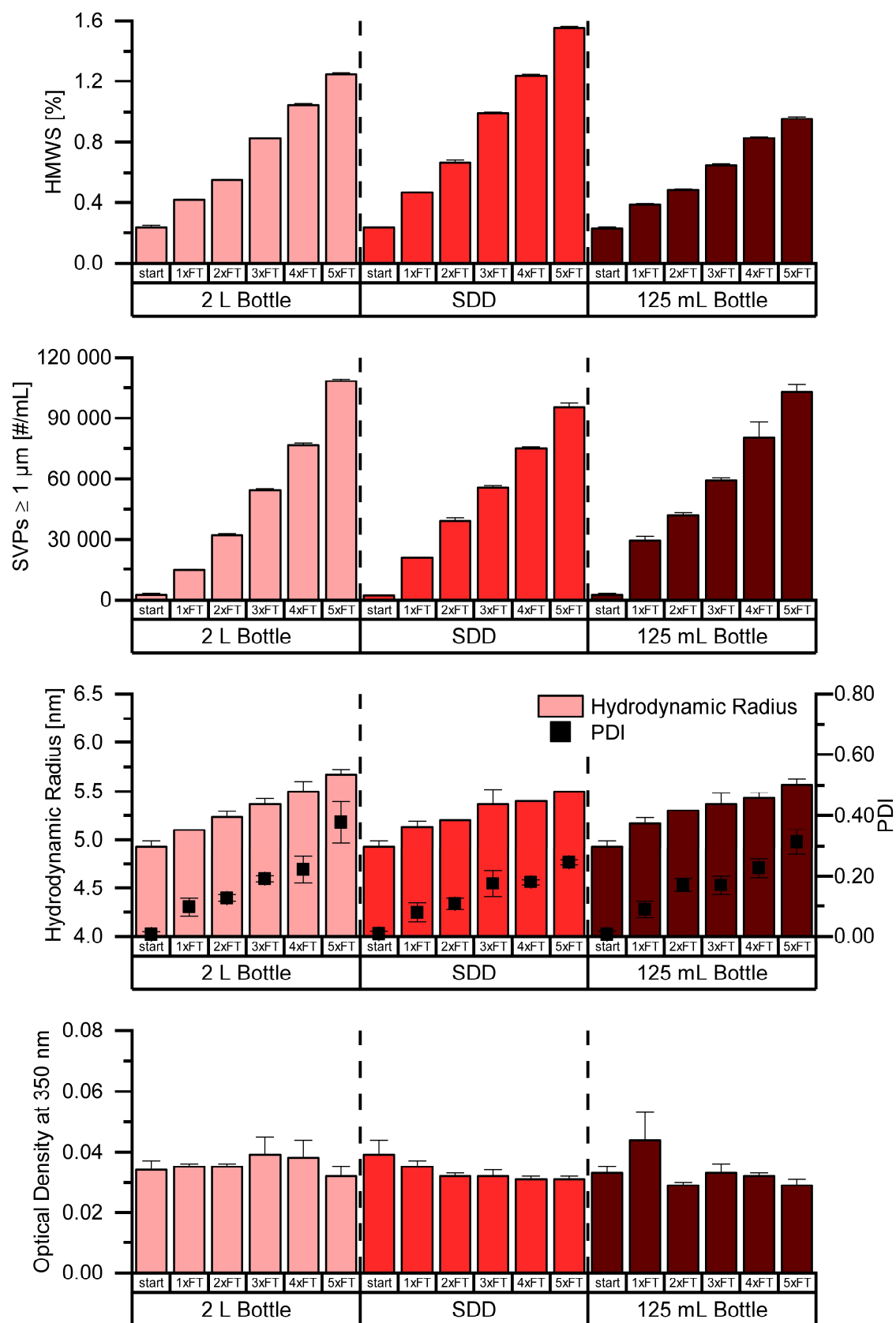


Figure 4 Comparison of mAb aggregation in the large-scale 2 L bottle, the SDD, and the unshielded 125 mL bottle upon repeated FT of a 1 mg/mL mAb2 solution in 25 mM adipic acid buffer at pH 5.2.

6.4.2 MAb Aggregation in 10 mL Vials and the mSDD

The 1 mg/mL mAb2 solution, that was sensitive to FT induced aggregation, was further used to characterise the performance of a newly developed mSDD. The mSDD reduces the volume required for stability testing from 100 mL in the SDD to 5.5 mL. To generate a general understanding of the processes in the mSDD, firstly temperature profiles in 10 mL PharmaTainer™ stability vials were recorded and compared to the set temperature (Figure 5). Secondly, mAb aggregation in the mSDD was characterised in comparison to the 2 L bottle (Figure 6). To evaluate the impact of the adapted FT in the mSDD, results were additionally compared to 10 mL PharmaTainer™ stability vials upon FT in the blast freezer and thawer used for the 2 L bottle.

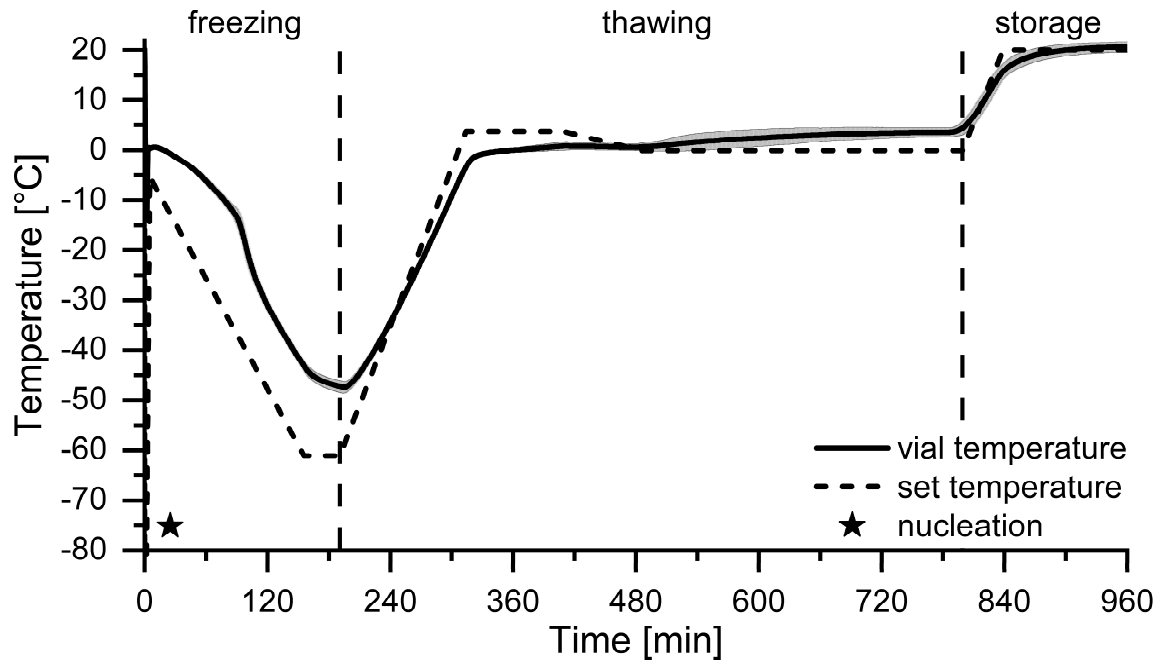


Figure 5 Comparison of set and vial temperature in the mSDD. The temperature in the vials was measured at the lowest possible position in direct contact to the bottom. The grey cloud indicates the standard deviation.

As for the SDD, the cumulative thermal history of a 2 L bottle calculated via CFD simulations was to be matched. In case of the SDD, the thermal history is manipulated by controlling the heat exchange of the small bottle with a 3D printed cover. Thereby, the SDD can be processed next to the bottle of interest. In case of the mSDD, the temperature in 10 mL stability vials is accurately controlled by cooling and heating from the bottom on a plate filled with ethanol. The time the sample spends between the freezing temperature and T_g' , during which molecular mobility is high (38), was extended. To this end, as shown in Figure 5, several ramps and plateaus are applied after controlled nucleation. The exact

profiles are adapted according to the bottle size that should be mimicked and the average heat exchange coefficient on the bottle wall during large-scale freezing. The heat exchange coefficient depends on the freezer and thawer and is estimated based on simulations. The temperature profiles at the vial bottom deviated from the set temperature. This was due to the 4 mm high ethanol layer, an air bubble underneath the bottom, and the lower heat transfer of the container material. The impact of these factors was considered during the development of the mSDD. Small standard deviation underlined the overall good homogeneity during FT, regardless of the position of the vial in the holder. The sudden drop in temperature after approximately 90 min indicated that freezing in the whole vial was completed. From this point in time on no more latent heat of crystallisation was released into the system. During thawing temperatures above 0 °C were reached after 480 min. Because of the negative thermal expansion of aqueous solutions, the thermocouple at the bottom of the vial quickly approached temperatures around 4 °C. Although the mAb2 solutions completely thawed near the bottom, visual inspection at this point in time revealed a large frozen fraction in the top region. This fraction experienced further stress until the vials were completely thawed.

As discussed above, a 1 mg/mL mAb2 solution showed a substantial increase in HMWS, SVPs, hydrodynamic radius, and PDI during FT in a 2 L bottle. In contrast, protein aggregation in 10 mL PharmaTainer™ vials treated in a blast freezer and thawer was by far less pronounced (Figure 6). HMWS levels remained on the initial 0.24%, SVP count only minimally increased from 2 600 SVPs $\geq 1 \mu\text{m}$ per mL at t_0 to 11 500 after five freeze-thaw cycles, hydrodynamic radius and PDI only changed from 4.9 nm to 5.1 nm and 0.01 to 0.15, respectively, and similar to the 2 L bottle no change in optical density at 350 nm was observed. By manipulating the temperature vs. time profile of the FT, the mSDD significantly enhanced FT induced mAb aggregation. In detail, 0.63% HMWS and 31 700 SVPs $\geq 1 \mu\text{m}$ per mL were detected after five freeze-thaw cycles. The marked increase of average hydrodynamic radius and PDI after five freeze-thaw cycles in the 2 L bottle was not well mimicked by the mSDD with 5.2 nm and 0.14, respectively. The optical density was not affected by repeated FT as seen for the 2 L bottle. Nevertheless, the mSDD equipped with 10 mL vials clearly better reflects FT stress of a 2 L bottle as compared to simply placing the 10 mL vials in the blast freezer and thawer.

Evaluation of Two Novel Scale-Down Devices for Testing mAb Aggregation during Large-Scale Freezing

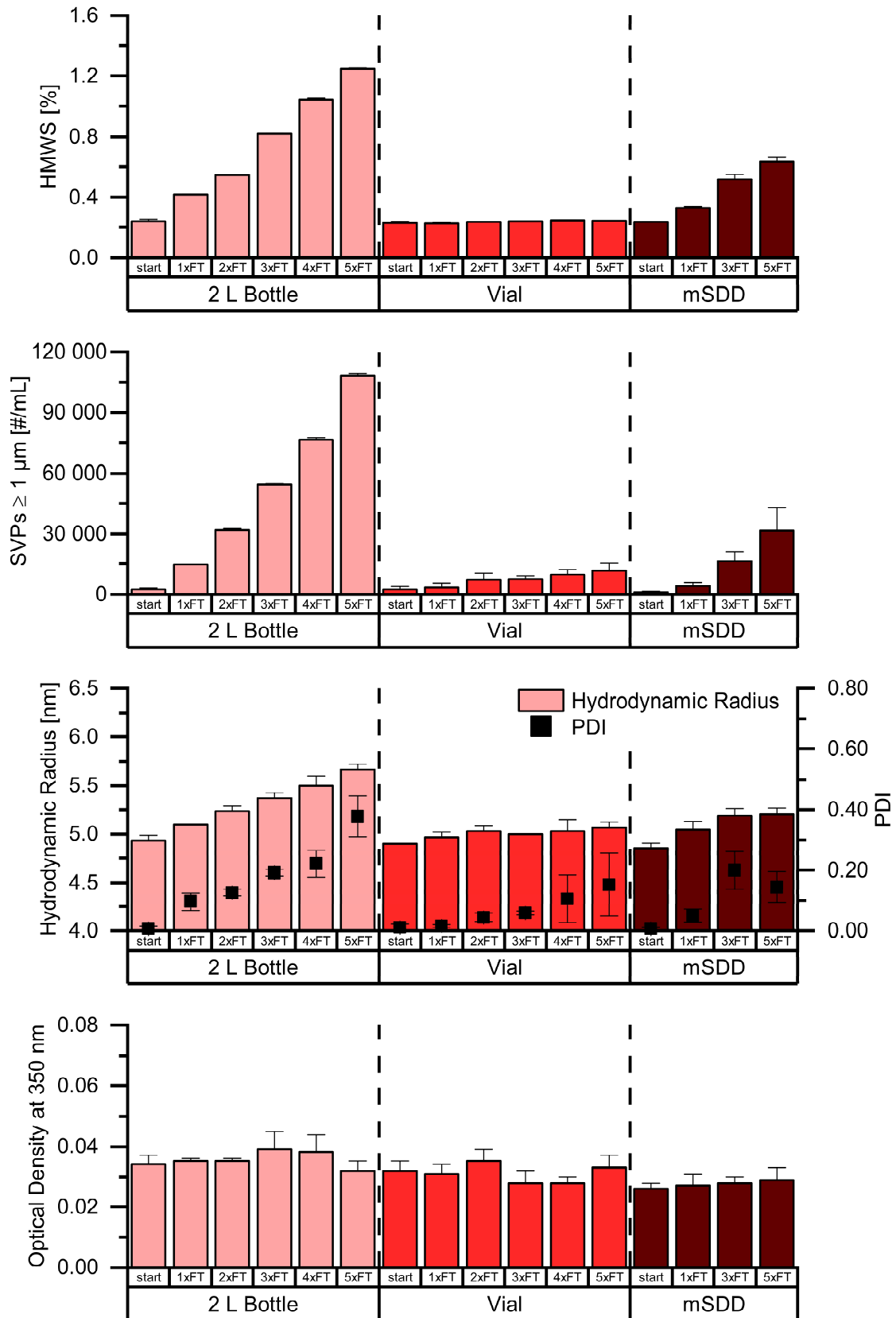


Figure 6 Comparison of mAb aggregation in the large-scale 2 L bottle, vials, and the mSDD upon repeated FT of a 1 mg/mL mAb2 solution in 25 mM adipic acid buffer at pH 5.2.

Vials freeze faster than larger bottles, resulting in smaller ice crystals (30). This larger surface might lead to the formation of SVPs. On the other hand, the exposure time of the protein to possible detrimental effects is shortened. In addition, the smaller volume and the reduced FT times mitigate cryoconcentration upon freezing and concentration gradients upon thawing (2,3). Eventually, less stress is observed during FT in vials. Though vials are regularly used for small-scale studies, our results emphasize that such experiments are not necessarily representative. Increasing the time period in between T_g' and the freezing temperature is a good approach to manipulate the total stress. Nevertheless, the mSDD did not perfectly match the large-scale FT stress of a 2 L bottle. Several hypotheses might explain this discrepancy. The CFD simulations that calculated the cumulative thermal history in the 2 L bottle considered FT from room temperature to $-80\text{ }^{\circ}\text{C}$. However, our large-scale experiments were practically limited to $-40\text{ }^{\circ}\text{C}$, which can generate an approximately two times larger stress time than set in the mSDD. Additionally, only one average heat transfer coefficient is used to calculate the set temperature in the mSDD. This might be realistic for high-capacity blast freezers, which freeze and thaw bottles homogeneously. In case of the blast freezer and thawer used in this study, the circulating air in the chamber is directed from the walls towards a fan in the back, which might result in slightly inhomogeneous FT. Therefore, one heat transfer coefficient cannot accurately describe the realistic process. In the mSDD vials are held at temperatures above $0\text{ }^{\circ}\text{C}$ for an extended period of time. As long as ice is present in the top region, this adds to the cumulative stress. According to the mSDD program ice should disappear 30 min before reaching the storage temperature. Visual inspection revealed ice in all vials after approximately 540 min, only in the two centre vials after 600 min, and after 780 min the ice had completely vanished in all vials as supposed. The observed deviations can be explained by variations in natural convection inside the vials or small differences in insulation that become relevant when the temperature difference (thermodynamic equilibrium and heat transfer surface) is small. In general, the mSDD aims to run a generic process suitable for all formulations, but solutes, which decrease the freezing temperature, could impact the outcome simply based on the freezing point depression.

6.5 Conclusion

The aim of this study was to evaluate mAb aggregation in two novel SDDs upon repeated FT in comparison to a large-scale 2 L bottle. Therefore, three different mAb solutions were subjected to five freeze-thaw cycles and the formation of HMWS and SVPs $\geq 1 \mu\text{m}$ per mL, the increase in hydrodynamic radius and PDI, and optical density at 350 nm determined.

Both the SDD and the mSDD were designed by SmartFreeZ via CFD simulations to preserve the overall stress upon FT of a 2 L bottle. In case of the 3D printed SDD, a 125 mL bottle is surrounded by the device and heat exchange at the walls manipulated by insulating two walls. Thereby, the material need is reduced 16-fold. MAb aggregation upon repeated FT of a 5 mg/mL mAb1 solution or an 85 mg/mL mAb2 solution in a 2 L bottle could be predicted by the SDD, but was equally mimicked by the unshielded 125 mL bottle. In contrast, aggregation of a much more sensitive 1 mg/mL mAb2 solution was underpredicted by the 125 mL bottle; the SDD overpredicted the formation of soluble aggregates, indicating that it could be used as a worst-case scenario in formulation or FT process development.

The mSDD follows the same CFD based approach of equivalent cumulative stress, but reduces the sample volume nearly 300-fold to 5.5 mL in vials. Instead of insulating areas of the container, the significant differences in size and geometry require a different approach to increase stress time in the mSDD. A defined cooling and heating program, which is adapted in respect of the bottle size and the freezer and thawer used, expands the time the sample spends at a temperature between the freezing temperature and T_g' . Vials that were equally frozen and thawed as the 2 L bottle in a blast freezer and thawer significantly underestimated soluble as well as insoluble mAb aggregate formation. The adapted cooling and heating by the mSDD significantly increased stress and mAb aggregation. Thus, the presented mSDD offers a novel approach to representatively scale-down FT in large-scale 2 L bottles, that requires only a fraction of the material. Nevertheless, optimisation is needed to close the gap between the mSDD and the 2 L bottle.

Acknowledgements

The Novartis Pharma AG provided mAb1 and mAb2 stock solutions.

References

1. Maity H, Karkaria C, Davagnino J. Mapping of solution components, pH changes, protein stability and the elimination of protein precipitation during freeze–thawing of fibroblast growth factor 20. *Int J Pharm.* 2009 Aug;378(1–2):122–35.
2. Miller MA, Rodrigues MA, Glass MA, Singh SK, Johnston KP, Maynard JA. Frozen-State Storage Stability of a Monoclonal Antibody: Aggregation is Impacted by Freezing Rate and Solute Distribution. *J Pharm Sci.* 2013 Apr;102(4):1194–208.
3. Rodrigues MA, Miller MA, Glass MA, Singh SK, Johnston KP. Effect of Freezing Rate and Dendritic Ice Formation on Concentration Profiles of Proteins Frozen in Cylindrical Vessels. *J Pharm Sci.* 2011 Apr;100(4):1316–29.
4. Padala C, Jameel F, Rathore N, Gupta K, Sethuraman A. Impact of Uncontrolled vs Controlled Rate Freeze-Thaw Technologies on Process Performance and Product Quality. *PDA J Pharm Sci Technol.* 2010;64(4):290–8.
5. Kolhe P, Badkar A. Protein and solute distribution in drug substance containers during frozen storage and post-thawing: A tool to understand and define freezing-thawing parameters in biotechnology process development. *Biotechnol Prog.* 2011 Mar;27(2):494–504.
6. Rathore N, Rajan RS. Current Perspectives on Stability of Protein Drug Products during Formulation, Fill and Finish Operations. *Biotechnol Prog.* 2008 Jun 6;24(3):504–14.
7. Kolhe P, Amend E, K. Singh S. Impact of freezing on pH of buffered solutions and consequences for monoclonal antibody aggregation. *Biotechnol Prog.* 2009 Dec 28;26(3):727–33.
8. Kuelz LA, Wang W e. i., Randolph TW, Carpenter JF. Effects of Solution Conditions, Processing Parameters, and Container Materials on Aggregation of a Monoclonal Antibody during Freeze-Thawing. *J Pharm Sci.* 2008 May;97(5):1801–12.
9. Roessl U, Leitgeb S, Nidetzky B. Protein freeze concentration and micro-segregation analysed in a temperature-controlled freeze container. *Biotechnol Reports.* 2015 Jun;6:108–11.
10. Hauptmann A, Hoelzl G, Loerting T. Distribution of Protein Content and Number of Aggregates in Monoclonal Antibody Formulation After Large-Scale Freezing. *AAPS PharmSciTech.* 2019 Feb 10;20(2):72.
11. Kolhe P, Mehta AP, Lary AL, Chico SC, Singh SK. Large-Scale Freezing of Biologics (Part III). *BioPharm Int.* 2012;25(October):40–8.
12. Duarte A, Rego P, Ferreira A, Dias P, Geraldes V, Rodrigues MA. Interfacial Stress and Container Failure During Freezing of Bulk Protein Solutions Can Be Prevented by Local Heating. *AAPS PharmSciTech.* 2020 Oct 1;21(7):251.

13. Mehta SB, Subramanian S, D’Mello R, Brisbane C, Roy S. Effect of protein cryoconcentration and processing conditions on kinetics of dimer formation for a monoclonal antibody: A case study on bioprocessing. *Biotechnol Prog.* 2019 Jul 15;35(4):1–7.
14. Rodrigues MA, Balzan G, Rosa M, Gomes D, de Azevedo EG, Singh SK, et al. The importance of heat flow direction for reproducible and homogeneous freezing of bulk protein solutions. *Biotechnol Prog.* 2013 Sep;29(5):1212–21.
15. Arsiccio A, McCarty J, Pisano R, Shea J-E. Heightened Cold-Denaturation of Proteins at the Ice–Water Interface. *J Am Chem Soc.* 2020 Mar 25;142(12):5722–30.
16. Correia C, Tavares E, Lopes C, Silva JG, Duarte A, Geraldes V, et al. Stability of Protein Formulations at Subzero Temperatures by Isochoric Cooling. *J Pharm Sci.* 2020 Jan;109(1):316–22.
17. Rosa M, Lopes C, Melo EP, Singh SK, Geraldes V, Rodrigues MA. Measuring and Modeling Hemoglobin Aggregation below the Freezing Temperature. *J Phys Chem B.* 2013 Aug 18;117(30):8939–46.
18. Connolly BD, Le L, Patapoff TW, Cromwell MEM, Moore JMR, Lam P. Protein Aggregation in Frozen Trehalose Formulations: Effects of Composition, Cooling Rate, and Storage Temperature. *J Pharm Sci.* 2015 Dec;104(12):4170–84.
19. Singh SK, Kolhe P, Mehta AP, Chico SC, Lary AL, Huang M. Frozen State Storage Instability of a Monoclonal Antibody: Aggregation as a Consequence of Trehalose Crystallization and Protein Unfolding. *Pharm Res.* 2011 Apr 7;28(4):873–85.
20. Hauptmann A, Podgoršek K, Kuzman D, Srčić S, Hoelzl G, Loerting T. Impact of Buffer, Protein Concentration and Sucrose Addition on the Aggregation and Particle Formation during Freezing and Thawing. *Pharm Res.* 2018 May 19;35(5):101.
21. Pikal-Cleland KA, Rodríguez-Hornedo N, Amidon GL, Carpenter JF. Protein Denaturation during Freezing and Thawing in Phosphate Buffer Systems: Monomeric and Tetrameric β -Galactosidase. *Arch Biochem Biophys.* 2000 Dec;384(2):398–406.
22. Arsiccio A, Pisano R. The Ice-Water Interface and Protein Stability: A Review. *J Pharm Sci.* 2020 Jul;109(7):2116–30.
23. Authelin J-R, Rodrigues MA, Tchessalov S, Singh SK, McCoy T, Wang S, et al. Freezing of Biologicals Revisited: Scale, Stability, Excipients, and Degradation Stresses. *J Pharm Sci.* 2020 Jan;109(1):44–61.
24. Thorat AA, Munjal B, Geders TW, Suryanarayanan R. Freezing-induced protein aggregation - Role of pH shift and potential mitigation strategies. *J Control Release.* 2020 Jul;323(April):591–9.
25. Zhang A, Singh SK, Shirts MR, Kumar S, Fernandez EJ. Distinct Aggregation Mechanisms of Monoclonal Antibody Under Thermal and Freeze-Thaw Stresses Revealed by Hydrogen Exchange. *Pharm Res.* 2012 Jan 30;29(1):236–50.
26. Shamlou PA, Breen LH, Bell W V., Pollo M, Thomas BA. A new scaleable freeze–thaw technology for bulk protein solutions. *Biotechnol Appl Biochem.* 2007 Jan 1;46(1):13.

27. Gerald V, Gomes DC, Rego P, Fegley D, Rodrigues MA. A New Perspective on Scale-Down Strategies for Freezing of Biopharmaceuticals by Means of Computational Fluid Dynamics. *J Pharm Sci.* 2020 Jun;109(6):1978–89.
28. Bluemel O, Buecheler JW, Rodrigues MA, Gerald V, Hoelzl G, Bechtold-Peters K, et al. Cryoconcentration and 3D Temperature Profiles During Freezing of mAb Solutions in Large-Scale PET Bottles and a Novel Scale-Down Device. *Pharm Res.* 2020 Sep 30;37(9):179.
29. Barnard JG, Singh S, Randolph TW, Carpenter JF. Subvisible Particle Counting Provides a Sensitive Method of Detecting and Quantifying Aggregation of Monoclonal Antibody Caused by Freeze-Thawing: Insights Into the Roles of Particles in the Protein Aggregation Pathway. *J Pharm Sci.* 2011 Feb;100(2):492–503.
30. Singh SK, Kolhe P, Wang W, Nema S. Large-Scale Freezing of Biologics A Practitioner’s Review, Part One: Fundamental Aspects. *Bioprocess Int.* 2009;7(9):32–44.
31. Sarciaux J-M, Mansour S, Hageman MJ, Nail SL. Effects of buffer composition and processing conditions on aggregation of bovine IgG during freeze-drying. *J Pharm Sci.* 1999 Dec;88(12):1354–61.
32. Nobbmann U, Connah M, Fish B, Varley P, Gee C, Mulot S, et al. Dynamic light scattering as a relative tool for assessing the molecular integrity and stability of monoclonal antibodies. *Biotechnol Genet Eng Rev.* 2007 Jan;24(1):117–28.
33. Svilenov H, Gentiluomo L, Friess W, Roessner D, Winter G. A New Approach to Study the Physical Stability of Monoclonal Antibody Formulations—Dilution From a Denaturant. *J Pharm Sci.* 2018 Dec;107(12):3007–13.
34. Hawe A, Hulse WL, Jiskoot W, Forbes RT. Taylor Dispersion Analysis Compared to Dynamic Light Scattering for the Size Analysis of Therapeutic Peptides and Proteins and Their Aggregates. *Pharm Res.* 2011 Sep 11;28(9):2302–10.
35. Stetefeld J, McKenna SA, Patel TR. Dynamic light scattering: a practical guide and applications in biomedical sciences. *Biophys Rev.* 2016 Dec 6;8(4):409–27.
36. Wang W. Lyophilization and development of solid protein pharmaceuticals. *Int J Pharm.* 2000 Aug;203(1–2):1–60.
37. Jiang S, Nail SL. Effect of process conditions on recovery of protein activity after freezing and freeze-drying. *Eur J Pharm Biopharm.* 1998 May;45(3):249–57.
38. Pansare SK, Patel SM. Practical Considerations for Determination of Glass Transition Temperature of a Maximally Freeze Concentrated Solution. *AAPS PharmSciTech.* 2016 Aug 18;17(4):805–19.

Chapter 7 Computational Fluid Dynamic Simulations of Temperature, Cryoconcentration, and Local Stress during Large-Scale Freezing and Thawing of mAb Solutions

Oliver Bluemel¹, Andraž Pavličič², Blaž Likozar², Miguel A. Rodrigues³, Vitor Geraldés⁴, Karoline Bechtold-Peters⁵, Wolfgang Friess¹

1 Pharmaceutical Technology and Biopharmaceutics, Department of Pharmacy, Ludwig-Maximilians-Universität München, 81377 Munich, Germany

2 Laboratory of Catalysis and Chemical Reaction Engineering, National Institute of Chemistry, 1000 Ljubljana, Slovenia

3 Centro de Química Estrutural, Department of Chemical Engineering, Instituto Superior Técnico, Lisboa 1049-001, Portugal

4 CeFEMA, Department of Chemical Engineering, Instituto Superior Técnico, Lisboa 1049-001, Portugal

5 Technical Research and Development, Novartis Pharma AG, 4002 Basel, Switzerland

Author contributions:

O.B., W.F., and K.B.P. conceived the study. M.A.R. and V.G. developed the solver. A.P. and B.L. performed the simulations. O.B. performed the experiments and evaluated the data. O.B. and A.P. wrote the paper. W.F., K.B.P., and A.P. contributed to the discussion of the results and revised the manuscript. W.F. and K.B.P. supervised the work.

7.1 Abstract

Purpose: Large-scale freezing and thawing experiments of monoclonal antibody (mAb) solutions are time and material consuming. Computational Fluid Dynamic (CFD) modeling of temperature, solute composition as well as the local stress, defined as the time between start of freezing and reaching T_g' at any point in the container, could be a promising approach to ease and speed up process development.

Methods: Temperature profiles at six positions were recorded during freezing and thawing of a 2 L rectangular bottle and compared to CFD simulations via OpenFOAM. Furthermore, cryoconcentration upon freezing and concentration gradients upon thawing of a mAb solution were predicted and the local stress calculated.

Results: Temperature profiles during freezing were accurately matched by the CFD simulation. Thawing time was only 45 min to 60 min longer in the model. The macroscopic cryoconcentration of the mAb was also matched by the simulation; only a highly concentrated region in the top and a diluted core in the geometrical centre of the 2 L bottle were not well reflected in the simulation. The concentration gradient after thawing obtained by simulation as well agreed with the experimental result. In addition, CFD simulations allowed to extract the global temperature distribution, the formation of ice, and thus the distribution of stress in the freezing liquid.

Conclusion: CFD simulations via OpenFOAM are a promising tool to describe large-scale freezing and thawing of mAb solutions and can help to generate a deeper understanding and to improve testing of the robustness of the processes.

Keywords: CFD, cryoconcentration, freeze-concentration, freezing and thawing, freeze-thaw, large-scale, monoclonal antibody, OpenFOAM, simulation

Abbreviations: CF – Concentration factor, CFD – Computational Fluid Dynamics, HTC – Heat transfer coefficient, mAb – Monoclonal antibody, TC – Thermocouple, VOF – Volume of Fluid

7.2 Introduction

During large-scale production of monoclonal antibody (mAb) solutions, freezing is commonly applied to increase stability and shelf life (1). Frozen storage reduces the risk of microbial growth, halts shaking and foaming during transportation, and provides flexibility in manufacturing processes (1,2). Although offering a variety of advantages, freezing and inevitable subsequent thawing are connected to several possible adverse effects. Microscopic and macroscopic changes in concentration, surface-induced aggregation at the ice interface, and cold denaturation can potentially outbalance the benefits of freezing (2). It has been shown that Computational Fluid Dynamics (CFD) modeling can be used to assess stresses potentially affecting mAb stability (3). Thereby, CFD can help to gain a better understanding of the process, accelerate robustness evaluation of a process, and enable to define optimal process parameters. In this communication, we explore if CFD simulations can depict large-scale freezing and thawing processes. Therefore, we compared CFD simulations to previously published experimental results including the temperature profiles during freezing and thawing at several positions and macroscopic cryoconcentration upon freezing and concentration gradients upon thawing in a rectangular 2 L bottle. In addition, we used the CFD simulations to gain insights into critical attributes that are not accessible via experiments, namely the global temperature distribution, the formation of ice, and an estimation of stress in different regions of the bottle.

7.3 Materials and Methods

All materials and methods for the practical part of this study were described previously (2). In this section, only the essential information will be given.

7.3.1 Materials

A 5 mg/mL IgG1 mAb solution in a 20 mM histidine buffer at pH 5.5 with 0.4 mg/mL polysorbate 80 was used. 2 L PharmaTainer™ polyethylene terephthalate bottles (Celon S.A., Bascharage, Luxembourg) were filled with 1.6 L mAb solution.

7.3.2 Temperature Mapping during Freezing and Thawing

Six type T thermocouples (TCs) connected to an HH520 handheld data logger thermometer (OMEGA Engineering GmbH, Deckenpfronn, Germany) were positioned as shown in Figure 1. Five TCs were evenly distributed in one fourth of the 2 L bottle at half liquid height; a sixth TC was positioned in the centre but at 75% liquid level. The bottles were

cooled for 10 h at -40 °C and heated for 15 h at 20 °C in an MKF 240 air-blast climate chamber (Binder GmbH, Tuttlingen, Germany). The measurement was performed in triplicate.



Figure 1 Positioning of TCs in the 2 L PharmaTainer™ bottle. On top a schematic drawing in cross-section is provided, below a representative picture of the bottle. The figure is adapted from Bluemel et al. (2).

7.3.3 Analysis of Changes in Concentration

Cryoconcentration and concentration gradients were analysed after freezing by cutting the frozen block into 234 equal segments of approximately 7 mL for subsequent analysis. In a separate experiment changes in concentration upon thawing were examined by taking

samples out of nine layers for analysis. For each layer five samples were taken in the edges and the centre of the 2 L bottle. For the contour plot the mean per layer was calculated and plotted without considering the centre samples. MAb concentration was quantified via size-exclusion chromatography.

7.3.4 Computational Fluid Dynamics Modeling

The detailed mathematical description of freeze-thaw systems is difficult due to the complex structure of the ice dendrites in the slushy layer. We used the enthalpy-porosity technique, which was implemented in an in-house developed solver using the OpenFOAM software. A more detailed description can be found elsewhere (3). With aid of the volume of fluid (VOF) technique the fluid/solid system of heat and mass transfer was modelled as depicted in Table 1. Single momentum and energy equation (eq. 4 and eq. 5) for overall mixture with density ρ , velocity \mathbf{U} , and effective thermal conductivity k was shared for all phases and the volume fraction of each phase was tracked throughout the domain. Following the enthalpy-porosity method, the momentum equation (eq. 4) has a drag force source, \mathbf{S}_d , which expresses the force that the ice matrix exerts on the fluid, due to the fluid percolation (correlation of \mathbf{S}_d is captured in eq. 10). Biomixture/gas interface was solved by advection of biomixture fraction (γ). Solute mass transport (with mass fraction w_A) was calculated as depicted in eq. 6. Ice fraction (α) was tracked by eq. 7 which is related with the ice mass source (S_{ice}) empirical crystallisation kinetics (eq. 9). The liquidus temperature was predicted by the classical equation (eq. 8) for estimation of the freezing point depression ($K_f = 2.60 \text{ K mol kg}^{-1}$) for an aqueous solution of sucrose. Geraldès et al. described the thermophysical properties used in the model (3).

Table 1 Equations used for the modeling of heat and mass transfer in the CFD simulations.

Advection of liquid volume fraction γ	$\frac{\partial \gamma}{\partial t} + \nabla \cdot (\gamma \mathbf{U}) = 0$	(1)
Mixture density	$\rho = \gamma (\rho_{ice} \alpha + \rho_{liq} (1 - \alpha)) + (1 - \gamma) \rho_{air}$	(2)
Continuity equation	$\frac{\partial \rho}{\partial t} + \nabla \cdot (\rho \mathbf{U}) = 0$	(3)
Momentum equation	$\frac{\partial \rho \mathbf{U}}{\partial t} + \rho (\mathbf{U} \cdot \nabla) \mathbf{U} = -\nabla p + \nabla \mu \cdot (\nabla \mathbf{U} + \nabla \mathbf{U}^T) + \rho \mathbf{g} + \mathbf{S}_d$	(4)

Energy equation	$\frac{\partial[\gamma(\alpha\hat{h}_{ice} + (1 - \alpha)\hat{h}_{liq}) + (1 - \gamma)\hat{h}_{air}]}{\partial t} + \nabla \cdot (\rho\mathbf{U}\hat{h}_f) - \nabla \cdot (k\nabla T) = 0$	(5)
	$\begin{aligned}\hat{h}_{ice} &= \hat{c}_{p,ice}(T - T_{ref}) - \Delta\hat{H}_{solidification} \\ \hat{h}_{liq} &= \hat{c}_{p,liq}(T - T_{ref}) \\ \hat{h}_{air} &= \hat{c}_{p,air}(T - T_{ref}) \\ \hat{h}_f &= \gamma\hat{h}_{liq} + (1 - \gamma)\hat{h}_{air} \\ k &= \gamma(\alpha k_{ice} + (1 - \alpha)k_{liq}) + (1 - \gamma)k_{air}\end{aligned}$	
Solute continuity equation	$\frac{\partial\rho_w w_A}{\partial t} + \nabla \cdot (\rho\mathbf{U}w_A) - \nabla \cdot [\rho_w D_{AB}\nabla w_A] = 0$ <p>where $\rho_w = \gamma(1 - \alpha)\rho_{liq} + (1 - \gamma)\rho_{air}$</p>	(6)
Ice continuity equation	$\frac{\partial\alpha}{\partial t} = \frac{S_{ice}}{\rho_{ice}}$	(7)
Liquidus temperature	$T_L = T_f - \frac{K_f w_A}{M_A(1 - w_A)}$	(8)
Ice mass source	$S_{ice} = \tau(1 - \alpha)^2\alpha(T - T_L)(w_{Ag} - w_A)$	(9)
Momentum source equation	$\mathbf{S}_d = \beta\mu\frac{\alpha^2}{(1 - \alpha)^3}\mathbf{U}$	(10)

7.4 Results and Discussion

7.4.1 Comparison of Temperature Profiles during Freezing

Temperature profiles at six positions were mapped and compared to the experimental outcome to verify the CFD simulations. The heat transfer at the bottle surface defines the temperature distribution and the freezing time. Therefore, it is crucial to use realistic heat transfer coefficients (HTCs). Based on own preliminary measurements in comparable blast freezers and thawers, the HTC was initially set to 25 W/(m²K). The temperature profiles

for a freezing simulation with $25 \text{ W}/(\text{m}^2\text{K})$ at all six surfaces, the four walls, the top, and bottom, are given in Figure 2.

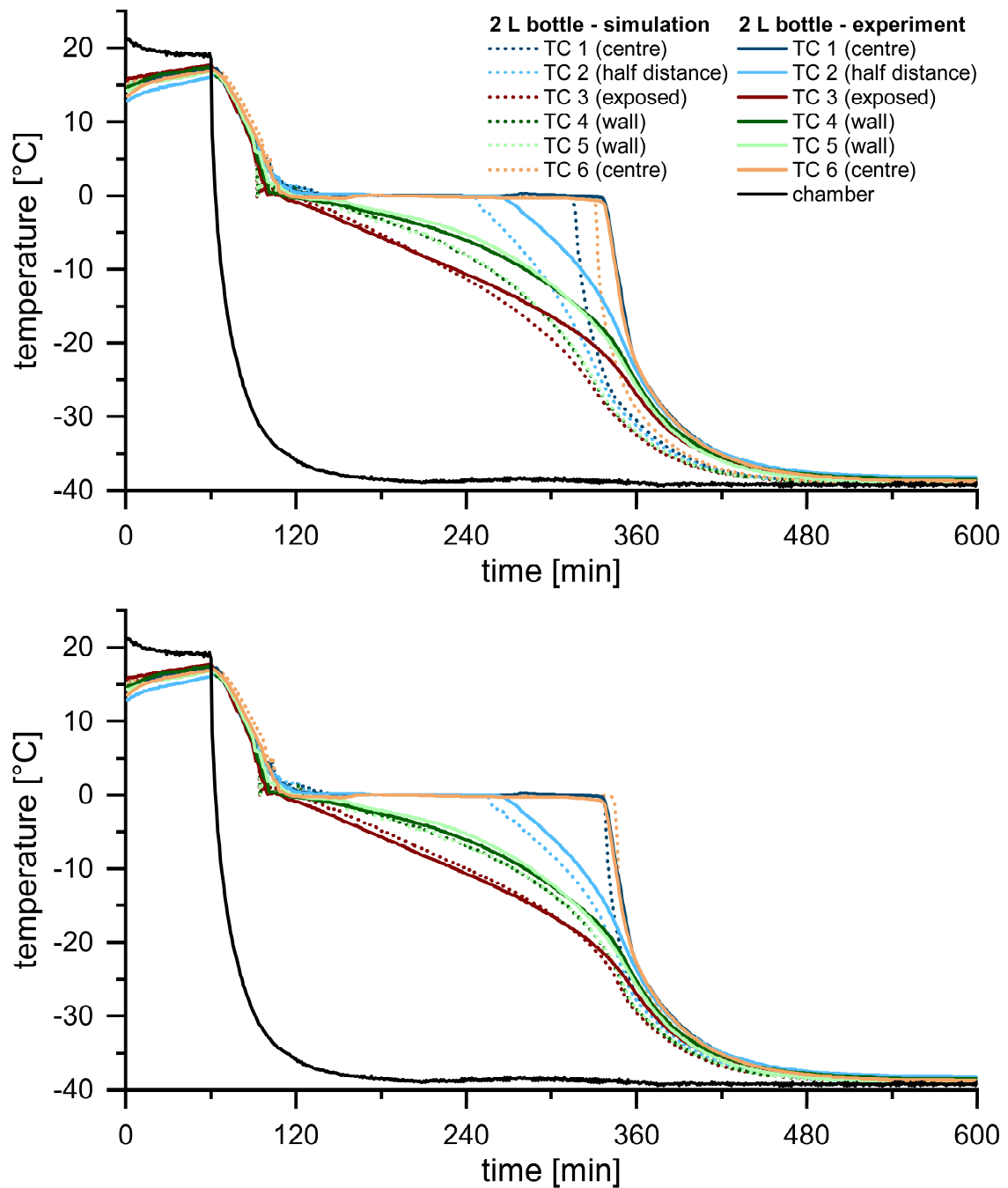


Figure 2 Temperature profiles as determined during the CFD simulation (dotted lines) and large-scale experiments (solid lines) during freezing. On top freezing was simulated with an HTC of $25 \text{ W}/(\text{m}^2\text{K})$ at all surfaces. Below the HTC was set to $24 \text{ W}/(\text{m}^2\text{K})$ at the walls and to $15 \text{ W}/(\text{m}^2\text{K})$ at the top and the bottom surface.

Overall, freezing time was shorter in the simulation compared to the experiment. Freezing time is defined as the time span between nucleation and the completion of ice formation

(2,4), indicated by a plateau in the temperature profiles. As soon as ice crystallisation is finished, no latent heat of crystallisation is released into the system and the temperature drops. Differences between simulation and experiment were more distinct at the later freezing points (TC 1 and TC 2), while the last point to freeze at TC 6 was again very close. This indicated that in the CFD simulation the HTC was set slightly too high and heat transfer from the bottom and the top should be reduced. Consequently, we set up a second simulation with an HTC of 24 W/(m²K) at the walls and 15 W/(m²K) at the bottom and the top surface. Thereby, the simulated temperature profiles matched the experimental outcome (Figure 2); only a small difference of 15 min was observed when comparing TC 2. With this setup further modeling was performed.

7.4.2 Comparison of Cryoconcentration

With the optimised simulation parameters, we characterised the mAb cryoconcentration upon freezing. Changes in concentration were expressed as the concentration factor (CF), which is the ratio of the sample concentration to the initial concentration. Experimentally, a CF between 0.54 and 1.37 was determined (Figure 3).

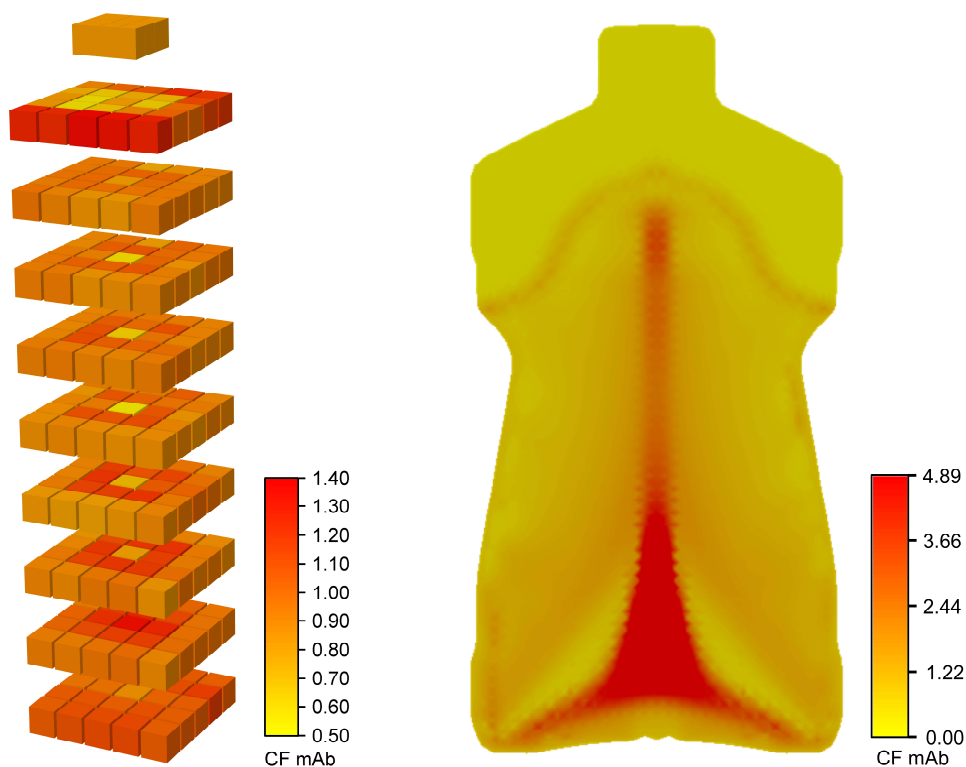


Figure 3 Experimentally determined mAb cryoconcentration (left) in comparison to simulated cryoconcentration (right) upon freezing.

The simulation displayed a CF between 0.12 and 4.89 (limited to 99% of the total mass; the highest simulated CF reflects a negligible fraction that is not of practical relevance). The cryoconcentration apparently appears to be increased in the simulation. However, since the sample size influences the experimental outcome (5), a deviation between experiment and simulation was expected. The simulation well predicted diluted areas at the walls and a highly concentrated centre near the bottom. Nevertheless, three results from the experiments were not covered by the simulations: i) the diluted core in the geometrical centre, ii) a highly concentrated region on top resulting from an eruption because of an upward volume expansion (2,6), and iii) the significant shift of the ratio between mAb and the buffer species histidine as the simulation only considers cryoconcentration of the mAb.

7.4.3 Comparison of Temperature Profiles during Thawing

Similar to the approach during freezing, temperature profiles were used to optimise the thawing simulation. The best agreement was found for an HTC of 26 W/(m²K) at the walls and 20 W/(m²K) at bottom and top (Figure 4). Overall, the TC profiles were matched. Optimisation could not completely eliminate the deviation towards the bottle centre (TC 1, TC 2, and TC 6). During thawing ice detaches and starts to float on top, driven by coincidence. This process cannot be implemented in the simulation which assumes ice as stationary. Consequently, thawing takes longer in the simulation. Additionally, only two HTC values can momentarily be set; different HTC values for the four walls depending on the positioning towards fans and blast freezer/thawer wall may allow even better adjustment. Nevertheless, differences between TC 1 and TC 6, which were experimentally seen upon thawing, were also detected by the simulation. The oscillation after complete thawing of ice is due to natural convection that was implemented in the solver.

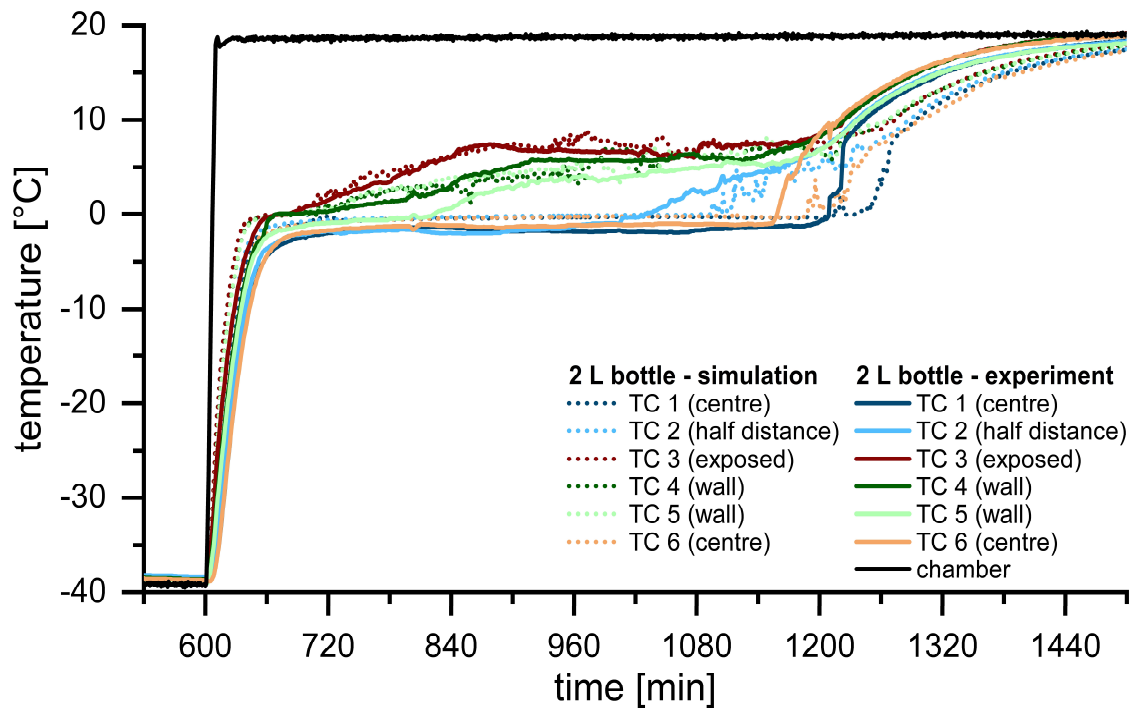


Figure 4 Temperature profiles as determined during the CFD simulation (dotted lines) and large-scale experiments (solid lines) during thawing. The HTC was set to $26 \text{ W}/(\text{m}^2\text{K})$ at the walls and to $20 \text{ W}/(\text{m}^2\text{K})$ at the top and the bottom surface.

7.4.4 Comparison of Concentration Gradients upon Thawing

Upon thawing, CF values between 0.54 and 2.86 were quantified experimentally (Figure 5). This indicates a strongly diluted top region and highly concentrated region at the bottom of the 2 L bottle. This gradient was predicted by the CFD simulations with CFs between 0.002 and 2.93 (limited to 99% total mass). Again, the extremely low CF towards the top is limited to a very small defined region and more of theoretical nature. Different diffusion coefficients for different solutes are not implemented in the solver and therefore additional relative changes in the composition depending on the position in the bottle cannot be predicted by the simulation.

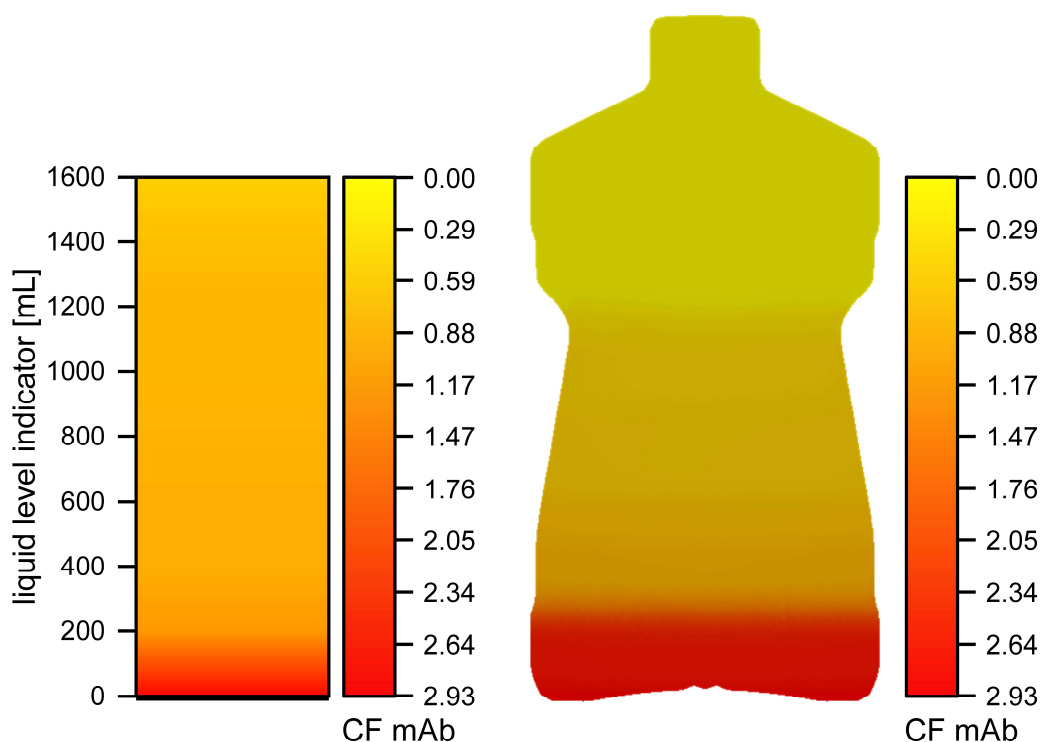


Figure 5 Experimentally determined mAb concentration gradient (left) in comparison to simulated concentration gradient (right) after thawing.

7.4.5 Additional Parameters Derived from the CFD Simulations

Temperature profiles and changes in concentration at any position in the bottle through freezing and thawing can be derived from CFD simulations. Additionally, the simulations calculate several parameters that can be of interest during large-scale freezing and thawing and that are not easily accessible via experiments. As displayed in Figure 6, the global temperature distribution during freezing as well as thawing can be extracted. This could be used to determine when set temperatures are reached throughout the entity. Furthermore, the proceeding of the freezing front and the formation of ice is pictured, which correctly displayed a volume expansion towards the top. It should be again noted that the ice is assumed stationary during thawing and thus does not start to float. In addition, the spatial stress upon freezing and thawing was simulated. Stress is defined in the solver as the time span a control volume stays below the freezing temperature and above the glass transition temperature of the maximally freeze-concentrated solution (T_g'). Upon freezing, this stress was highest at the walls of the bottle and lowest in the centre according to the simulations. Upon thawing, the latest thawing region in the centre experienced highest stress. It should be noted that the formation and the thawing of ice, indicated by time consuming plateaus in the temperature profiles, are not considered as stress.



Figure 6 Simulated development of mAb concentration (CF), temperature (°C), local stress, and the formation of ice during cooling and heating.

7.5 Conclusion

CFD simulations accurately described temperature distribution at six distinct positions during freezing and thawing in a rectangular 2 L bottle. Temperature profiles during thawing were slightly less accurate, probably because in the experiments ice detaches during thawing and starts to float. The experimentally determined cryoconcentration upon freezing as well as concentration gradients after thawing were well reflected in detail in the simulation. Only a small diluted core region and a small highly concentrated region in the top region upon freezing were not reflected in the simulation. Effects of differences in the diffusion coefficient of solutes due their size on cryoconcentration are not yet implemented in the simulation, but can be added in the future. An enormous asset of the CFD simulations is that they enable to calculate parameters that cannot be directly assessed experimentally including the global temperature distribution, the formation of ice, and the distribution of stress.

CFD modeling helps to gain a better understanding of large-scale freezing and thawing processes and associated phenomena. Thus, simulations can be used to define optimal process parameters and to evaluate the robustness of processes, i.e. the effect variations in fill volume, bottle size, and cooling and heating ramps have on the outcome. Furthermore, the information about the distribution of stress is used to develop novel scale-down devices.

References

1. Rodrigues MA, Miller MA, Glass MA, Singh SK, Johnston KP. Effect of Freezing Rate and Dendritic Ice Formation on Concentration Profiles of Proteins Frozen in Cylindrical Vessels. *J Pharm Sci.* 2011 Apr;100(4):1316–29.
2. Bluemel O, Buecheler JW, Rodrigues MA, Geraldes V, Hoelzl G, Bechtold-Peters K, et al. Cryoconcentration and 3D Temperature Profiles During Freezing of mAb Solutions in Large-Scale PET Bottles and a Novel Scale-Down Device. *Pharm Res.* 2020 Sep 30;37(9):179.
3. Geraldes V, Gomes DC, Rego P, Fegley D, Rodrigues MA. A New Perspective on Scale-Down Strategies for Freezing of Biopharmaceuticals by Means of Computational Fluid Dynamics. *J Pharm Sci.* 2020 Jun;109(6):1978–89.
4. Singh SK, Kolhe P, Wang W, Nema S. Large-Scale Freezing of Biologics A Practitioner’s Review, Part One: Fundamental Aspects. *Bioprocess Int.* 2009;7(9):32–44.
5. Kolhe P, Mehta AP, Lary AL, Chico SC, Singh SK. Large-Scale Freezing of Biologics (Part III). *BioPharm Int.* 2012;25(October):40–8.
6. Duarte A, Rego P, Ferreira A, Dias P, Geraldes V, Rodrigues MA. Interfacial Stress and Container Failure During Freezing of Bulk Protein Solutions Can Be Prevented by Local Heating. *AAPS PharmSciTech.* 2020 Oct 1;21(7):251.

Chapter 8 Summary

Due to material limitations, particularly during early-stage development, scale-down devices (SDDs) are needed that preserve the characteristics of large-scale freezing and thawing, but require only a fraction of the material. So far, no SDD is marketed to predict freezing and thawing and possible detrimental effects in industrially widely used disposable bottles.

Chapter 1 highlighted advantages and possible drawbacks that are associated with freezing and thawing of monoclonal antibody (mAb) solutions. Additionally, the current scientific knowledge in respect of ideal process and storage conditions was summarised. Several approaches to scale-down large-scale freezing and thawing were discussed and two SDDs, which development was assisted by Computation Fluid Dynamics (CFD), were introduced.

At first, freezing in a novel SDD was compared to a large-scale 2 L bottle and a 125 mL bottle (**Chapter 2**). The 3D printed SDD is a cover that surrounds a 125 mL bottle and controls the heat exchange via insulation of critical regions. Thereby, matching cumulative thermal histories between the SDD and the 2 L bottle are generated. The SDD accurately predicted 3D temperature profiles and cryoconcentration of a mAb and the buffer histidine compared to the 2 L bottle. Unforeseen events, such as a diluted core at the last point to freeze as well as shifts in the mAb to histidine ratio, were preserved. In contrast, freezing was markedly shorter and cryoconcentration reduced in the 125 mL bottle. High initial mAb concentration suppressed cryoconcentration, while low initial mAb concentrations led to substantial freeze-concentration. The higher dynamic viscosity, which further increased upon cooling, was found to limit cryoconcentration.

Furthermore, the SDD mimicked temperature profiles that were observed during large-scale thawing in a 2 L bottle (**Chapter 3**). Substantial concentration gradients of mAb, the buffer histidine, and the surfactant polysorbate 80 (PS80), leading to marked density gradients, were detected in the SDD and the large-scale 2 L bottle. Concentration gradients were considerably smaller in the 125 mL bottle, because of the significantly reduced thawing time. Differences in diffusivity between mAb, histidine, and PS80 resulted in a rapid equilibration of histidine during and after thawing of the mAb solution.

Eventually, mAb aggregation upon repeated freezing and thawing in the SDD was compared to the 2 L bottle and the 125 mL bottle (**Chapter 6**). Three different mAb solutions were subjected to five freeze-thaw cycles. In comparison to the 2 L bottle, the

125 mL bottle underestimated aggregation in mAb solutions that are sensitive to freezing and thawing induced denaturation. In contrast, the use of the SDD had a marked effect on mAb stability. While mAb aggregation upon large-scale freezing and thawing of highly stable mAb solutions was matched in the SDD, the formation of soluble aggregates was overpredicted in instable solutions. Thus, the SDD can mimic the worst-case scenario during development and formulation optimisation. A novel micro SDD (mSDD) that utilises vials reduces the material needed to characterise large-scale freezing and thawing nearly 300-fold. Whereas the SDD matched the thermal history of a 2 L bottle via insulation of critical regions, the significant differences in size and geometry required a different approach in the mSDD. Defined cooling and heating rates expand the time the sample spends between the freezing temperature and the glass transition temperature of the maximally freeze-concentrated solutions (T_g') and thereby increase stress time. MAb aggregation was significantly underestimated in 10 mL vials that were frozen identical to the 2 L bottle. In contrast, the use of the mSDD markedly increased soluble and insoluble aggregate levels.

In summary, the novel 2 SDD can be used to mimic freezing and thawing and associated phenomena, e.g. cryoconcentration, in a 2 L bottle by using only a fraction of the material. During early-stage development, it can be utilised for process and formulation optimisation. The novel mSDD further reduces the material need and proves that the manipulation of cooling and heating profiles is an effective method to increase stress upon freezing and thawing.

Chapter 4 examined the effect of cryoconcentration, which comes with a change in mAb to histidine ratio, on long-term frozen storage stability below and above T_g' . To determine T_g' of protein samples that do not contain glass formers via differential scanning calorimetry, an optimised sample preparation was established. Increasing the sample concentration via lyophilisation and subsequent reconstitution with less water resulted in distinct glass transition signals. T_g' of the samples was defined by the mAb to histidine ratio. Storage at $-80\text{ }^\circ\text{C}$, significantly below T_g' , did not lead to mAb aggregation, whereas storage above T_g' , at $-20\text{ }^\circ\text{C}$ or $-10\text{ }^\circ\text{C}$, markedly affected stability. Long-term storage stability above T_g' was an interplay of ΔT between T_g' and the storage temperature, the ionic strength in the non-solidified freeze-concentrated matrix, and mAb concentration. Transferred to cryoconcentration in a 2 L bottle, apparently small changes in mAb and

histidine concentration, associated with a shift in the mAb to excipient ratio, have a considerable effect on long-term frozen storage stability.

In **Chapter 5** a more systematic study was presented that addressed the effects variations in mAb and buffer concentration have on long-term frozen storage stability. Increasing mAb concentration negatively impacted insoluble aggregation, but decreased the oxidised fraction that was found after six-month storage at -10 °C. An increase in buffer concentration decreased mAb stability. This effect could be correlated to weaker repulsive protein-protein interactions with increasing ionic strength. Buffer-free samples displayed overall highest levels of soluble aggregates.

During the development of the SDDs, CFD simulations were used to calculate the thermal history and thereby stress during large-scale freezing and thawing. **Chapter 7** compared optimised CFD simulations to experimental temperature profiles and cryoconcentration and concentration gradients upon freezing (**Chapter 2**) and thawing (**Chapter 3**), respectively. After adapting heat transfer coefficients, the simulations precisely described the experimental temperature distribution. While the concentration gradient upon thawing was accurately predicted, macroscopic cryoconcentration upon freezing was slightly increased. However, the samples size influences the experimental outcome. In addition, CFD modeling allowed to extract the distribution of stress, the global temperature, and the formation of ice. Thus, the simulations are a promising tool to characterise freezing and thawing of mAb solutions and to generate a holistic understanding of the process.

This thesis focused on the characterisation of novel SDDs to predict freezing and thawing behaviour of mAb solutions in large-scale bottles. To this end, we evaluated i) temperature profiles at distinct positions, ii) changes in concentration upon freezing and thawing, and iii) mAb aggregation. Overall, the SDD proved great predictive power. In contrast, an unshielded 125 mL bottle significantly underestimated process time and changes in concentration and should not be used to scale down large-scale freezing and thawing processes. The material need was further reduced in a mSDD which controls the freezing and thawing process in 10 mL vials. Compared to regularly frozen 10 mL vials, the mSDD was much closer to the increased soluble and insoluble aggregate levels of the large-scale bottles. Long-term frozen storage stability studies underlined the marked effect apparently small changes in mAb and excipient concentration due to cryoconcentration might have

when the storage temperature is above T_g' . The SDD can be stored to study these effects or used to determine cryoconcentration and shifts in mAb to excipient ratio to prepare samples accordingly.